Geochemical and Hydraulic Modeling of Cavernous Structures in Potash Seams

---

Geochemische und hydraulische Modellierung kavernöser Strukturen in Kaliflözen

Kumulative Dissertation

zur Erlangung des akademischen Grades

Doktor-Ingenieur (Dr.-Ing.)

in der Wissenschaftsdisziplin Hydrogeologie

eingereicht an der

Mathematisch-Naturwissenschaftlichen Fakultät

der Universität Potsdam

und dem

Helmholtz-Zentrum Potsdam

Deutsches GeoForschungsZentrum GFZ

vorgelegt von

Svenja Steding

am 26. Oktober 2021

Ort und Datum der Disputation: Potsdam, 25. Februar 2022

Betreuer

Prof. Dr. Michael Kühn

Deutsches GeoForschungsZentrum GFZ

Department Geochemie

Sektion Fluidsystemmodellierung

und

Universität Potsdam

Mathematisch-Naturwissenschaftliche Fakultät

Institut für Geowissenschaften

Dr. Thomas Kempka

Deutsches GeoForschungsZentrum GFZ

Department Geochemie

Sektion Fluidsystemmodellierung

und

Universität Potsdam

Mathematisch-Naturwissenschaftliche Fakultät

Institut für Geowissenschaften

Prof. Dr. Max Wilke

Universität Potsdam

Mathematisch-Naturwissenschaftliche Fakultät

Institut für Geowissenschaften

Gutachter:innen

Prof. Dr. Michael Kühn

Deutsches GeoForschungsZentrum GFZ

Department Geochemie

Sektion Fluidsystemmodellierung

und

Universität Potsdam

Mathematisch-Naturwissenschaftliche Fakultät

Institut für Geowissenschaften

Prof. Dr. Wilfried Schneider

Technische Universität Hamburg

Studiendekanat Bauwesen

Institut für Wasserressourcen und Wasserversorgung

Dr. habil. Elke Bozau

Technische Universität Clausthal

Institut für Geologie und Paläontologie

Abteilung Hydrogeologie

Online veröffentlicht auf dem
Publikationsserver der Universität Potsdam:
https://doi.org/10.25932/publishup-54818
https://nbn-resolving.org/urn:nbn:de:kobv:517-opus4-548182

Abstract

Salt deposits offer a variety of usage types. These include the mining of rock salt and potash salt as important raw materials, the storage of energy in man-made underground caverns, and the disposal of hazardous substances in former mines. The most serious risk with any of these usage types comes from the contact with groundwater or surface water. It causes an uncontrolled dissolution of salt rock, which in the worst case can result in the flooding or collapse of underground facilities. Especially along potash seams, cavernous structures can spread quickly, because potash salts show a much higher solubility than rock salt. However, as their chemical behavior is quite complex, previous models do not account for these highly soluble interlayers. Therefore, the objective of the present thesis is to describe the evolution of cavernous structures along potash seams in space and time in order to improve hazard mitigation during the utilization of salt deposits.

The formation of cavernous structures represents an interplay of chemical and hydraulic processes. Hence, the first step is to systematically investigate the dissolution and precipitation reactions that occur when water and potash salt come into contact. For this purpose, a geochemical reaction model is used. The results show that the minerals are only partially dissolved, resulting in a porous sponge like structure. With the saturation of the solution increasing, various secondary minerals are formed, whose number and type depend on the original rock composition. Field data confirm a correlation between the degree of saturation and the distance from the center of the cavern, where solution is entering. Subsequently, the reaction model is coupled with a flow and transport code and supplemented by a novel approach called 'interchange'. The latter enables the exchange of solution and rock between areas of different porosity and mineralogy, and thus ultimately the growth of the cavernous structure. By means of several scenario analyses, cavern shape, growth rate and mineralogy are systematically investigated, taking also heterogeneous potash seams into account. The results show that basically four different cases can be distinguished, with mixed forms being a frequent occurrence in nature. The classification scheme is based on the dimensionless numbers Péclet and Damköhler, and allows for a first assessment of the hazard potential. In future, the model can be applied to any field case, using measurement data for calibration.

The presented research work provides a reactive transport model that is able to spatially and temporally characterize the propagation of cavernous structures along potash seams for the first time. Furthermore, it allows to determine thickness and composition of transition zones between cavern center and unaffected salt rock. The latter is particularly important in potash mining, so that natural cavernous structures can be located at an early stage and the risk of mine flooding can thus be reduced. The models may also contribute to an improved hazard prevention in the construction of storage caverns and the disposal of hazardous waste in salt deposits. Predictions regarding the characteristics and evolution of cavernous structures enable a better assessment of potential hazards, such as integrity or stability loss, as well as of suitable mitigation measures.

Kurzfassung

Salzlagerstätten bieten eine Vielzahl an Nutzungsmöglichkeiten. Diese umfassen den Abbau von Steinsalz und Kalisalz als wichtige Rohstoffe, die Speicherung von Energie in künstlich erzeugten Hohlräumen, sowie die Entsorgung gefährlicher Substanzen in stillgelegten Bergwerken. Die größte Gefahr bei jeder dieser Nutzungsarten ist der Kontakt mit Grund- oder Oberflächenwasser. Er bewirkt eine unkontrollierte Lösung des Salzgesteins, was im schlimmsten Fall zur Flutung oder zum Einsturz unterirdischer Infrastrukturen führt. Insbesondere entlang von Kaliflözen können sich kavernöse Strukturen schnell ausbreiten, da Kalisalze eine wesentlich höhere Löslichkeit besitzen als Steinsalz. Ihr chemisches Verhalten ist jedoch komplex, weshalb bisherige Modelle diese hochlöslichen Zwischenschichten vernachlässigen. Ziel der vorliegenden Doktorarbeit ist es daher, die Ausbreitung kavernöser Strukturen entlang von Kaliflözen räumlich und zeitlich zu beschreiben und damit die Möglichkeiten zur Gefahrenprävention bei der Nutzung von Salzlagerstätten zu verbessern.

Die Bildung kavernöser Strukturen ist ein Zusammenspiel chemischer und hydraulischer Prozesse. Zunächst wird daher mithilfe eines geochemischen Reaktionsmodells systematisch untersucht, welche Lösungs- und Fällungsreaktionen beim Kontakt von Wasser und Kalisalz auftreten. Die Ergebnisse zeigen, dass nur ein Teil der Minerale gelöst wird, wodurch sich eine poröse, schwammartige Struktur bildet. Mit zunehmender Aufsättigung der Lösung treten verschiedene Sekundärminerale auf, deren Anzahl und Art vom Ausgangsgestein abhängen. Felddaten belegen dabei eine Korrelation zwischen Sättigungsgrad und Abstand vom Kavernenzentrum, wo die Lösung ein- und austritt. Anschließend wird das Reaktionsmodell mit einem Strömungs- und Transportcode gekoppelt und um einen neuartigen Ansatz namens "interchange" ergänzt. Dieser ermöglicht den Austausch von Lösung und Gestein zwischen Bereichen unterschiedlicher Porosität und Mineralogie, und damit letztlich das Wachstum der kavernösen Struktur. In mehreren Szenarienanalysen werden Kavernenform, Ausbreitungsgeschwindigkeit und Mineralogie systematisch untersucht und dabei auch heterogene Kaliflöze betrachtet. Die Ergebnisse zeigen, dass grundsätzlich vier Fälle zu unterscheiden sind, wobei in der Natur häufig Mischformen auftreten. Die Klassifizierung erfolgt auf Basis der dimensionslosen Kennzahlen Péclet und Damköhler und ermöglicht eine erste Abschätzung des Gefahrenpotentials. In Zukunft kann das Modell auf beliebige Feldbeispiele angewandt und mithilfe von Messdaten kalibriert werden.

Die vorliegende Arbeit liefert ein reaktives Transportmodell, mit dem die Ausbreitung kavernöser Strukturen entlang von Kaliflözen erstmals räumlich und zeitlich beschrieben werden kann. Auch Mächtigkeit und Zusammensetzung der Übergangszone zwischen Kavernenzentrum und unberührtem Salzgestein können damit bestimmt werden. Letzteres ist insbesondere im Kalibergbau von Bedeutung, um natürliche kavernöse Strukturen rechtzeitig zu lokalisieren und damit das Risiko für eine Flutung von Bergwerken zu verringern. Auch bei der Herstellung von Speicherkavernen und der Einlagerung gefährlicher Substanzen im Salzgestein können die Modelle zu einer besseren Gefahrenprävention beitragen. Sie ermöglichen Prognosen über Beschaffenheit und Ausbreitungsverhalten kavernöser Strukturen, wodurch sowohl potentielle Gefahren, wie der Verlust von Dichtigkeit oder Stabilität, als auch geeignete Gegenmaßnahmen besser abschätzbar werden.

Table of Contents

List of Figures

List of Tables

List of Abbreviations

Abbreviations

1D	One-dimensional
2D	Two-dimensional
3D	Three-dimensional
DepV	Deponieverordnung
K+S	K+S Aktiengesellschaft
StandAG	Standortauswahlgesetz
TRANSE	TRANsport Simulation Environment
TU	Technische Universität
z1KHe	Potash seam 'Hessen'
z1KTh	Potash seam 'Thüringen'
z1NAa	Lower Werra rock salt
z1NAb	Middle Werra rock salt
z1NAc	Upper Werra rock salt

Names and molecular formula of salt minerals can be found in Table 2.2.

Symbols

c_f	Fluid compressibility	1/Pa
$contact\_area$	Contact area between non-equilibrated minerals and solution	cm^2
D_f	Diffusion coefficient	m^2/s
Da	Damköhler number	-
di	Cell diameter perpendicular to the dissolution front	cm
dt	Time step length	s
$factor$	Factor between 1 and ∞ to calculate $contact\_area$	-
K	Equilibrium constant	-
k_f	Permeability	m^2
k_{max}	Maximum dissolution rate of a mineral	cm/s
l	Characteristic length	m

Min	Minerals present in a cell	mol
Min_{add}	Minerals added from Min_{dry} to permeated sub-cell	mol
Min_{dry}	Minerals in the dry sub-cell	mol
Min_{eq}	Minerals equilibrated with solution	mol
Min_{neq}	Minerals not equilibrated with solution	mol
Min_{sol}	Minerals dissolved via interchange	mol
$Min_{sol,dry}$	Minerals dissolved from Min_{dry} via internal dissolution	mol
$Min_{sol,neq}$	Minerals dissolved from Min_{neq} via internal dissolution	mol
Pe	Péclet number	-
Q	Activity product	-
r	Average dissolution rate (all minerals)	cm/s
$rate$	Saturation-dependent dissolution rate	cm/s
S_{per}	Permeation state of a cell	-
SI	Saturation index	-
v	Flow velocity	m/s
V_{cell}	Cell volume	m^3
V_{neq}	Volume of non-equilibrated minerals	cm^3
V_{per}	Volume of permeated sub-cell	m^3
Φ	Porosity	-
Φ_{per}	Porosity of permeated sub-cell	-

Indices

A	Cell A
B	Cell B
n	Interchanged mineral

1 | Introduction

Utilization of the geological subsurface is essential to master some of the major challenges of our time. Thereby, salt deposits belong to the most versatile rock types. First, they provide important raw materials: each year, over 300 million tons of rock salt and potash salt are mined in order to produce more than 10,000 industrial products (Bolen 2021; Jasinski 2021). Among others, these include table salt, soap and medical products, but also potash fertilizers with the latter being essential to meet the global food demand (Elsner 2016). Second, salt rock is particularly suitable for underground energy storage due to its low permeability. In Germany, more than 370 storage caverns for gas and oil have been built in salt formations (LBEG 2021). All over the world, storage caverns are an important means for bridging gaps in energy supply and, in the near future, they are expected to gain in importance since the production of renewable energies is associated with large fluctuations. In this context, technical caverns can be used to store, for example, hydrogen, compressed air or synthetic methane (Gasanzade et al. 2021; Letcher 2016). Finally, salt deposits represent a promising host rock for the geological disposal of harmful substances. In Germany, all underground disposal sites for toxic waste are located in rock salt (§3 DepV). In addition, it is considered as potential host rock for nuclear waste repositories, together with claystone and crystalline rocks, due to its high thermal conductivity and self-healing characteristics (§ 1 StandAG, IAEA 2020). However, each of these usage types is also associated with risks. To ensure an efficient and safe long-term utilization, thorough knowledge about the formation, exploration and operational properties of salt deposits is essential.

1.1 Utilization of Salt Deposits: Requirements and Risks

Salt deposits are formed by the evaporation of seawater and consist of layers with different solubilities (Braitsch 1971). The largest ones are rock salt layers, which are usually several tens of meters thick. If diapirism causes the formation of salt pillows or salt domes, their vertical extension can be increased to several hundreds of meters. Rock salt layers mainly consist of halite (NaCl), but considerable amounts of anhydrite ($CaSO_4$), carbonates or clay can be included as well. These minerals either occur as inclusions or as thin interlayers and are nearly insoluble compared to halite. Another type of salt layers are potash seams. They are only formed if >98% of the original seawater have evaporated and therefore do not occur in peripheral areas of salt deposits. Furthermore, they are rarely more than a few meters thick and their mineralogical composition varies widely, depending upon the conditions during and after evaporation. Potash seams show the highest solubility of all salt minerals. Between

salt deposits and aquifers, layers from gypsum, anhydrite or mudstone act as aquitards, preventing the inflow of groundwater and thus the dissolution of salt deposits.

For the construction of technical caverns, water is pumped into a salt deposit to deliberately dissolve the rock salt. Simultaneously, NaCl-saturated brine is pumped out, resulting in the formation of a cavity 500-2000 m below the surface (Figure 1.1a). To produce regular cavern shapes, the purity of rock salt should be at the highest possible level. In practice, however, intersecting layers of low or high solubility in comparison with halite are a common phenomenon (Thoms and Gehle 1999). The first ones break off and sink down to the bottom of the cavern as soon as the halite around them has been dissolved (Figure 1.1a). The fragments block parts of the previously formed storage volume and therefore reduce the storage capacity (Li et al. 2018). Conversely, highly soluble potash seams cause a preferential expansion of caverns along them. The resulting irregular shapes endanger the mechanical stability of technical caverns (Cyran 2020; Fokker 1995; Keime et al. 2012). Additionally, the risk of encountering another storage cavern or an aquifer is increased. Both cases would be equivalent to an integrity loss (Figure 1.1a).

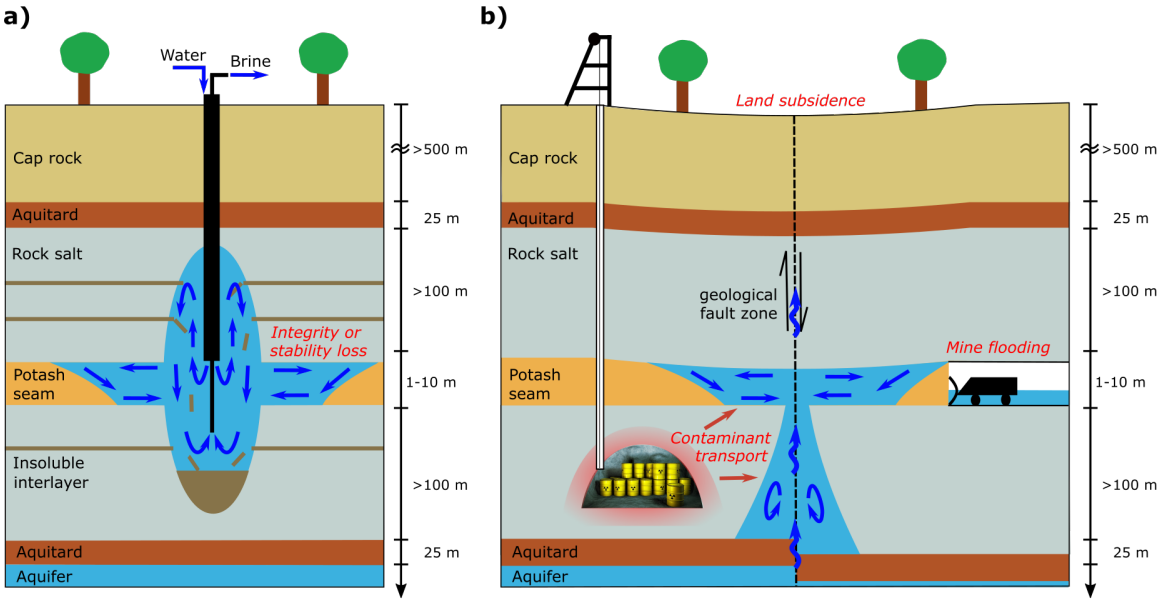

Figure 1.1: Utilization of salt deposits and its risks: a) Construction of a technical cavern. Insoluble interlayers reduce the storage volume, potash seams increase the risk of integrity/stability loss. b) Formation of a natural cavern. Its preferential expansion along potash seams increases the risk of land subsidence, mine flooding and the transport of contaminants from waste repositories into aquifers.

For the mining of salt rock, thick layers with a high level of purity are preferable as well. Furthermore, they should be located close to the surface in order to reduce costs for production and treatment. However, care must be taken that the aquitard is not damaged by mining activities. Otherwise, groundwater or surface water can get into contact with salt rock, leading to the formation of natural cavern systems (Johnson 2008). The same phenomenon can also occur due to geological fault zones disrupting the aquitard (Figure 1.1b) (Anderson and Kirkland 1980; Höntzsch and Zeibig 2014).

Generally, natural caverns represent the greatest threat to any underground facility in salt deposits (Warren 2017). In case they encounter a mine, a dynamic outlet is created, enabling flow and dissolution rates to grow significantly. As a result, the inflow of water increases over time, until the mine finally is flooded. With regard to potash mining, this has been the most common reason for an unwanted early closure of mines within the past 150 years (Prugger and Prugger 1991). The reason why potash mines are particularly endangered is the high solubility of potash minerals and the resulting preferential expansion of caverns along them (Figure 1.1b). However, not every brine occurrence in mines is related to external water inflow. Many of them were formed and enclosed millions of years ago and do not represent a significant danger. To distinguish between them, brine amount and composition are important indicators (Herbert and Schwandt 2007; Wittrup and Kyser 1990). Moreover, an early detection of natural caverns, based on rock samples from the surrounding, is beneficial with regard to risk mitigation (Boys 1993).

Natural cavern systems also represent a great threat to geological repositories. In the worst case, the surrounding rock salt is dissolved and contaminants are directly released into the groundwater. However, even if caverns occur in proximity to geological repositories, the thickness of the surrounding rock salt, and thus its function as a barrier, is significantly lower (Figure 1.1b). Again, the presence of potash salt intensifies the problem due to its high solubility and the associated increase in the formation of new pathways (Mengel et al. 2012). Finally, the collapse of natural caverns can lead to land subsidence (Figure 1.1b). This risk increases as well if potash seams enable a preferential, faster expansion in horizontal direction (Höntzsch and Zeibig 2014).

In summary, uncontrolled dissolution processes in salt deposits pose high potential hazards. In order to assess and minimize them, it is essential to understand the evolution of technical and natural caverns, particularly along potash seams. Only then, a safe utilization of salt deposits can be ensured.

1.2 Modeling Salt Leaching: History and Current Challenges

Technical and natural caverns in salt rock are the result of a complex interaction between chemical reactions, transport and, in the long term, mechanical processes. To ensure an efficient and safe utilization of salt deposits, laboratory and field experiments have been conducted within the last 120 years, complemented by model approaches aiming to understand and reproduce the underlying processes. The following section gives an overview of the research that has been done so far, asking the question which steps are necessary to fully comprehend the evolution of caverns in salt rock. In this context, particular emphasis is placed on the availability of data and models dealing with potash salt. Although rock salt layers make up the largest part of salt deposits, potash seams are especially important with regard to cavern evolution due to the

preferential expansion along them and the above-mentioned risks resulting out of that (Figure 1.1).

Understanding the chemistry of salt-water systems is essential to predict the evolution of caverns. For every temperature, pressure and solution composition, it has to be known which salt phases occur and what the properties of the ion containing solution are. In case of rock salt, this is rather simple since only halite (NaCl) is dissolved, resulting in a binary system ($NaCl-H_2O$) with well-known thermodynamic properties. In contrast, potash brines usually contain all six major components of seawater (Na, Cl, K, Mg, SO_4 and Ca) from which more than sixty different salt minerals can be formed (Voigt 2015). During the 20^{th} century, many dissolution experiments were performed, investigating the solubility equilibria of the hexary oceanic salt system $Na-K-Mg-Cl-SO_4-Ca-H_2O$ and its subsystems. Based on the results, thermodynamic models have been developed in order to easily quantify saturation states as well as dissolution and precipitation processes for arbitrary solution compositions and varying temperatures (Altmaier et al. 2011; Harvie and Weare 1980). To account for high salinity, the Pitzer approach (Pitzer 1973) is commonly applied. By means of computer programs such as PHREEQC (Parkhurst and Appelo 2013), Geochemist's Workbench (Bethke 2007) or EQ3/6 (Wolery and Jarek 2003), it has been possible to classify salt brines (Herbert and Schwandt 2007) and to reproduce chemical reactions that occur during the formation of salt deposits (e.g. Debure et al. 2019; Krupp 2005). Nevertheless, the dissolution behavior of potash seams has only been studied for a few cases of mine flooding yet (Bach 2010; Bohn 2014; Herbert 2000). Systematic investigations for different potash salt compositions are still missing as well as a characterization of the so-called transition zone that surrounds caverns in potash seams, offering the possibility of localizing them.

Another important factor in cavern evolution are flow and transport processes. Natural, density-driven convection is considered as the main driving force in the formation of natural caverns (Anderson and Kirkland 1980) and the construction of technical caverns (Cyran 2020; Velema et al. 2010). It is caused by large density gradients between the inflowing solution, which is undersaturated with respect to the occurring salt minerals, and saturated brines (Dijk and Berkowitz 2000; Gechter et al. 2008). The latter show fluid densities of up to $1{,}230\,kg/m^3$ within rock salt layers and even $>1{,}300\,kg/m^3$ within potash seams (Herbert 2000). Density-driven convection forces the undersaturated, less dense solution to flow towards the cavern top, whereas saturated brine sinks down, leading to constant solution exchange and upward cavern enlargement (Weisbrod et al. 2012). However, modeling density-driven flow is challenging (Herbert et al. 1988; Wooding et al. 1997). Already in porous media, where laminar flow can be assumed, large density variations and salinity-dependent viscosity effects lead to a set of strongly coupled, nonlinear equations, necessitating sophisticated numerical approaches (Diersch and Kolditz 2002). In open cavities, turbulent flow conditions complicate the calculation of the concentration field even more (Küch-

ler 2014). To properly reproduce it, the Navier-Stokes equations have to be solved, requiring a high computational effort. Thus, these models are still under development, whereas commercial software tools for technical cavern construction usually assume strongly simplified flow fields and concentration distributions (Wan et al. 2019). In case of potash seams, multi-species transport has to be taken into account and gaseous components may lead to the formation of gas bubbles at the cavern top (Gechter et al. 2008), necessitating multiphase flow to be incorporated as well (Olivella et al. 1994). Finally, species diffusion coefficients in brines are not constant but depend on the composition of the solution (Felmy and Weare 1991). Thus, hydraulics and chemical reactions within salt caverns are strongly coupled, calling for the application of reactive transport models.

Reactive transport models aim to simulate the complex interplay of fluid flow and rock-liquid interactions in order to reproduce cavern evolution in space and time. In general, a broad range of numerical reactive transport codes already exists, especially for porous media (Steefel et al. 2015). Some of them also take heat transport and the resulting changes in flow parameters into account (Graf and Therrien 2007; Kuhlman 2014; Stauffer et al. 2013). To couple transport and chemical reaction equations, either the global implicit approach or the split-operator technique is used. The latter allows to relatively easily combine different submodels dealing with individual processes, i.e., to couple geochemical reaction modules with flow and transport simulators (Mao et al. 2006). However, these approaches alone are insufficient to reproduce cavern development because chemical reactions can only take place where water is present. Due to the fact that intact, dry salt rock is basically impermeable, the inflow of solution is inhibited, preventing dissolution processes and thus any progress of the solid-fluid boundary. In case of rock salt, mass transfer rates are commonly used to overcome this limitation: by means of empirical functions, the dissolution rate of halite, and therefore the moving rate of the cavern wall, is determined, with the brine concentration and the inclination of the solid-fluid interface being the main variables of influence (Jinlong et al. 2020; Li et al. 2018; Wan et al. 2019; Zidane et al. 2014). Several experimental and numerical studies have been conducted dealing with the dissolution behavior of halite under various flow conditions and saturation states (Alkattan et al. 1997; Durie and Jessen 1964; Liu et al. 2016; Stiller et al. 2016; Weisbrod et al. 2012; Yang and Liu 2017). Nevertheless, the influence of surface roughness and rock fibre is still poorly understood (Cyran 2020; Field et al. 2019). While some reactive transport models account for the effects of insoluble interlayers on a macro scale (e.g. Jinlong et al. 2020), they are usually incapable of considering highly soluble potash seams. In order to reproduce the preferential expansion of caverns along them and to evaluate the potential risks resulting out of that (Figure 1.1), further development of reactive transport models is necessary.

The main difficulty about developing reactive transport models for potash seams is the complex chemistry described above. In contrast to rock salt, it is insufficient

to only distinguish between dry rock and a cavity filled with solution, because the solubility of the different components varies significantly. For example, kieserite and anhydrite dissolve considerably slower than carnallite or sylvite (Hoppe and Winkler 1974; Röhr 1981), and halite is nearly insoluble in the presence of magnesium salts (Fokker 1995). As a result, potash seams do not dissolve completely, but a porous rock matrix remains, consisting of regions with different porosities and mineralogical compositions (Velema et al. 2010). Chemical reactions are no longer limited to the cavern wall but may occur in any region with water present, causing strong changes in porosity and permeability. Thereby, it may happen that previously formed pores are fully sealed again due to the precipitation of secondary minerals (Xie et al. 2011). To simulate the progress of multiple precipitation/dissolution fronts being formed within potash seams, the dissolution behavior of all occurring minerals has to be known. However, the dissolution kinetics of potash salts have been explored only rudimentarily yet. Studies indicate that in most cases, they are comparable to halite, with the dissolution rate being transport-controlled and decreasing linearly with saturation, whereas a few potash minerals show reaction-controlled or mixed dissolution behavior (Hoppe and Winkler 1974; Husband and Ozsahin 1967; Karsten 1954; Sdanowski 1958). Unfortunately, empirical functions considering both, the saturation state of the solution and the hydrodynamic boundary conditions, rarely exist for the dissolution rates of potash minerals. Consequently, current reactive transport models usually oversimplify the chemical reactions within potash seams and their interactions with fluid flow (Luo et al. 2012; Velema et al. 2010). Xie et al. (2011) presented a benchmark where various mineralogical regions and the resulting changes in permeability are reproduced, but density-driven flow was not considered. In summary, a reactive transport model suitable to describe the temporal and spatial evolution of caverns within potash seams has not been developed yet.

Cavern evolution is also affected by the mechanical behavior of salt rock. On the one hand, high local stresses due to cavern formation can induce microcracks or even collapse structures, increasing rock permeability and creating new hydraulic pathways (Lux and Eberth 2007; Minkley et al. 2013; Zhang et al. 2019). On the other hand, salt creep can effect self-healing and, in the long term, the closure of cavities (Munson 1997). Several mechanical models have been developed to evaluate the stability and tightness of technical caverns during the phases of excavation, operation and abandonment (Khaledi et al. 2016; Lux 2005; Wang et al. 2015), with some of them taking thermal effects into account (Bérest et al. 2001; Lux et al. 2015; Mahmoudi et al. 2016). In addition to that, coupled (thermo-) hydraulic-mechanical models have been developed to investigate the integrity of natural barriers in nuclear waste repositories (Hou 2003; Kuhlman 2014; Minkley et al. 2013; Pudewills 2012). It was shown that in the long term, creep and thermo-mechanical loading can cause significant changes in porosity and permeability. However, in the short term, the effects are rather small compared to dissolution processes, which can cause rapid changes in a matter of days,

weeks or years (Johnson 2008). An exception are collapse structures, leading to large permeability changes within a very short time frame. To account for them, a coupling of (thermo-) mechanical and reactive transport models would be required. However, this is still in the initial stages of development (Steefel et al. 2015). Furthermore, it is uncertain if the mechanical models existing already are applicable to caverns that preferentially expand along potash seams. Most of them assume pure rock salt, whereas only a few studies deal with the influence of non-salt interlayers (Nazary Moghadam et al. 2015). The mechanical behavior of potash salt has only been investigated in a rudimentary way so far (Campos de Orellana 1996; Fokker 1995), and for partly dissolved rock matrices, constitutive laws do not exist at all. Consequently, current models are incapable of predicting the stability of cavernous structures within potash seams.

All in all, the formation of caverns in salt rock is mainly controlled by the interplay between chemical reactions, namely the dissolution and precipitation of salt minerals, and hydraulics, with natural, density-driven convection being especially important. In contrast, mechanical processes are only relevant in the long term or if the stability of the cavern is endangered. To adequately reproduce the temporal and spatial evolution of technical and natural cavernous structures, sophisticated reactive transport models are required. Thereby, the complex geochemical behavior of potash salts represents a particular challenge and has not been investigated systematically yet. Current reactive transport models either neglect potash seams or oversimplify the chemical reactions within them. Hence, what is needed is the development of a more comprehensive approach to understand the preferential expansion of caverns along potash seams and to evaluate the associated risks.

1.3 Thesis Objectives

The preferential expansion of technical and natural caverns along potash seams represents a considerable risk for the utilization of salt deposits (Figure 1.1). Based on the previous explanations, three main research objectives are formulated for this thesis in order to reproduce the evolution of leaching zones within potash seams and to asses their hazard potential for subsurface utilization:

The **first objective** is to systematically investigate the chemical reactions within potash seams, aiming to quantify the brine and rock composition along transition zones between the center of cavernous structures and unaffected salt rock (Chapter 2). The **second objective** is to integrate these findings into a reactive transport model in order to temporally and spatially reproduce the evolution of leaching zones and to identify parameters that allow for a classification as well as a first assessment of the hazard potential (Chapter 3). Since most potash seams are not homogeneous, the **third objective** is to examine the influence of mineral heterogeneity and saturation-dependent

dissolution rates on the leaching zone evolution, focusing on insoluble inclusions and interlayers within potash seams (Chapter 4).

1.4 Organization of the Thesis and Author Contribution

This cumulative doctoral thesis consists of three articles, which are published in international, peer-reviewed journals. In Chapters 2 to 4, the publications are presented in detail, followed by a discussion about the main findings in Chapter 5. Conclusions with respect to the thesis objectives as well as an outlook for future research are given in Chapter 6. The following section shortly summarizes the three articles and indicates the respective author and co-author contributions.

In Chapter 2, geochemical reaction models are used to systematically investigate the dissolution behavior of various potash salts. It is shown that one liter of NaCl solution can affect several tens of kilograms of rock with the reaction path depending on the ratio between kieserite and sylvite. Field data from a natural brine occurrence are used to validate the results. With the help of a 1D model, the transition zones between cavernous structures and unaffected salt rock are quantified, finding that cavitation only occurs close to the central part of a cavern. Furthermore, it is shown that cavern enlargement requires an open system with frequent brine exchange. The chapter is published as '*Geochemical Reaction Models Quantify the Composition of Transition Zones between Brine Occurrence and Unaffected Salt Rock*' in *Chemical Geology*. As the first author, I was responsible for designing and performing the research, analyzing the data and illustrating the simulation results. Axel Zirkler provided unpublished field data and supported the model conceptualization. Michael Kühn co-designed the research and supervised my scientific activities. I was mainly responsible for the preparation and revision of the manuscript with my co-authors contributing to review and editing. It is citet as Steding et al. (2020) in the following.

In Chapter 3, a reactive transport model is developed and complemented by an innovative approach to simulate water-rock interactions at the solid-liquid interface. By means of scenario analyses, the temporal and spatial evolution of leaching zones within carnallite-bearing potash seams is examined. The results show that their shape, growth rate and mineralogy mainly depend on the dissolution rate of potash salt and its relation to the flow velocity governed by density-driven flow. A classification scheme based on the dimensionless Péclet and Damköhler number is used to assess the hazard potential. The chapter is published as '*Spatial and Temporal Evolution of Leaching Zones within Potash Seams Reproduced by Reactive Transport Simulations*' in *Water*. As the first author, I was designing and performing the research, analyzing the data and illustrating the simulation results. Axel Zirkler provided unpublished field data and contributed to the elaboration of the manuscript. The model development was done in close collaboration with Thomas Kempka who supervised my scientific activities together with Michael Kühn. Both of them contributed to the manuscript by

reviewing and editing it. I was mainly responsible for the preparation and revision of the manuscript. It is citet as Steding et al. (2021b) in the following.

In Chapter 4, the reactive transport model from Chapter 3 is used to examine the influence of insoluble inclusions and intersecting layers on cavern evolution. For this purpose, it is extended by mineral-specific, saturation-dependent dissolution rates. A scenario analysis for a carnallite-bearing potash seam is carried out, showing that heterogeneous rock distributions only affect transport-dominated systems (Damköhler > 1). Insoluble inclusions result in less regular, steeper dissolution fronts, with the upper end advancing slower. Intersecting layers lead to several independent convection cells and, if the layers are inclined, to asymmetric cavern shapes. In general, it is found that heterogeneous potash seams exhibit a lower hazard potential as long as mechanical stability is maintained. The chapter is published as '*How Insoluble Inclusions and Intersecting Layers Affect the Leaching Process within Potash Seams*' in *Applied Sciences*. As the first author, I was designing and performing the research, analyzing the data and illustrating the simulation results. Thomas Kempka and Michael Kühn supervised my scientific activities and contributed to the manuscript by reviewing and editing it. I was mainly responsible for the preparation and revision of the manuscript. It is citet as Steding et al. (2021a) in the following.

2 | Geochemical Reaction Models Quantify the Composition of Transition Zones between Brine Occurrence and Unaffected Salt Rock

Abstract

Brine occurrences belong to the most significant risks in salt mining as they can lead to mine flooding and land subsidence. Especially within highly soluble potash seams, which contain some of the economically most interesting types of salt, the interactions between brine and salt rock result in cavernous structures surrounded by moisture penetration zones with different mineralogical regions. In order to facilitate an early detection of cavernous structures, the brine and rock composition along these transition zones was modeled. The results show that the potash salt composition, or more precisely the ratio between kieserite and sylvite, determines the dissolution behavior and therefore which types of secondary minerals occur. According to the volume balance, cavitation is only possible close to the center of a cavernous structure, where the solid-fluid-ratio is low. Furthermore, an open system with frequent brine exchange is required. Along the transition zone, the solid-fluid-ratio can increase to several tens of kilograms before the water is fully consumed and the unaffected salt rock is reached. A comparison with measured data from a natural brine occurrence validates the model results and confirms a correlation between the brine composition and the distance from the center of a cavernous structure. In conclusion, the models are suitable to determine the location of the central part of a cavernous structure based on rock and brine samples from the vicinity. However, in order to simulate the temporal and spatial development of geogenic cavities, a coupling of chemistry and hydraulics will be necessary.

2.1 Introduction

In Germany, salt deposits play an important role as industrial raw material, which is won by mining. One of the most significant risks in mining is the access of groundwater due to geological fault zones which may lead to the formation of moisture penetration zones and local cavities within the salt body. Stability and tightness of the salt rock are significantly reduced in these areas and encountering them, in the worst case, can lead to the flooding of a mine (Baumert 1953; Warren 2017; Wittrup and Kyser 1990). Among the different salt layers, potash seams are particularly endangered as they have a significantly higher solubility than rock salt (Gimm and Meyer 1968). Their dissolution

behavior is very complex and has only been investigated for a few individual cases (Bach 2010; Bohn 2014; Herbert 2000). Therefore, there is little academic literature on the composition of transition zones between a brine occurrence and the unaffected salt rock.

In this paper, geochemical modeling is the basis to systematically investigate the dissolution behavior of various potash salts. The results are transferred to the mine system, whereby a natural brine occurrence in a potash mine serves as case study. Extensive investigation measures during the last decades provide comprehensive information on the geological extent and the chemical composition of the brine occurrence and the surrounding transition zone. The aim of the modeling is to quantify the dissolution processes within potash seams in order to facilitate an early detection of brine occurrences and minimize risks for mining industry.

2.2 Modeling Approaches

Potash salts not only contain the main components Na^+ and Cl^- but also Mg^{2+}, K^+, $SO_4{}^{2-}$, Ca^{2+} and crystal water. Upon contact with groundwater all components enter into the solution and a hexary system forms. This system was modeled by using the program code PHREEQC (Parkhurst and Appelo 2013). The dataset 'THEREDA_PIT_PHRC_r01' (Altmaier et al. 2011) serves as database that, among other things, takes temperature dependency into account. Due to the high salinity also the Pitzer approach (Pitzer 1973) is used.

It can be assumed that within a cavernous structure in salt rock, the system is always saturated with NaCl (Herbert and Schwandt 2007; Stadler et al. 2012). Depending on the relationship between the other ion concentrations, the solution is in thermodynamic equilibrium with different minerals. This can be seen, for example, at the Jänecke projection (Jänecke 1912) for a Ca-free, NaCl-saturated system (Figure 2.1). Points such as P, Q or R denote concentration ratios where the solution is in equilibrium with three other minerals besides halite. The location of these points is temperature-dependent. In addition, it should be noted that in this representation, not the absolute concentrations are taken into account but only their relationship to each other. Thus, a solution may have the same concentration ratio as, for example, at point P, but still be undersaturated with all adjacent mineral phases. Therefore, it is important to always consider the absolute concentrations and saturations of the solution as well. Nevertheless, the Jänecke projection is useful to graphically show the reaction path of a solution.

When considering a hexary system, the solution composition does not move across the surface shown in Figure 2.1 but through a tetrahedon whose fourth vertex is formed by the calcium concentration (Herbert and Schwandt 2007). The stability fields become stability spaces and additional minerals, such as anhydrite, polyhalite or syngenite, occur within the tetrahedron. The starting point of a reaction path always corresponds

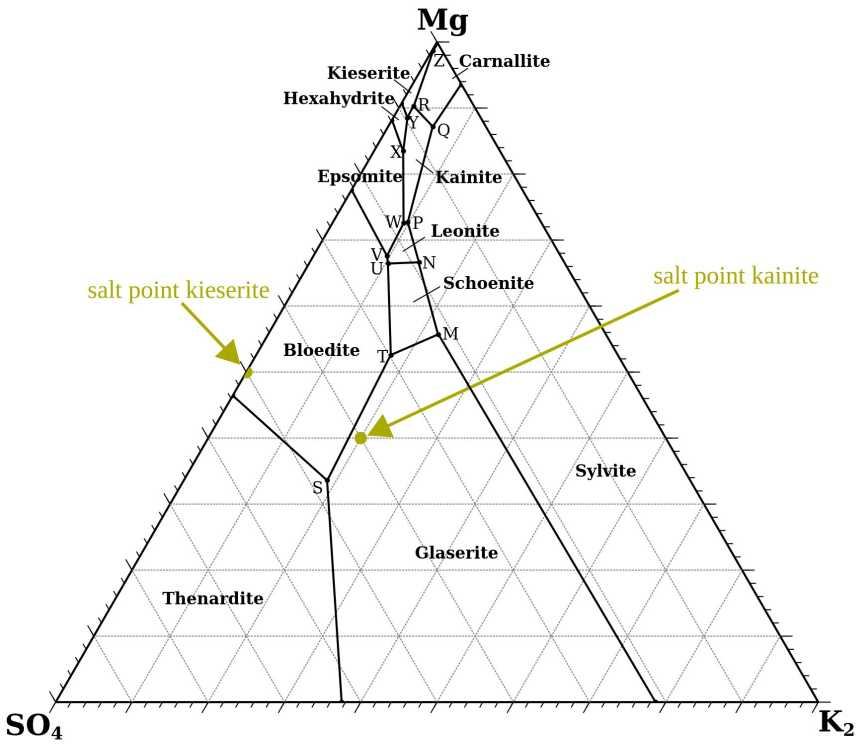

Figure 2.1: Jänecke projection for an NaCl-saturated, quinary system Na−K−Mg−Cl−SO_4−H_2O at 22°C; at points S, T, U... the solution is in equilibrium with all minerals of the adjacent stability fields.

to the salt point of the dissolved rock, which results from the ratio of the ion concentrations in it. For example, the salt point of kieserite ($MgSO_4 \cdot H_2O$) is located at the left border of the Jänecke projection midway between Mg and SO_4 vertex (Figure 2.1). For kieseritic potash salt, the salt point is usually located within the stability field of glaserite or more specifically, within the stability space behind it. Since the calcium concentration is very low in comparison with the other ion concentrations, the reaction path is projected onto the side surface K_2−Mg−SO_4 for purposes of illustration. However, calcium containing minerals are considered in the calculations as well as the absolute concentrations and saturations. Table 2.1 shows with which minerals the solution is in equilibrium at the points mentioned in the following. The chemical composition of every mineral can be taken from Table 2.2.

The models themselves were designed as so-called titration models, where potash salt is gradually added to a saturated NaCl solution. This corresponds to the situation in a mine, because the influent solution has to pass through rock salt layers before reaching the potash seams. At the beginning, the model contains 1 kg of water and 6 mol of dissolved NaCl. At every step, 1 mol of potash salt is added to the solution. Assuming that thermodynamic equilibrium is archieved, the progressive evolution of the solution composition can be quantified. The temperature is set at 22°C, which is in accordance with the natural conditions in the mine in the area of brine occurrence.

Table 2.1: Invariant points and their adjacent stability spaces in the hexary system Na–K–Mg–Cl–SO_4–Ca–H_2O at 22°C.

Point	Minerals the solution is in equilibrium with (besides halite)
M	glaserite, schoenite, sylvite, polyhalite
N	leonite, schoenite, sylvite, polyhalite
P	kainite, leonite, sylvite, polyhalite
Q	carnallite, kainite, sylvite, polyhalite
R	carnallite, kainite, kieserite, polyhalite
T	glaserite, schoenite, bloedite, polyhalite
U	leonite, schoenite, bloedite, polyhalite
V	epsomite, leonite, bloedite, polyhalite
W	epsomite, kainite, leonite, polyhalite
X	hexahydrite, kainite, epsomite, polyhalite
Y	hexahydrite, kainite, kieserite, polyhalite

Table 2.2: Salt minerals taken into account.

Mineral	Molecular formula	Mineral	Molecular formula
Anhydrite	$CaSO_4$	Kainite	$K_4Mg_4Cl_4[SO_4]_4 \cdot 11\,H_2O$
Bloedite	$Na_2Mg[SO_4]_2 \cdot 4\,H_2O$	Kieserite	$MgSO_4 \cdot H_2O$
Carnallite	$KMgCl_3 \cdot 6\,H_2O$	Langbeinite	$K_2Mg_2[SO_4]_3$
Epsomite	$MgSO_4 \cdot 7\,H_2O$	Leonite	$K_2Mg[SO_4]_2 \cdot 4\,H_2O$
Glaserite	$K_6Na_2[SO_4]_4$	Polyhalite	$K_2MgCa_2[SO_4]_4 \cdot 2\,H_2O$
Glauberite	$Na_2Ca[SO_4]_2$	Schoenite	$K_2Mg[SO_4]_2 \cdot 6\,H_2O$
Gypsum	$CaSO_4 \cdot 2\,H_2O$	Sylvite	KCl
Halite	NaCl	Syngenite	$K_2Ca[SO_4]_2 \cdot H_2O$
Hexahydrite	$MgSO_4 \cdot 6\,H_2O$	Thenardite	$Na_2[SO_4]$

The aim is to determine which precipitates are formed upon the contact of potash salt and NaCl solution, which amount of rock is affected and under which conditions the dissolution process stops. The composition of the solution and the surrounding rock are assumed to be spatially homogeneous. Therefore, this titration model applies only to closed systems where a limited amount of NaCl solution is in contact with potash salt over a longer period of time.

However, especially in the vicinity of geological fault zones, open systems with regular brine exchange may occur. This is particularly the case in layers located close to the edges of salt deposits. The 1D model used in this study shows which interactions occur if a NaCl-saturated solution flows through a potash seam. In particular, the changing solution composition as well as precipitations along the flow path are considered. The 1D model consists of several successively arranged cells which initially contain the same amount of NaCl solution (Figure 2.2). Based on the titration model, 1 mol of potash salt is added to each cell and the dissolutions and precipitations are calculated assuming thermodynamic equilibrium. Subsequently, the solution is moved one cell to the right, while from the left a 6-molar NaCl solution flows into the first cell. Solid minerals remain in their cells. Thereafter, 1 mol of potash salt is added to each cell, the solution is moved one cell to the right and so forth. In this way, the evolution

of the rock and solution composition along a flow path within the potash seam can be modeled. The 1D model is dimensionless in both, space and time. To be able to interpret the model on a temporal scale, the amount of NaCl solution per cell is varied between 0.01 and 1 kg. This allows different ratios between the amount of solution and rock to be simulated, which corresponds to different exchange rates.

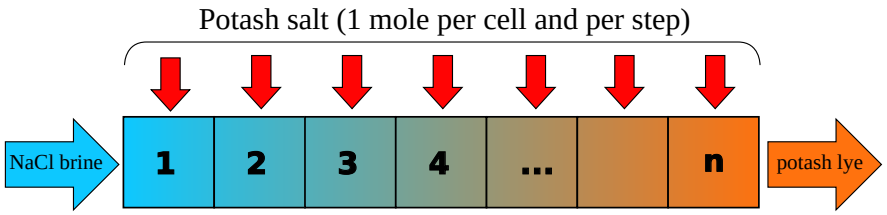

Figure 2.2: Schematic diagram of the 1D model for an open system.

2.3 Model Validation

Titration models have already been used by Herbert (2000) in order to model the evolution of the solution composition during the solution process of potash salt. The comparison of the model results with 6-year readings from the flooded Hope mine showed a very good agreement in the front part of the reaction path. Solution composition, precipitations, amount of water, and activity of the individual components have been described precisely (Herbert 2000) and the solution compositions in mines that were flooded long time ago indicate that the predicted reaction pathways are also reliable for longer periods of time (Bohn 2014). For example, the entire calculated reaction pathway for carnallitite was experimentally detected in an in-situ large-scale test at the Asse mine (Herbert 2000) and was also confirmed in laboratory experiments (Bach 2010).

Herbert (2000) used the program code EQ3/6 and the database of Harvie et al. (1984) in order to model the dissolution process of potash salt at 25°C. On the webpage of the THEREDA project, a link is provided to research results from TU Bergakademie Freiberg, where a comparison is made between the THEREDA database and the database of Harvie et al. (1984). Obviously, the two databases show only minor differences. However, in order to verify that the solution process can also be simulated by using PHREEQC (Parkhurst and Appelo 2013) and the THEREDA database (Altmaier et al. 2011), the titration model was used to determine the reaction path for the potash salt in Hope. It is a sylvinitic hard salt with 61.4% halite, 31.7% sylvite, 3.4% kieserite and 1.7% anhydrite (% by mass). The results agree very well with those of Herbert (2000). Therefore, we conclude that the titration model is suitable both fundamentally and specifically with the data set chosen here to quantify the dissolution behavior of potash seams at 22°C.

2.4 Application to a Natural Brine Occurrence

2.4.1 Analysis of Rock and Brine Samples from the Field

The potash seams considered in this study belong to the Zechstein formation in Germany and mainly consist of kieseritic potash rocks (hardsalt). However, the exact composition within the seams varies considerably. Analyses show kieserite contents between 3.5% and 43%. In the area of the brine occurrence, the potash seams 'Hessen' and 'Thüringen' can be found (Figure 2.4), which consist mainly of halite, kieserite and sylvite. The minor constituents carnallite and anhydrite or polyhalite, as well as insoluble constituents (e.g. clay), make up just under 5% of the potash seams. Furthermore, small amounts of kainite or langbeinite can be found.

The type and amount of the individual components have a strong influence on the dissolution behavior of a potash salt (Herbert and Schwandt 2007). For this reason, the reaction paths for different potash salt compositions were examined and compared to each other. Exemplarily, a kieserite-rich potash salt from the potash seam 'Hessen' and a kieserite-poor potash salt from the potash seam 'Thüringen' are considered in this paper (Figure 2.3). Minor components kainite and langbeinite are neglected.

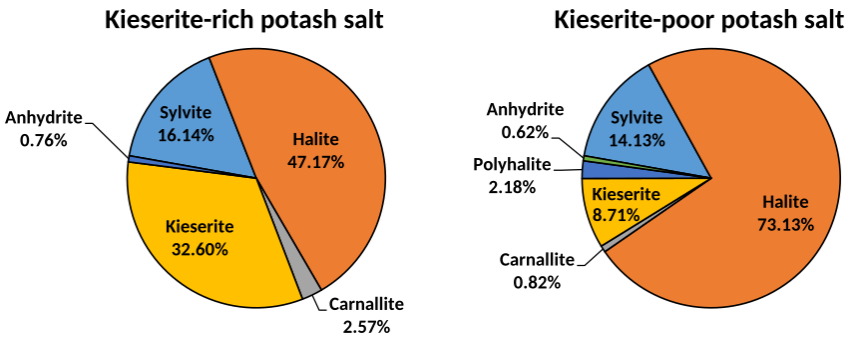

Figure 2.3: Composition of the considered potash salts without neglected minor components (% by mass).

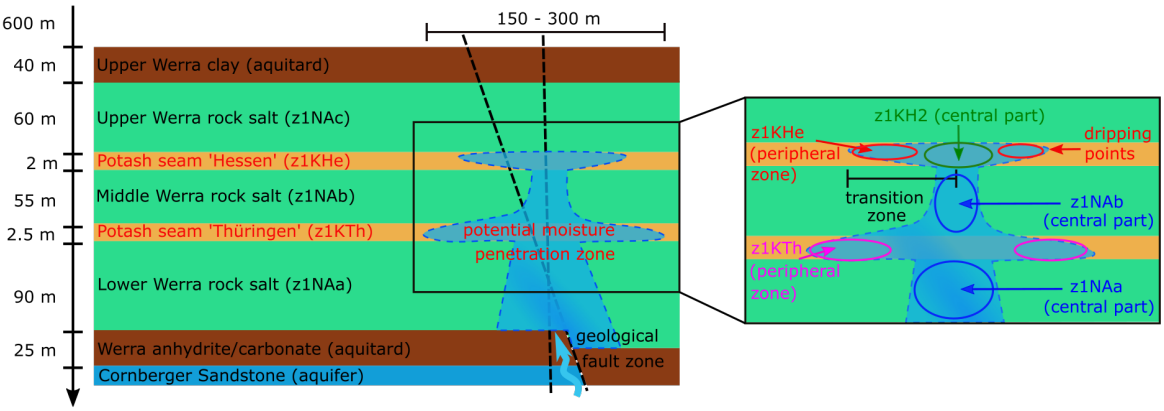

Figure 2.4: Geological context of the potash seams and (simplified) geometry of the cavernous structure (left) and sampling locations relative to the brine occurrence (right).

The brine occurrence exemplarily examined in this study has been continuously monitored and sampled for more than 60 years. It was most likely formed by leakage of the hydrological barrier in the footwall due to multiple, crosscutting fault systems underneath the salt formation (Höntzsch and Zeibig 2014) (Figure 2.4). However, the exact geometry of the cavernous structure is not known. The relative position of a sampling point can therefore only be estimated on the basis of the amount of brine solution occurring. Areas, where large amounts of brine (several liters per minute over a long period of time) where encountered, are therefore called 'central part' of the brine occurrence. On the other hand, areas with only gas or small amounts of brine (<1 l per minute) are called 'peripheral zone' (Figure 2.4).

The composition of some selected brine samples is shown in Figure 2.5; their labels provide information on location and date of sampling. First analyses originate from individual dripping points at the level of the potash seam 'Hessen' (z1KHe). From 1957 to July 1977, average compositions of brine solutions found in boreholes into the central part of the brine occurrence (z1KHe) are available. Subsequently, the inflow rate of brine solution increased while the density decreased. At the same time, there were strong fluctuations in the composition of the brine from the central part of the cavern. During further exploration work, brine solutions were also found in deeper layers like the potash seam 'Thüringen' (z1KTh), the Middle (z1NAb) and the Lower (z1NAa) Werra rock salt (Figure 2.4). It is assumed that they belong to the same reservoir as the brine occurences found in potash seam 'Hessen'. In August 1978, the calcium concentration was determined for the first time. It never exceeds 50 mmol/kgw and in highly concentrated potash solutions it even drops below 1 mmol/kgw. Therefore, no data are available for such samples, but only for NaCl solutions and low-concentrated potash solutions.

Figure 2.6 shows where the solution compositions from Figure 2.5 and some other samples are located within the Jänecke projection (projected onto the side surface $K_2-Mg-SO_4$). In addition, PHREEQC was used to determine their saturation indices (SI). A value equal or less than -0.1 is interpreted as undersaturation, a value equal or greater than 0.1 as supersaturation, which means a potential for corresponding dissolution or precipitation reactions (Monnin and Ramboz 1996). If the value is between those two, it is assumed that the solution is in equilibrium in regard to the particular mineral. The saturations were determined for the respective outflow temperature; the fluctuation range is 20 to 26°C.

Red and magenta indicate samples from dripping points and boreholes, where only small amounts of brine solution appeared (Figure 2.4). They were taken at various locations in the vicinity of the brine occurrence. The 1957 sample is in equilibrium with epsomite and hexahydrite, while kieserite is marginally undersaturated (SI = -0.12). Noticeable is its undersaturation on halite (SI = -0.88), which occurs only in three other cases. Samples from the dripping points 1960 and 1961 show supersaturations of carnallite (SI $\leq$ 0.28) and kainite (SI $\leq$ 1.06); additionally, the first one is in equilibrium with

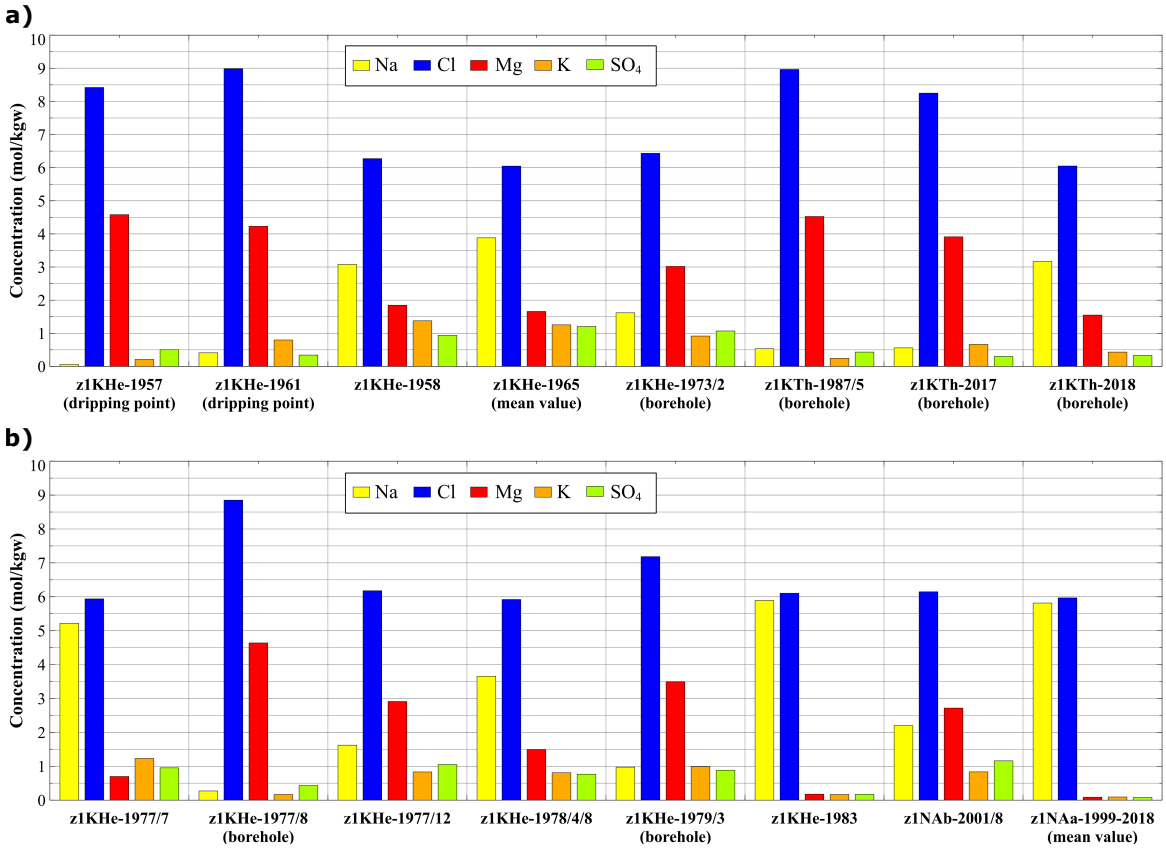

Figure 2.5: Composition of selected brine solution samples a) from the potash seam 'Hessen' (z1KHe) before 1977 and exploration drill holes in the potash seam 'Thüringen' (z1KTh) and b) from the potash seam 'Hessen' after July 1977 and from the Middle (z1NAb) and Lower (z1NAa) Werra rock salt (labeling: [layer]-[year/month/day] of sampling).

sylvite and kieserite, while the second one is supersaturated with sylvite (SI = 0.18). Thus, the samples are located in the immediate vicinity of the points Y, R and Q. The samples from potash seam 'Thüringen' (magenta) plot close to those invariant points as well, but their supersaturations are substantially lower. While the 1987 samples are in equilibrium with kainite, hexahydrite and either epsomite or carnallite and kieserite, the 2017 sample from another borehole is saturated exclusively with sylvite (besides halite). Although the 2018 sample has an ion concentration ratio near point P, the absolute values show an equilibrium only with halite and anhydrite. The sample from February 1973 (potash seam 'Hessen') is located at point U and is (nearly) saturated with halite, schoenite, bloedite, leonite and epsomite ($-0.05 \leq SI \leq 0.01$) as well as hexahydrite (SI = -0.09). Except for the 2018 sample ($1.23\,g/cm^3$), all brine solutions from the peripheral zone have a density of 1.29 to $1.31\,g/cm^3$. This is in a typical range for highly saturated potash solutions.

In green, samples from the central part of the cavernous structure are shown, where larger amounts of brine solution were encountered. From 1958 to 1975, the brine compositions are located in the vicinity of point T, whereby they are saturated with respect to halite, bloedite and/or schoenite and sometimes leonite. In almost all cases, glaserite is supersaturated (SI = 0.1 to 0.31). During this time span, the density is

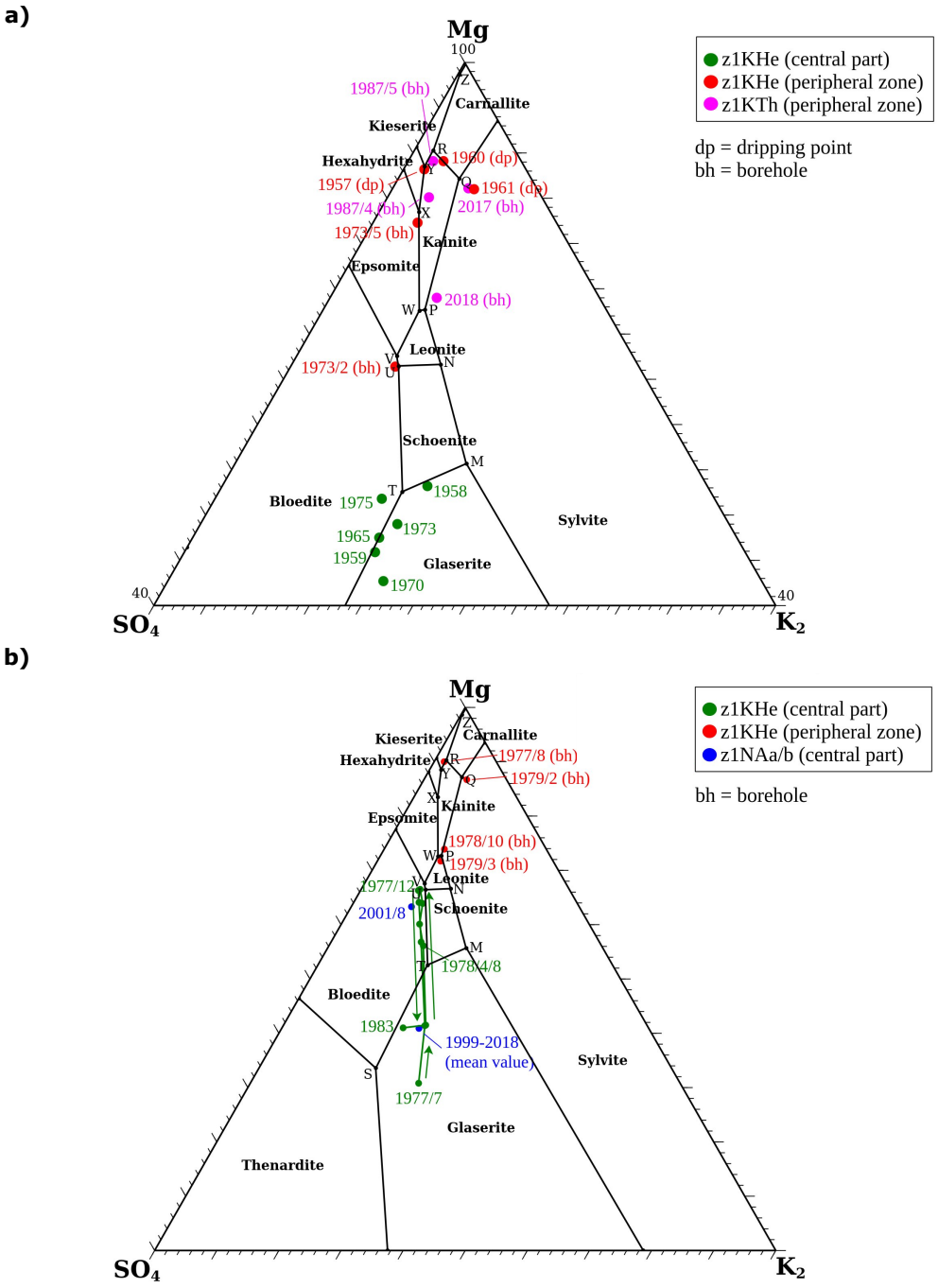

Figure 2.6: Composition of the samples from a) Figure 2.5a (zoomed) and b) Figure 2.5b with additional data in the Jänecke projection (labeling: date [year/month/day] of sampling).

between 1.28 and 1.3 g/cm^3. In July 1977, the inflow rate increases sharply and the density drops below 1.27 g/cm^3. The brine solution is now saturated only with halite and glaserite. In the following months, the density increases again to 1.29 g/cm^3. As Figure 2.6b shows, in December 1977 the concentration of Mg^{2+} reaches its peak and the solution is in equilibrium with epsomite. Halite, bloedite, schoenite, leonite and hexahydrite are now slightly undersaturated (-0.16 $\leq$ SI $\leq$ -0.11). This corresponds to a composition near point V. In April 1978, the Mg^{2+} concentration drops significantly, leaving only an equilibrium with halite. While the composition of the brine solution in

the center of the cavernous structure shows great fluctuations during this time, samples from the peripheral area prove that highly saturated potash solutions are still present there (Figure 2.6b, red).

Since 1989, the brine solution has been extracted from a borehole below both potash seams. Since then, only one time in 2001 the density increased again to $1.3\,\mathrm{g/cm^3}$ and (super-) saturations with respect to schoenite and bloedite (SI = 0.14) occurred. Otherwise, the density has since been about $1.21\,\mathrm{g/cm^3}$, which corresponds to a NaCl-saturated brine solution. The average composition of 1999-2018 shows that during this period, only halite was in geochemical equilibrium with the solution. In addition, the brine solution was almost always in equilibrium with anhydrite and/or gypsum or, respectively, had slight supersaturations (SI $\leq$ 0.3) with respect to these minerals.

Overall, most of the samples from a natural brine occurrence showed either no or only slight supersaturations. However, a comparison of the saturations for 20°C and 25°C has shown that even small temperature deviations can significantly affect the saturation index. The difference is particularly large in cases of glaserite and kainite ($0 \leq \Delta SI \leq 0.3$). For bloedite and leonite, ΔSI was up to 0.13, for carnallite and epsomite up to 0.11. Therefore, slight super- or undersaturations should not be given too much importance, the absolute values of the ion concentrations are decisive.

2.4.2 Results of the Closed Titration Model

Figure 2.7 shows the chemical evolution of a saturated NaCl solution if potash salt is gradually added. The first two are the potash salts in Figure 2.3 and the third one is an hypothetical salt consisting of 30% of both sylvite and kieserite, 39% of halite and 0.5% of both carnallite and anhydrite (all mole-%). The ion concentrations were projected onto the side surface $K_2-Mg-SO_4$.

The results show that salt point and reaction path differ significantly, depending on the ratio between kieserite and sylvite. If the potash salt contains more kieserite than sylvite, the salt point is located near the stability field of bloedite and the reaction path leads along the points T, U, V, W, X and Y to the point R, where halite, kieserite, carnallite, kainite and polyhalite are in equilibrium with the brine solution. If, on the other hand, the kieserite content is lower than the sylvite content, the salt point shifts in the direction of the stability field of sylvite and the reaction path leads along the points M, N and P to point Q, where the brine solution is in equilibrium with halite, sylvite, carnallite, kainite and polyhalite. The decisive factor here is the molar proportion of kieserite and sylvite. Accordingly, from now on, all potash salts with a higher molar fraction of kieserite than sylvite will be referred to as kieserite-rich and the others as kieserite-poor.

In the case that kieserite and sylvite have almost the same molar fraction, a third reaction path can occur. It progresses from the salt point via point T first through the stability fields of schoenite and possibly leonite to point N or P and from there to point Q (Figure 2.7c). For this to happen, the potash salt has to contain a little more

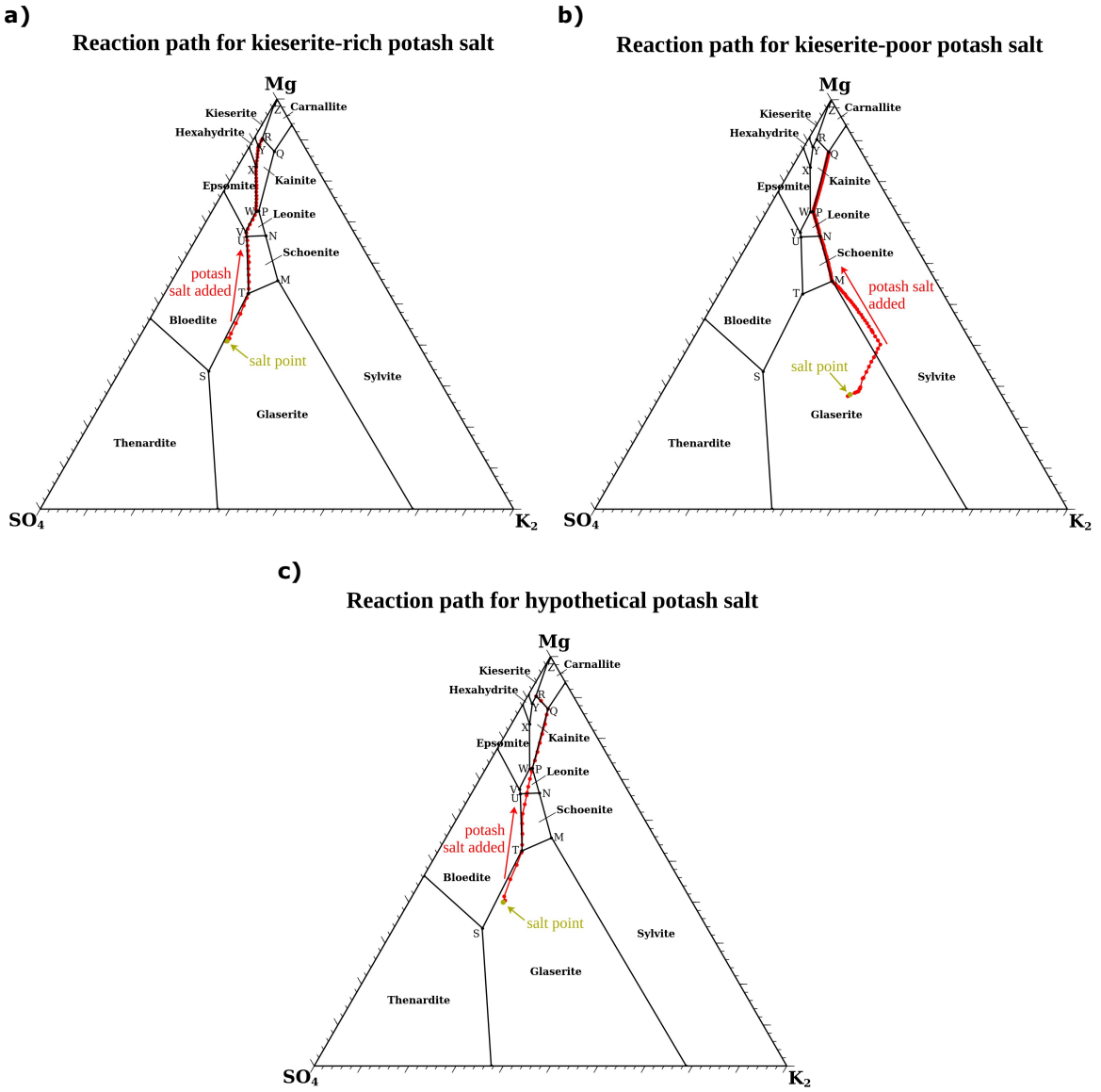

Figure 2.7: Chemical evolution of a NaCl-saturated brine solution if potash salt with three different ratios of kieserite and sylvite is added.

sylvite than kieserite or else carnallite as a minor constituent. In addition, if anhydrite is contained or if the kieserite content in the presence of carnallite is slightly higher than the sylvite content, the reaction path finally moves from point Q to point R. The precipitations at the beginning are glaserite, bloedite, schoenite and leonite, later kainite and carnallite. Because this case hardly occurs, it will not be considered here. In principle, it should be noted that the transition point between the reaction pathways in Figures 2.7a and 2.7b also depends on the anhydrite and carnallite content. However, since both occur only as minor components, the influence is usually negligible.

The ratio between kieserite and sylvite is also affecting the ion concentrations and in particular the precipitations. While glaserite, schoenite, leonite, kainite and polyhalite always occur as conversion products, bloedite, epsomite and hexahydrite precipitate only if kieserite-rich potash salts are dissolved (Figure 2.8b). The re-dissolution of some

of these conversion products regularly results in periods of constant concentrations. For example, at point W all the leonite must first be re-dissolved before the reaction path can leave the point and proceed to point X (Figure 2.8a,b). During such periods, significant amounts of potash salt are converted without a change in brine composition.

Even at point Q or R, the solution process of the potash salt does not come to an end since there is still no equilibrium reached between all mineral components and the brine. A look at the Jänecke projection shows that this is just not possible (at 22°C) for potash salts containing sylvite as well as kieserite. Instead, both components are converted to kainite until one of them is no longer available or there is no water left. Since in the titration model steadily potash salt is provided, the solution process only stops when the water is fully consumed due to the fact that the conversion products kainite and polyhalite contain more water than the dissolved minerals (Figure 2.8a). The amount of converted minerals is always similar and corresponds to about 4.3 kg of kieserite, 2.3 kg of sylvite, 0.3 kg of carnallite and 0.2 kg of anhydrite (per kg of water):

Reaction equation for kieserite-rich potash salt:

$$\underset{\text{2.34 kg sylvite}}{31.4\,KCl} + \underset{\text{4.73 kg kieserite}}{34.2\,MgSO_4 \cdot H_2O} + \underset{\text{6.85 kg halite}}{117.2\,NaCl} + \underset{\text{0.375 kg carnallite}}{1.35\,KMgCl_3 \cdot 6\,H_2O} + \underset{\text{0.111 kg anhydrite}}{0.81\,CaSO_4} +$$

$$\underset{\text{1 kg 6-molal NaCl solution}}{55.5\,H_2O + 6\,Na^+ + 6\,Cl^-} \longrightarrow \underset{\text{7.39 kg kainite}}{7.56\,K_4Mg_4Cl_4[SO_4]_4 \cdot 11\,H_2O} + \underset{\text{0.482 kg carnallite}}{1.73\,KMgCl_3 \cdot 6\,H_2O} +$$

$$\underset{\text{7.20 kg halite}}{123.2\,NaCl} + \underset{\text{0.44 kg kieserite}}{3.16\,MgSO_4 \cdot H_2O} + \underset{\text{0.245 kg polyhalite}}{0.41\,K_2MgCa_2[SO_4]_4 \cdot 2\,H_2O}$$

Reaction equation for kieserite-poor potash salt:

$$\underset{\text{6.77 kg sylvite}}{90.8\,KCl} + \underset{\text{4.17 kg kieserite}}{30.1\,MgSO_4 \cdot H_2O} + \underset{\text{35.05 kg halite}}{599.7\,NaCl} + \underset{\text{0.383 kg carnallite}}{1.38\,KMgCl_3 \cdot 6\,H_2O} + \underset{\text{0.297 kg anhydrite}}{2.18\,CaSO_4} +$$

$$\underset{\text{1.05 kg polyhalite}}{1.74\,K_2MgCa_2[SO_4]_4 \cdot 2\,H_2O} + \underset{\text{1 kg 6-molal NaCl solution}}{55.5\,H_2O + 6\,Na^+ + 6\,Cl^-} \longrightarrow$$

$$\underset{\text{6.83 kg kainite}}{6.99\,K_4Mg_4Cl_4[SO_4]_4 \cdot 11\,H_2O} + \underset{\text{0.684 kg carnallite}}{2.46\,KMgCl_3 \cdot 6\,H_2O} + \underset{\text{35.4 kg halite}}{605.7\,NaCl} + \underset{\text{4.44 kg sylvite}}{59.6\,KCl} +$$

$$\underset{\text{1.71 kg polyhalite}}{2.83\,K_2MgCa_2[SO_4]_4 \cdot 2\,H_2O}$$

The amount of potash salt that is required until the reaction stops differs: in case of the kieserite-rich potash salt, 14.5 kg are necessary, while in case of the kieserite-poor potash salt, it is 48 kg. This is due to the fact that they contain different amounts of the limiting component – for kieserite-rich potash salts this is sylvite, for kieserite-poor potash salts it is kieserite. This component is always completely dissolved, while the others are only partially dissolved. For example, the halite remains almost completely unaffected. If the limiting component makes up a smaller part of the rock, a larger total mass of potash rocks must take part in the reactions to allow the reaction path move forward. Accordingly, a larger rock mass is affected by the dissolution process. It also has an influence on the structure of the remaining rock: while 48.5% by mass of

a)

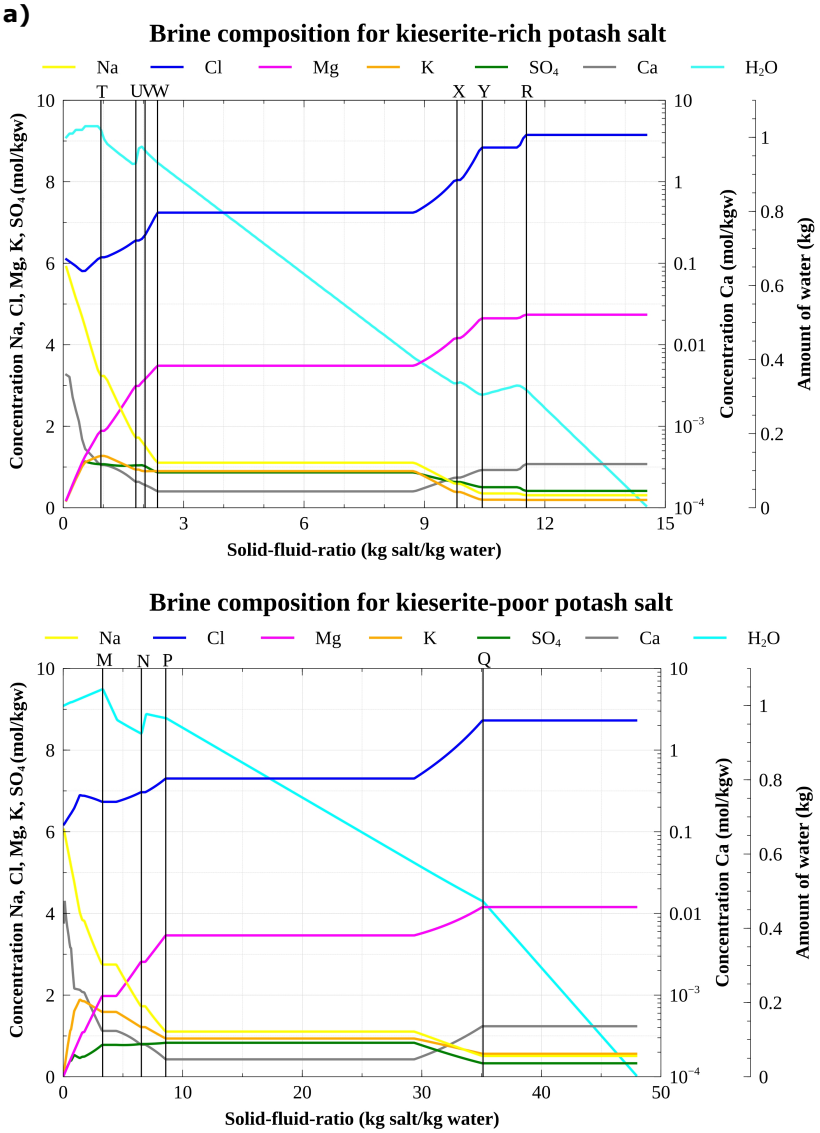
Brine composition for kieserite-rich potash salt
Na
Cl
Mg
K
SO4
Ca
H2O
T
UVW
X
Y
R
Concentration Na, Cl, Mg, K, SO4 (mol/kgw)
Concentration Ca (mol/kgw)
Amount of water (kg)
Solid-fluid-ratio (kg salt/kg water)
Brine composition for kieserite-poor potash salt
M
N
P
Q

b)

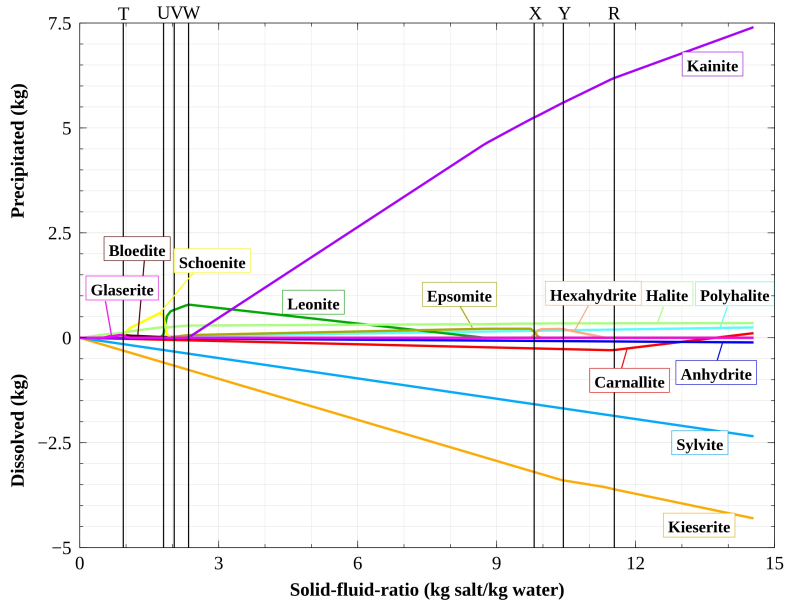
Precipitated and dissolved minerals for kieserite-rich potash salt
T
UVW
X
Y
R
Precipitated (kg)
Dissolved (kg)
Solid-fluid-ratio (kg salt/kg water)
Kainite
Bloedite
Schoenite
Glaserite
Leonite
Epsomite
Hexahydrite
Halite
Polyhalite
Carnallite
Anhydrite
Sylvite
Kieserite

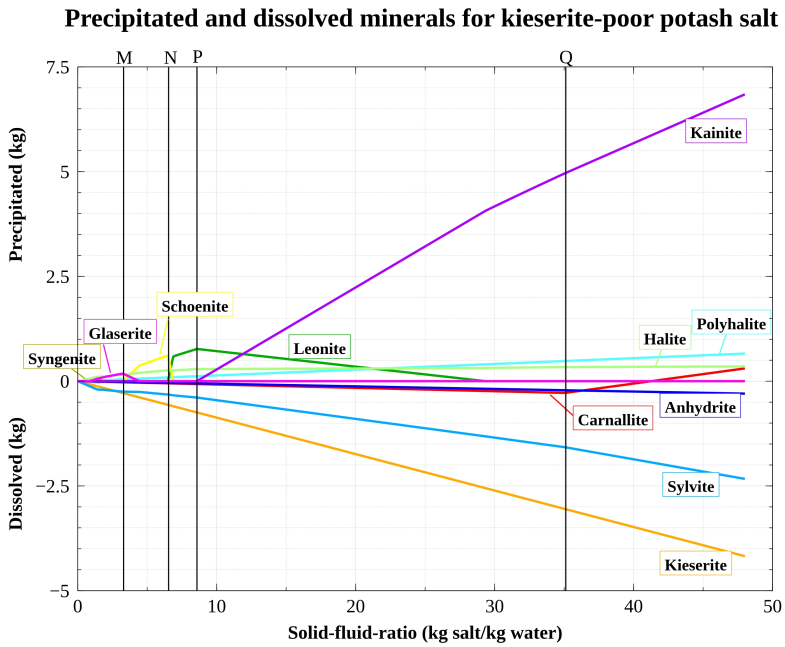

Figure 2.8: Comparison of the a) brine compositions and b) precipitations over the reaction path for kieserite-rich and kieserite-poor potash salt.

the kieserite-rich potash salt dissolve and recrystallize as secondary minerals, in case of the kieserite-poor potash salt, it is only 14.8%.

Assuming thermodynamic equilibrium, anhydrite is completely dissolved as well. The more anhydrite is contained in the salt rock in relation to kieserite or sylvite, respectively, the more polyhalite is precipitated. This, in turn, binds water and other ions, significantly changing the composition of the precipitated minerals compared to a Ca-free system. For example, less kainite is precipitated, instead various Ca-containing salts occur. Point Q or R is already reached with much lower solid-fluid-ratios, whereby more carnallite is precipitated. In addition, more water is consumed, which means that up to 25% less rock mass is affected by the dissolution process. Therefore, anhydrite must always be considered as a minor component. Another important minor component is carnallite as it significantly influences the reaction path. Calculations have shown that without carnallite, the solution composition would remain at point W or P instead of wandering to point R or Q, respectively. On the other hand, small amounts ($\ll$1%) of langbeinite and kainite can be neglected without falsifying the results.

2.4.3 Results of the Open 1D Model

The dimensionless titration model represents a closed system, where no in- or outflow takes place. By contrast, the 1D model allows for different exchange rates and determines the resulting brine solution and rock composition along a flow path. The latter is shown in Figure 2.9 after five times of flow through the system. In the case of the kieserite-rich potash salt, with each step 0.5 kg of water (plus NaCl) flow in from the left; in case of the kieserite-poor potash salt, it is 0.1 kg.

In the case of the kieserite-rich potash salt, the first cells contain mainly halite, glaserite and bloedite as well as small amounts of polyhalite. In the posterior cells, the reaction path has progressed further, so that first schoenite, then leonite, kainite and in the last cells possibly also epsomite and hexahydrite are formed (Figure 2.9a). Sylvite, kieserite, carnallite and anhydrite have been completely dissolved. In the case of the kieserite-poor potash salt, the same exchange rate would only cover the first part of the reaction path; therefore, the rock composition was calculated for an inflow of 0.1 kg of water (plus NaCl) per step (Figure 2.9b). The mineralogy is different as well: sylvite is not completely dissolved and instead of glauberite, syngenite is the first Ca-containing precipitate. In relation to the other minerals, polyhalite accounts for a significantly higher proportion.

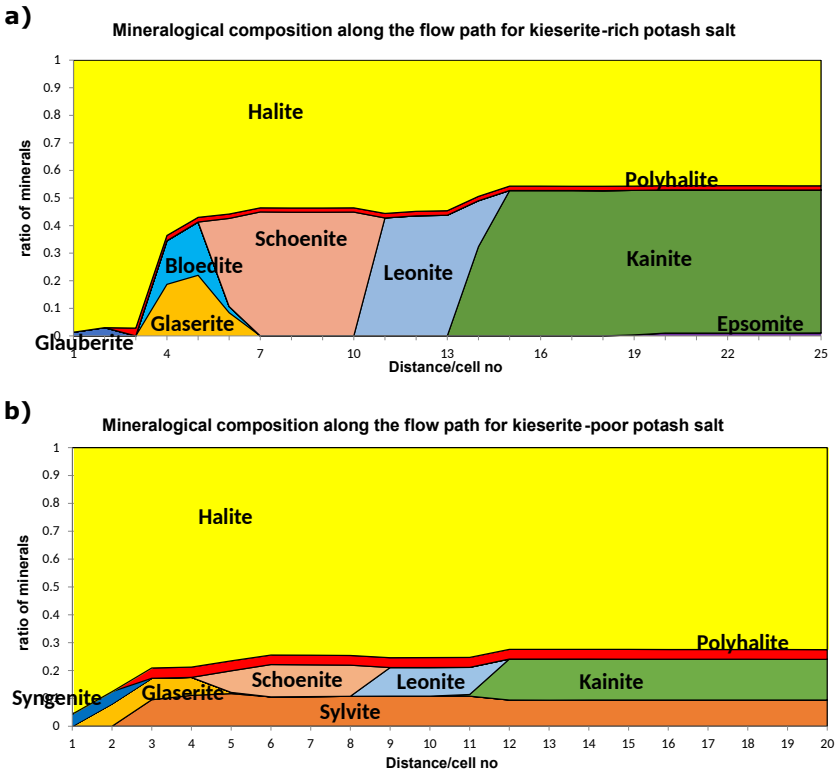

Figure 2.9: Composition of the transition zone after five flow throughs for a) kieserite-rich and b) kieserite-poor potash salt.

The results show that the reaction path calculated with the titration model basically transfers to the spatial level along the cells. The higher the exchange rate, the more cells or larger amounts of potash salt are required to cover the entire titration path. The same applies if a smaller amount of the limiting component, kieserite or sylvite, is contained in the potash salt. This is due to the fact that an increase in exchange rate results in a decrease of the solid-fluid-ratio. However, the reaction paths from the titration model can not be linearly transferred to the 1D model. The evolution along the flow path is more fluent and no periods of constant concentrations occur anymore (Figure 2.10b), because conversion products such as glaserite or schoenite do not have to be re-dissolved for the reaction path to move on. Instead, they now occur

consecutively within zones which show different states of thermodynamic equilibrium. It is important to notice that points such as U or V are not matched by the brine composition anymore because e.g. schoenite, bloedite and leonite do not occur in the same cell (Figure 2.9a). Therefore, the reaction path along the transition zone slightly differs from that in the titration model (Figure 2.10a).

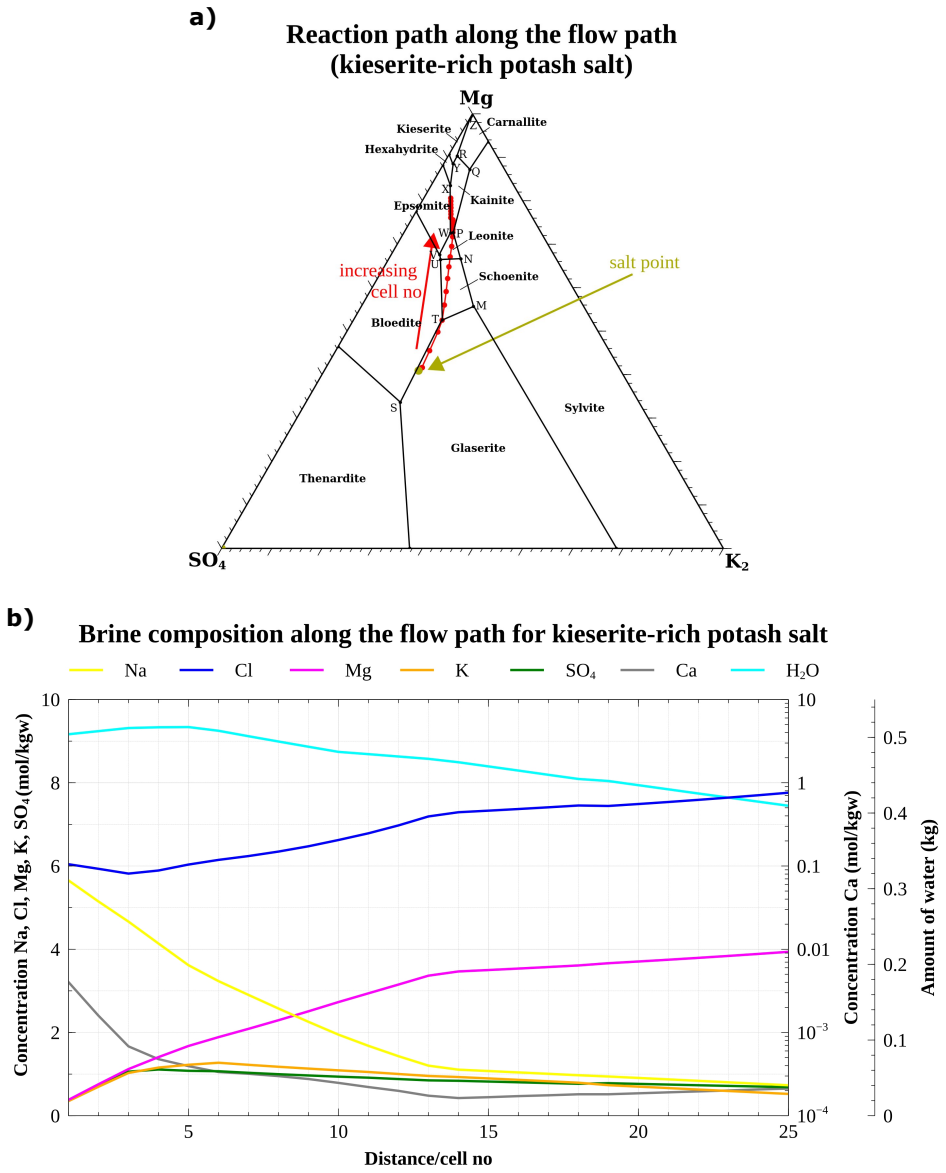

Figure 2.10: a) Flow path and b) brine composition along the transition zone after five flow throughs.

The volume analyses show that at the beginning of the flow path, the volume of the dissolved minerals is always higher than that of the precipitated ones (Figure 2.11). However, if a certain point of the reaction path is reached and water-rich components, such as schoenite, leonite and later kainite, are precipitated, the volume balance of a cell becomes negative. This means that in this area, a larger volume of salt is precipitated than it was previously dissolved. The reason for this is that the minerals dissolved in the first cells are now precipitated again as secondary minerals. In the process, parts of the existing water are incorporated into the precipitations as water of crystallization.

Thus, the amount of water within the posterior cells decreases, while mass and volume of the precipitated minerals increase.

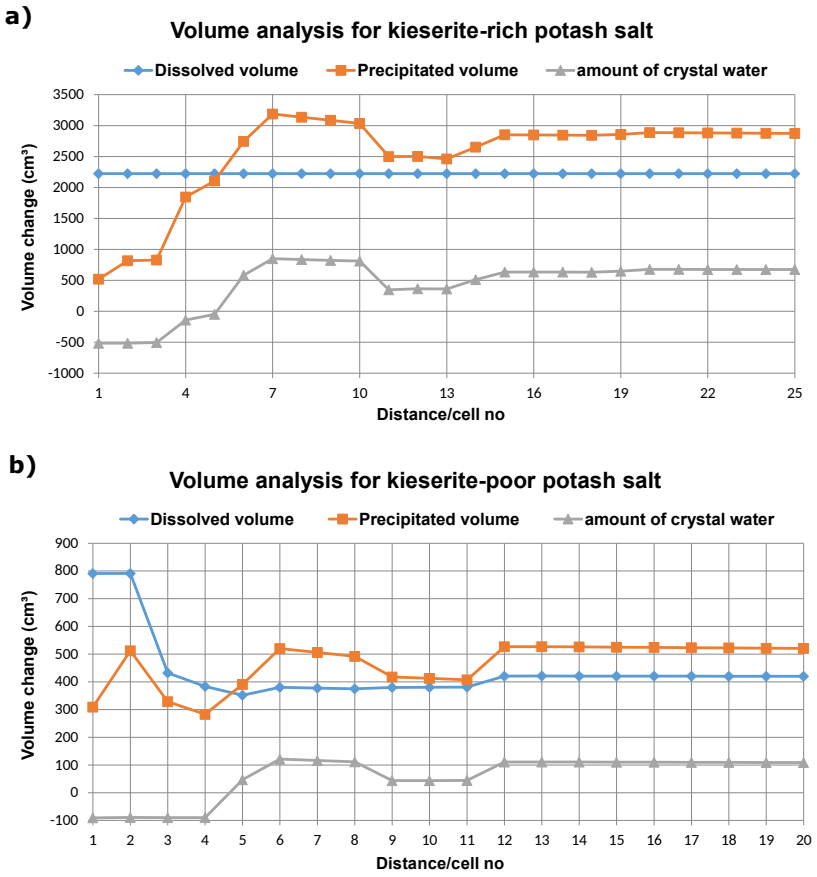

Figure 2.11: Volume balance along the flow path after five flow throughs for a) kieserite-rich and b) kieserite-poor potash salt.

2.5 Comparison between Model Results and Field Data

In the following, the calculated reaction paths from Figure 2.7 are compared with the measured values shown in Figure 2.6. For this purpose, the absolute deviations between the calculated ion concentrations for a closed system (Figure 2.8a) and the measured ion concentrations are determined at each point of the reaction path. Where their sum is the lowest, the measured brine composition is best described by the reaction path. In Figures 2.12 and 2.13, the measured values are entered at the corresponding location of the reaction path which showed a better match with the brine composition. As mentioned in Section 2.4.1, the Ca^{2+} concentration is not available for most of the samples. Therefore, only very few measurements in Figures 2.12 and 2.13 include Ca^{2+} (grey).

Samples from the central part of the cavernous structure within the potash seam 'Hessen' (green) consistently show a better agreement with the reaction pathway for kieserite-rich potash salt. All of these samples are quite far left; the solid-fluid-ratio is only 0 to 2 (Figure 2.12a). Samples taken from 1958 to 1975 show a very high

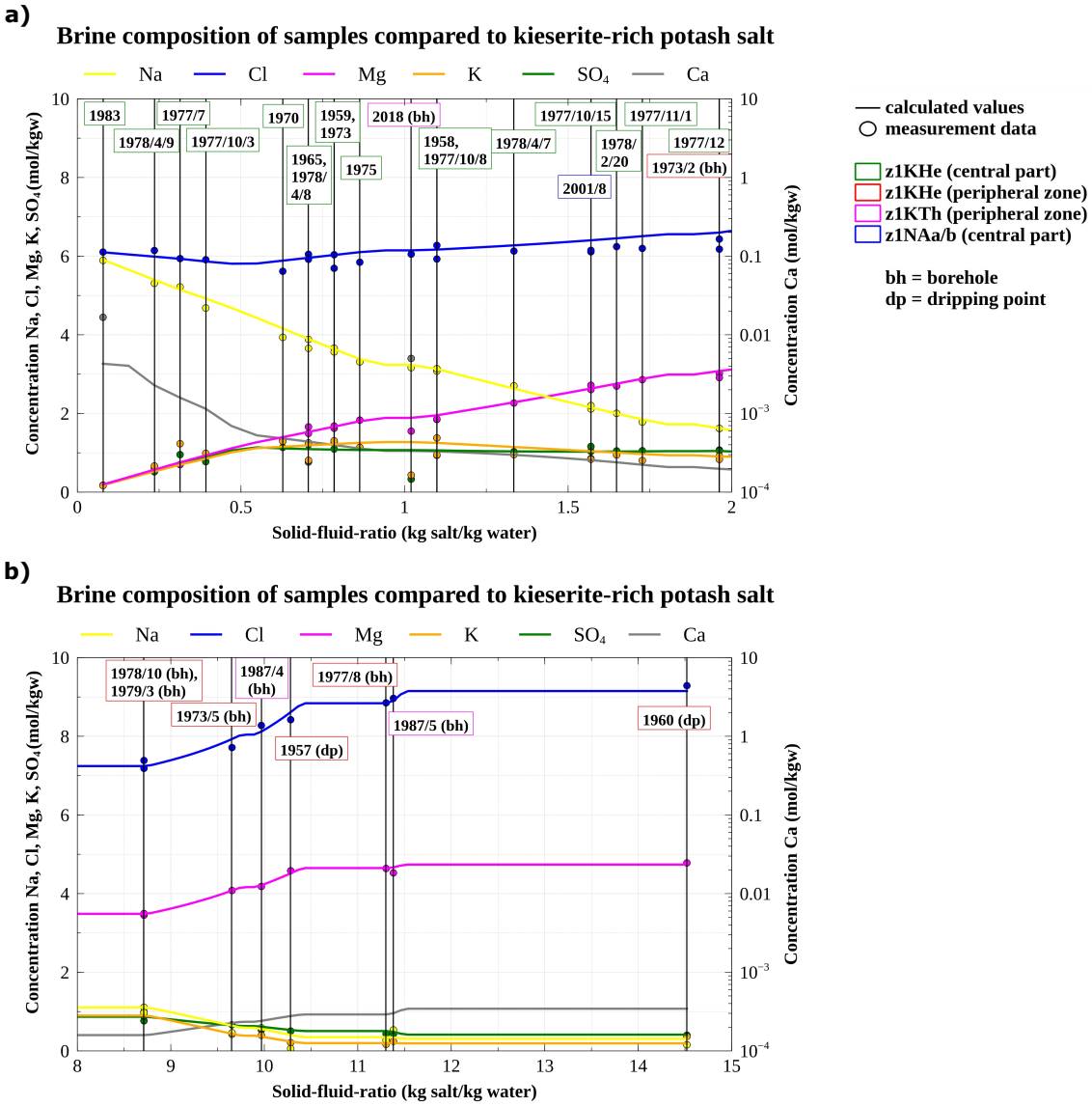

Figure 2.12: Comparison of the measured data with the reaction path for kieserite-rich potash salt at a) small and b) high solid-fluid-ratios (labeling: date [year/month/day] of sampling).

level of agreement with the calculated ion concentrations. The relative deviations are mostly well below 10%; only in four cases does the K^+ or SO_4^{2-} concentration differ by 10-15%. The composition of the brine solution hardly changes during this time, the solid-fluid-ratio for all samples is between 0.6 and 1.1 kg potash salt per kgw. With the increase of the inflow rate in July 1977, the solid-fluid-ratio initially decreases to 0.3 kg/kgw and the deviations of the K^+ and SO_4^{2-} concentrations increase to 25-50%. In the following months, the solid-fluid-ratio increases again to over 1 kg/kgw and the deviations decrease. In December 1977, the solid-fluid-ratio reaches a peak of 1.96 kg/kgw and for the first time, the deviations again fall below 10% for all concentrations. This condition is maintained until April 1978, when the composition of the solution again changes significantly and the solid-fluid-ratio drops to 0.24 kg/kgw within a few days, combined with deviations of up to 50% for K^+ and SO_4^{2-}. In 1983, with 0.08 kg/kgw hardly any potash is contained in the solution. However, apart from

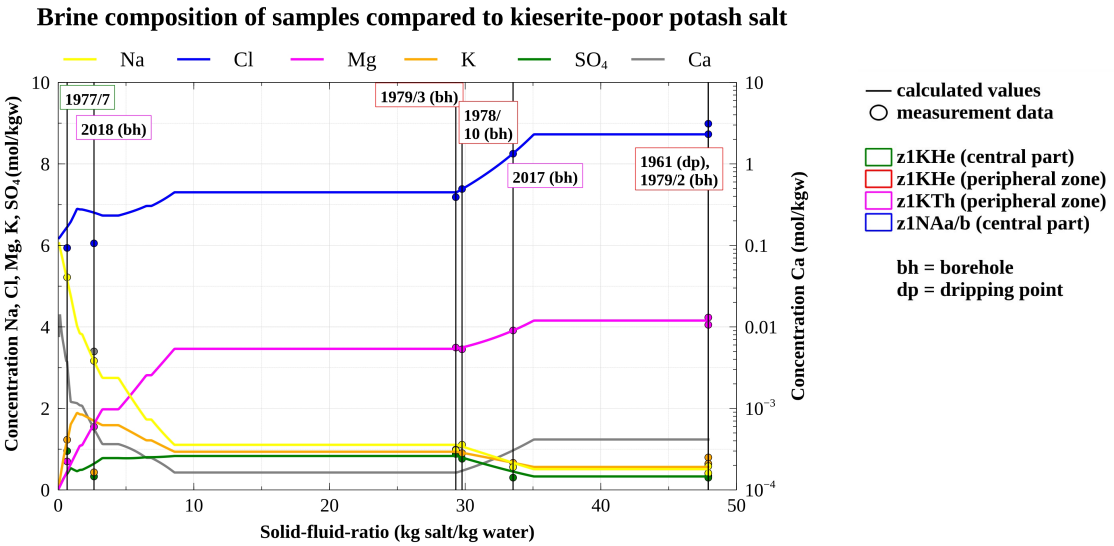

Figure 2.13: Comparison of the measured data with the reaction path for kieserite-poor potash salt (labeling: date [year/month/day] of sampling).

the Ca^{2+} concentration, the composition is in good agreement with the reaction path of kieserite-rich potash salt (maximum 11% deviation).

The increased deviations in 1977/78 in the central part of the cavernous structure are probably due to mixing effects, which can not be reproduced by the model. The inflow rate increased sharply during this period and the system became dynamic: NaCl solution from deeper layers mixed with the potash solution, which had previously been in equilibrium with the surrounding rock, and so the solid-fluid-ratio dropped. On the other hand, the increase in the solid-fluid-ratio in October 1977 indicates a communication of the brine occurrence with other, previously isolated, highly concentrated potash solutions within the potash seam. As a result of these effects, some solution compositions do not match any of the reaction paths during this time (Figure 2.7b). Only in 1983, when NaCl solution has completely displaced the original potash solution and the system is again static, the high agreement with the reaction path for kieserite-rich salt is observed.

However, in the peripheral zone of the cavernous structure, the fluctuations in the inflow rate show little effect. Samples taken from this area within potash seam 'Hessen' (red) originate from dripping points or boreholes and their position on the reaction path lies mostly far to the right (Figures 2.12b and 2.13). They are thus highly saturated potash solutions. In most cases, there is a better agreement with the reaction path for kieserite-rich salt. Only a dripping point in 1961 and a borehole in February 1979 contained a brine solution located at point Q, which suggests a contact with kieserite-poor potash salt. The deviations amount up to 13% (1979/2) and 30% (1961) respectively. Two samples from October 1978 and March 1979 are located close to the points W and P and can thus be assigned to both reaction paths. In both cases, the deviations are low with a maximum of 14%. All other samples from the potash seam 'Hessen' better match the reaction path for kieserite-rich potash

salt. However, the measured Na^+ concentrations are significantly lower (30–600%) than the calculated values, especially at the dripping points. This explains the partial undersaturations with respect to halite. In addition, the K^+ concentration deviates by 13 to 47% in three cases. These concentrations are calculated from the KCl and the NaCl content of the samples, with the latter in particular being very low (3 to 8 g/l) at the dripping points. Accordingly, measurement inaccuracies can cause significant deviations. Since sufficient amounts of halite are available both in rock salt and in the potash salt, undersaturation is unrealistic and the high deviations can probably be attributed to measurement inaccuracies.

The brine solution samples from the level of the potash seam 'Thüringen' (magenta) all stem from the peripheral zone of the cavernous structure. The samples from 1987 were taken from the same borehole with an interval of one week. The conformity with the reaction path for kieserite-rich potash salt is quite high in both cases (maximum 15% deviation in 1987/4 and, respectively, 36% in 1987/5 for Na^+). The second sample is located further down the reaction path, suggesting new solution processes after the first sampling. In 2017 and 2018, two more samples were taken from different boreholes. While that of 2017 with maximum deviations of 19% for Na^+ and 49% for $SO_4{}^{2-}$ is more consistent with the reaction path for kieserite-poor potash salt, that of 2018 does not match either of the two. Especially the K^+ and $SO_4{}^{2-}$ concentrations show 100 to 300% deviation in comparison with both of them. This could be due to various reasons: Besides mixing effects and measurement inaccuracies, inhomogeneities in the rock composition may lead to a lack of consistency.

In 1989, the water level in the center of the cavernous structure was lowered and since then the solution has been extracted from a borehole within the Lower Werra rock salt below the two potash seams. The average composition of 1999-2018 indicates no further contact with potash salt; the solid-fluid-ratio is 0 kg/kgw. Only in 2001 did the water level rise again. The sample from this time (blue) indicates the solution process of a kieserite-rich potash salt. The deviations amount up to 25%.

For all samples, the deviations of the Ca^{2+} concentration are significantly higher than for the other concentrations (up to 93%). As in the case of the Na^+ concentration at the dripping points, this is presumably due to measurement inaccuracies. The measured values for $CaSO_4$, from which the Ca^{2+} concentration is calculated, are at 0 to 3 g/l and therefore even lower than the NaCl contents found there.

Overall, most of the samples are more consistent with the reaction path for kieserite-rich potash salt. Thereby, compositions from the center of the cavernous structure, where larger amounts of brine solution are present, mostly are located at the beginning of the reaction path. In contrast, at the dripping points and boreholes that are located in the peripheral zone and contain only small amounts of brine solution, the reaction path has almost reached its end. Since, until 1977, the brine had enough time to equilibrate to the surrounding rock, it can be concluded that these regions have different mineralogical compositions. Within the transition zone between the center of the cav-

ernous structure and dripping points, secondary minerals such as glaserite, schoenite, leonite, bloedite and kainite were found. Epsomite and hexahydrite were observed as efflorescence on the rock surface near dripping points. This matches the results of the 1D model, after which areas with the above-mentioned minerals arise along flow paths within a potash seam.

2.6 Discussion

The titration model describes the development in a closed system where more and more potash salt in the vicinity of a brine occurrence is converted into secondary minerals. It can be assumed that the precipitations considerably hinder the access to further kieserite and sylvite and possibly even stop the dissolution process. Additionally, Bach (2010) mentions the inclusion of kieserite within carnallite as well as rock pressure and the resulting creep deformation as reasons why the dissolution process in a closed system can come to an end before the existing water is fully consumed. However, the comparison with field data in Section 2.5 proves that the end of a reaction path can indeed be reached. The amount of rock that is affected until then mainly depends on the original composition of the potash seam. Model results show that solid-fluid-ratios of up to 50 kg salt/kg water are necessary to deplete the water entirely.

In contrast to rock salt, where cavities are formed (Gechter et al. 2008), the potash salt is only partly dissolved. Field investigations have shown that this results in a sponge like structure inside the potash seam. Their porosity and permeability are determined on the one hand by the proportion of dissolved minerals, on the other hand by the conversion products formed from them. Laboratory experiments of Bach (2010) have shown that in case of stratified potash salts, some salt beds are completely dissolved so that others may loose stability. However, since the mass balance in a closed system must be zero, the formation of new cavities would only be possible with an increase in rock density. Accordingly, the titration model is incapable of explaining cavitation in potash seams. In order to simulate the progressive growth of the investigated natural cavern system, the model must be at least partially open to enable NaCl-saturated brine to flow in and potash lye to flow out. Furthermore, the titration model assumes all the converted rock to be in equilibrium with the brine and can not explain zones of different mineralogical and brine compositions. Therefore, a 1D model representing an open system was needed to further investigate the development of transition zones between the central part of the cavern and the peripheral zone.

According to the 1D model, the ratio of available salt and water determines the composition of the solution-influenced transition zone. In the close vicinity of geological fault zones, where the solid-fluid-ratio is low, halite is almost exclusively to be found, while along the further flow path within the potash seam more potash salt is dissolved and precipitations occur. The volume analyses show that cavity formation stops as soon as water-rich components, such as schoenite and leonite, are precipitated. However,

as long as the brine solution has access to kieserite and sylvite, the conversion process will continue. Brine and rock samples confirm this: the brine composition in the central part of the cavernous structure, where large amounts of solution are present, corresponds to the calculation results at the beginning of the reaction path. The brine is saturated with respect to halite and anhydrite, possibly glaserite, schoenite and bloedite. Conversely, in peripheral zones, where small amounts of brine face a large amount of unaffected rock, the composition coincides with the results at the end of the reaction path. It is in equilibrium with halite, polyhalite, kainite, carnallite and kieserite or, respectively, sylvite. Thus, the mineralogical composition of the transition zone between a cavernous structure and the unaffected rock can be estimated by using the 1D model. The flow itself is probably density-driven (Anderson and Kirkland 1980) as long as boreholes do not enforce convection.

The good agreement between the measurements and the model results assuming thermodynamic equilibrium shows that kinetic processes do not play a significant role in the system. However, it is not known how long the dissolution process takes. The titration model can only reproduce the temporal evolution of the brine composition in qualitative terms. For example, Bohn (2014) assumes a metastable state to take place at point Q if carnallitite is dissolved. During that state, kainite is supersaturated and it is not known when it precipitates so the composition can move further to point R. Depending on the rates of dissolution and precipitation as well as the size of the system, it may take days, months, or even (thousands of) years to reach thermodynamic equilibrium (Bach 2010; Herbert 2000). Stiller et al. (2016) have shown that the dissolution rates of salt exponentially depend on the saturation index, the ratio of solution volume to surface area and the flow conditions of the brine. The field samples taken here proved that if large amounts of brine are extracted, for some minerals supersaturation occurs. At which exchange rate this effect becomes relevant is not known yet. Another important factor is the temperature; a difference of 5°C can already change the saturation index by up to 0.3.

Spatially, the 1D model can only qualitatively describe the composition of the transition zone. For example, the analyses from dripping points and flooded mines (Herbert 2000; Stadler et al. 2012) show that point Q or R can indeed be reached, although the volume balance seems to contradict this. In order to model this, chemistry and hydraulics need to be coupled so that mass transport and density layering within the cavernous structure can be taken into account. Both of them are known to have substantial effect on the dissolution process (Anderson and Kirkland 1980; Bach 2010). The formation of gas bubbles at the cavity roof (Gechter et al. 2008) and preferential flow paths (Weisbrod et al. 2012) might be important factors as well.

Overall, it has to be conceded that the natural cavernous system considered here is extremely complex. The mineralogy and fault zones are distributed in an inhomogeneous manner, so that no uniform, radial distribution of the cavernous structure can be assumed, but a large number of independent systems, which are only partially

in contact with each other. Whether these are closed or open systems depends on many factors. This includes the pressure conditions, the distance to the next outflow, the extraction volume and the characteristics of the flow paths. Therefore, to model the cavernous structure considered here, 3D models are required which can also take into account inhomogeneities in the rock and include them in the calculation of the dissolution process.

2.7 Conclusions and Outlook

Overall, the titration models of the dissolution processes within potash seams show that the contact with NaCl solution causes different reaction paths depending on the ratio between sylvite and kieserite. Since equilibrium of the brine solution with both components is impossible at 22°C - the ambient temperature of the investigated brine occurrence -, the dissolution process continues until one of the minerals or the water is fully consumed. Transferred to the mine scale, this means that in a solution-filled, cavernous structure with no in- or outflow more and more of the surrounding potash salt is converted over time. As a result, a transition zone with a porous sponge like structure is formed. With increasing saturation of the brine precipitations occur, which seal the previously formed cavities. However, as long as there is still access to unaffected potash salt, the dissolution process continues and the transition zone expands into the surrounding rock. In this regard, the model shows that one liter of NaCl solution can affect several tens of kilograms of salt rock. During this process, precipitations often have to be re-dissolved while, in return, other ones occur. In these periods, the solution composition remains constant, although the dissolution process is still ongoing. This might be an explanation why measurements show an apparent stop of the dissolution process before the calculated final state is reached (Bach 2010). Another explanation is that precipitations block the access to unaffected potash salt.

Formation of new cavities occurs only in open systems. Calculations with a 1D model have shown that near an inflow of NaCl solution only halite remains. Then, along the flow path, precipitations occur, forming zones of different mineralogy. The solution composition along the flow path follows the reaction path. As soon as water-rich compounds, such as schoenite and leonite, are precipitated, cavitation stops. Transferred to the mine scale, this means that in contact with a geological fault zone, a cavernous structure can only form if a minimum exchange rate is guaranteed. In this case, near the fault, where NaCl solution enters, the center of the cavernous structure forms, where all minerals except from halite are dissolved. At a further distance, the exchange rate decreases so that the reaction path can progress further and precipitations occur. In radial direction, a transition zone is formed, of which the temporal and spatial evolution can be qualitatively described using the 1D model. This makes it possible to draw conclusions about the distance to the central part of the cavernous structure based on the rock and solution composition within the vicinity of a brine occurrence. For exam-

ple, if exploratory work reveals kainite, leonite and finally schoenite, this may suggest approaching geological fault zones related to significant contact with saline solution. Thus, it is possible to recognize the risk of brine inflow and to determine the location of cavernous structures without directly drilling into the potential brine occurrence.

For the future, a spatial and temporal scaling of the models is planned. For this purpose, the thickness of real transition zones in the mine is investigated. Furthermore, a consideration in 2D and 3D is striven in order to determine the geometry of the resulting cavernous system. In this context, not only the stratification of the rock has to be considered, but also the distribution of mass within the cavernous structure due to diffusion, free and forced convection. The associated coupling of chemistry and hydraulics allows for a temporal scaling of the model based on the exchange rate. In order to achieve these goals and to finally make detailed prognosis on the long-term development of geogenic cavities, the presented reaction models provide a reliable basis.

3 | Spatial and Temporal Evolution of Leaching Zones within Potash Seams Reproduced by Reactive Transport Simulations

Abstract

Leaching zones within potash seams generally represent a significant risk to subsurface mining operations and the construction of technical caverns in salt rocks, but their temporal and spatial formation has been investigated only rudimentarily to date. To the knowledge of the authors, current reactive transport simulation implementations are not capable to address hydraulic-chemical interactions within potash salt. For this reason, a reactive transport model has been developed and complemented by an innovative approach to calculate the interchange of minerals and solution at the water-rock interface. Using this model, a scenario analysis was carried out based on a carnallite-bearing potash seam. The results show that the evolution of leaching zones depends on the mineral composition and dissolution rate of the original salt rock, and that the formation can be classified by the dimensionless parameters of Péclet (Pe) and Damköhler (Da). For $Pe > 2$ and $Da > 1$, a funnel-shaped leaching zone is formed, otherwise the dissolution front is planar. Additionally, $Da > 1$ results in the formation of a sylvinitic zone and a flow barrier. Most scenarios represent hybrid forms of these cases. The simulated shapes and mineralogies are confirmed by literature data and can be used to assess the hazard potential.

3.1 Introduction

The formation of leaching zones within potash seams represents a significant safety risk in salt mining (Baumert 1953; Warren 2017) and the construction of technical caverns (Edler 2010; Thoms and Gehle 1999). The latter are needed in the course of the energy transition, for example for the storage of hydrogen (Welder et al. 2018). Due to the increased solubility of potash salts, even NaCl-saturated solutions, if available, can penetrate deeply into potash seams and initiate leaching processes that generate fluid flow paths (Figure 3.1) and affect the mechanical stability (Höntzsch and Zeibig 2014; Warren 2017). In order to model the temporal and spatial evolution of leaching zones, coupling of chemical reactions with density-driven species transport is required (Dijk and Berkowitz 2000). One main difficulty is the description of transport and chemical reactions within regions of strongly varying porosities, such as the dissolution

front. If impermeable (dry) salt rock inhibits the inflow of solution, chemical reactions cannot take place and the dissolution front is immobile. Accordingly, a sequential coupling of transport and chemistry as described in Steefel et al. (2015) does not suffice but an additional approach to describe the process interaction at the solid-liquid interface is required. Reactive transport models dealing with rock salt often use a mass transfer rate to overcome this limitation (Jinlong et al. 2020; Li et al. 2018; Zidane et al. 2014). Laouafa et al. (2015; 2019) introduced a local non-equilibrium diffuse interface model to describe the dissolution of halite and gypsum at the interface. However, these approaches have only been applied to binary systems yet. Furthermore, they do not consider precipitations, which may inhibit the solution inflow into permeated areas as well. Therefore, a more sophisticated approach is required when dealing with potash salt, which consists of several minerals and causes the precipitation of secondary minerals. So far, only simplified approaches (Velema et al. 2010) and benchmarks on selected rocks (Xie et al. 2011) are available for the development of leaching zones within potash seams.

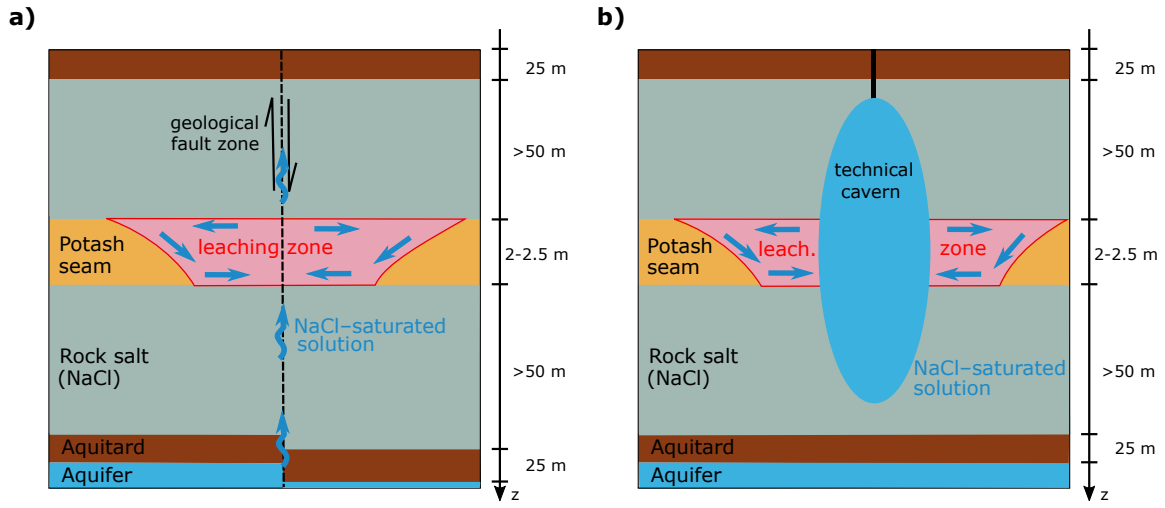

Figure 3.1: Sketch of leaching zones a) in salt mining (symmetrical in x- and y-direction) and b) in the construction of technical caverns (radially symmetrical).

The paper discusses a modeling approach, which allows to qualitatively reproduce the temporal and spatial evolution of leaching zones within potash seams. For this purpose, the TRANsport Simulation Environment (TRANSE) (Kempka 2020) was coupled with the geochemical reaction module PHREEQC (Parkhurst and Appelo 2013), and extended by a new approach to describe the interchange of minerals and solution at the water-rock interface. A carnallite-bearing potash seam is used in the simulations to validate the results against literature data. Hereby, the present study especially focuses on density-driven flow, which governs natural leaching processes and cavern formation according to Anderson and Kirkland (1980). By means of scenario analyses, the dissolution rate and the rock composition of the potash seam are varied, and it is determined under which conditions the leaching zone growth is transport-

or reaction-dominated, whether advection or diffusion dominates the transport and to what extent the evolution of the leaching zone is affected in this way.

3.2 Materials and Methods

To simulate the spatial and temporal formation of leaching zones within potash seams, a numerical reactive transport model has been developed in the present study and is discussed in the following sections. An overview of all the calculation steps is shown in Figure 3.2. At the beginning of each time step, the simulation of fluid flow and transport of chemical species are carried out using TRANSE. Thereafter, saturation and fluid density are updated in order to minimize mass balance errors in the chemical reaction calculations. Saturation and fluid density as well as chemical reactions are determined by using the PHREEQC simulation module with the THEREDA database (Altmaier et al. 2011). Between them, an additional step called 'interchange' is performed. Finally, the calculated concentrations, fluid densities, viscosities and porosities are transferred back to the TRANSE simulator and used to calculate the fluid flow and mass transport of the next time step (Figure 3.2).

The term 'saturated' is used in view of the chemical equilibration of the solution with respect to certain minerals. The fluid saturation in the pore space is referred to as 'dry' or 'permeated'. This subdivision is necessary, since pores within unaffected potash salt usually do not contain any water.

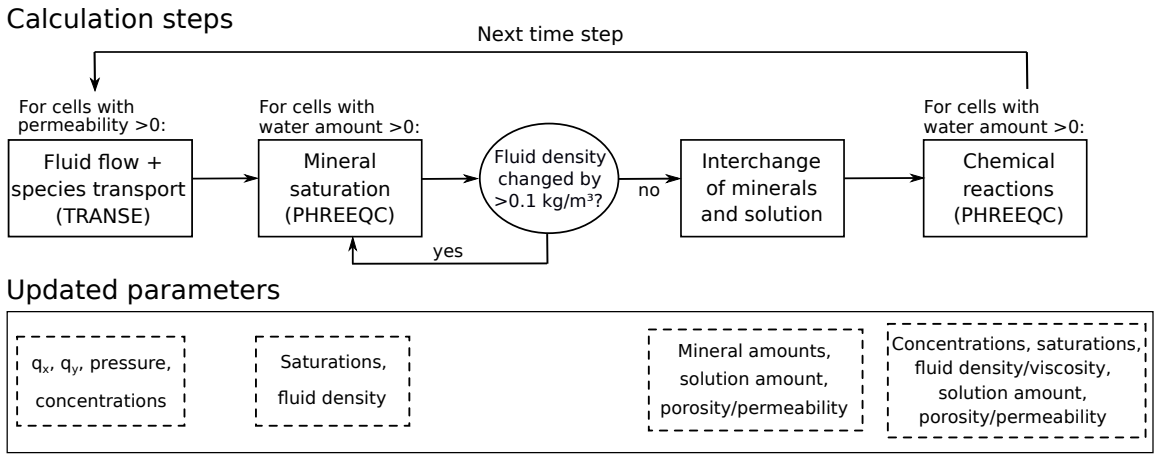

Figure 3.2: Flow sheet of the coupled reactive transport model: calculation steps in each time step and associated output parameters.

3.2.1 Fluid Flow and Transport of Chemical Species

TRANSE is a fluid flow and transport code that is based on the Finite Difference Method (Kempka 2020). Due to the fact that the solution crosses several rock salt layers before it reaches the potash seam (Figure 3.1), it is generally NaCl-saturated with the consequence that halite is not dissolved during the formation of leaching zones.

Hence, a porous medium is established within the potash seams (Velema et al. 2010) and consequently, Darcy flow in a medium fully saturated with a single phase fluid (further referred to as permeated) is applied in the present study. A fully-implicit numerical scheme is used to solve the density-driven formulation of the Darcy flow equation, coupled with the equations for transport of reactive chemical species. Therein, advective and diffusive species transport are taken into account. Input parameters from the previous time step are the spatial distribution of minerals and species concentration, fluid density and viscosity as well as porosity Φ and permeability k_f. Using these input data, the numerical simulator computes the spatial distribution in flow velocities, fluid pressure and species concentration for the current time step. The coupled modeling results were thoroughly checked for any appearance of oscillations at locations with sharp concentration fronts. The choice of strict convergence criteria for the solution of both coupled partial differential equation systems, flow and transport, ensured that flow velocity and concentration changes due to oscillations were negligible during the entire simulation time. Alternative oscillation mitigation schemes such as artificial diffusion terms, cross-wind streamline diffusion correction, etc., were neither required nor applied. All details on the mathematical model and its numerical implementation are provided in Kempka (2020).

3.2.2 Mineral Saturation and Fluid Density

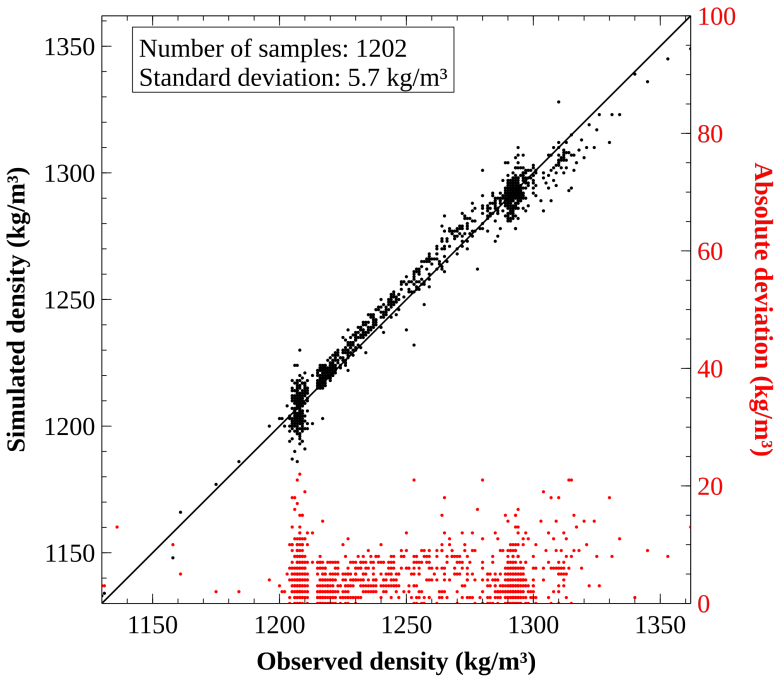

Figure 3.3: Comparison between observed and simulated densities.

When using the updated concentrations after the flow and transport calculation in the chemical reaction calculations, an accurate fluid density is most important to mini-

mize mass balance errors. For this purpose, the updated species concentrations are transferred to the PHREEQC simulation module to update the fluid density and saturation. In this regard, the THEREDA database was extended by molar volumes for the involved species. Its validation showed a very good agreement with the PHREEQC simulation results with more than 1,000 fluid density measurements from a potash salt mine of K+S (Figure 3.3). If the updated fluid density differs by more than 0.1 kg/m^3 from the input value, the process is iteratively repeated until a deviation of <0.1 kg/m^3 is achieved. The saturation of the solution is needed for the interchange as well as for the chemical reaction calculations representing the final two calculation steps in each time step (Figure 3.2).

3.2.3 Interchange of Minerals and Solution at the Water-Rock Interface

Describing the water-rock interface represents a particular challenge in the simulation of leaching zone growth. The porosity of dry, unaffected salt rock is negligible ($\ll$1%). Even if completely permeated with brine, the result would be such a high solid-fluid-ratio that all water present is converted into crystal water, while the very small existing pore space would be sealed by secondary minerals (Steding et al. 2020; Xie et al. 2011). Accordingly, further fluid flow into the salt rock and resulting chemical reactions would cease. However, observations from the lab and the field prove that this is not the case if adjacent open pore space contains undersaturated solution. In order to manage the solid-liquid dissolution at the water-rock interface, a mineral and solution interchange modeling approach was developed in the present study. It describes the processes of mineral dissolution and transfer of solution between dry or permeated cells with very low porosities and adjacent cells with high porosity (Figure 3.4).

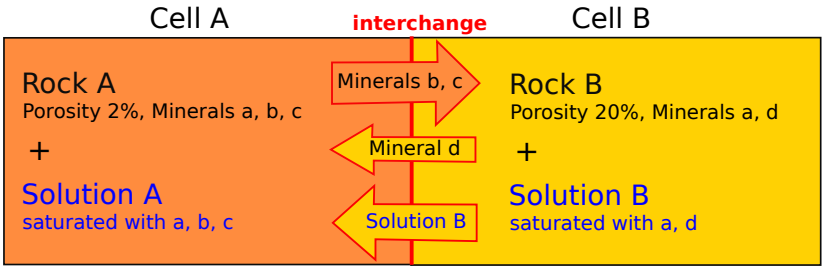

Figure 3.4: Sketch of the implemented interchange approach. A defined amount of minerals according to Equation 3.1 is dissolved into an adjacent cell if the solution present there is undersaturated with respect to the minerals. To fill the newly formed pore space, solution is transferred into the cell with the larger quantity of dissolved minerals (in this case Cell A).

In our approach, a pre-determined amount of the minerals in Cell A is dissolved into Cell B, provided that solution is present in Cell A and that it is undersaturated with respect to the corresponding minerals (Figure 3.4). This is also realized in reverse direction and at each interface between two cells within the model. In order to keep the volume of both cells constant, a corresponding fluid volume is transferred from the cell with the lower quantity of dissolved minerals into the cell with the larger quantity

of dissolved minerals (Figure 3.4). The maximum amount of minerals that can react Min_{sol} (mol) is given by a rate law, which considers the dissolution rate and also the contact area between solution and rock. Between Cell A and Cell B the amount is calculated by Equation 3.1:

$$Min_{sol} = r \cdot Min_A/di \cdot \Phi_B \cdot dt \tag{3.1}$$

The r (cm/s) represents the average dissolution rate of all minerals within the salt rock. Min_A (mol) is the sum of minerals present in Cell A. Divided by the cell diameter perpendicular to the dissolution front di (cm), it gives the affected amount of minerals if 1 cm rock from Cell A is dissolved. By multiplying this amount with the porosity in Cell B Φ_B (-), the contact area between the rock in Cell A and the solution in Cell B is taken into account. dt (s) is the length of the time step. The resulting amount of minerals represents a sum that is split among all minerals present in Cell A according to their molar fractions. This ensures that the different mineral densities are considered. Only those minerals are dissolved which are undersaturated in regard to the solution in Cell B. Based on the saturation calculation after the transport (Section 3.2.2) it is deduced which minerals are added to Cell B. The excess minerals remain in Cell A, so that the dissolution process is selective. After calculating the interchange, the rock composition in each cell is updated accordingly (Figure 3.2). Chemical reactions are calculated afterwards and are described in Section 3.2.4.

At the dissolution front, where permeated and dry potash salt are in contact, the dissolution of minerals is only allowed in one direction (Figure 3.5a). After calculating the interchange, the rock composition in each cell is updated. Again, the dissolution front represents a special case: originally dry cells that received solution for the first time are divided into a permeated and a dry sub-cell (Figure 3.5b). The permeated one contains those minerals that remained in the cell due to selective dissolution at the interface. Only this sub-cell is in contact with the solution transferred in the present modeling approach. The other part of the cell remains dry and is not considered in the subsequent calculation of chemical reactions. By this procedure, the immediate drying out of cells due to the high solid-fluid-ratio, and thus the requirement for re-permeation, are avoided. Dry and permeated sub-cells consist of different minerals. When the interchange between a partly permeated cell and an adjacent cell is calculated, both sub-cells are taken into account by weighting their volume fractions. However, mineral dissolution and inflow of solution from an adjacent cell can only occur in the permeated sub-cell.

In addition to the interchange between two cells, an internal permeation of the partly permeated cells at the dissolution front is taken into account. Here, dry minerals are gradually added to the permeated sub-cell, which may lead to the precipitation of new minerals (Figure 3.5c). The amount of minerals added Min_{add} (mol) follows the rate law in Equation 3.2:

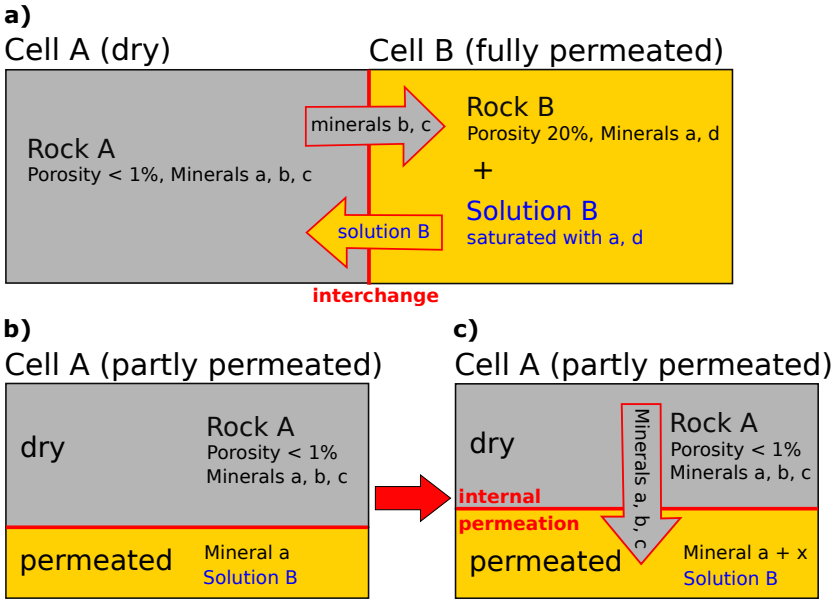

Figure 3.5: a) Interchange at the dissolution front leads to b) partly permeated cells; c) internal dissolution of dry minerals causes further permeation of the cell as well as mineral precipitation.

$$Min_{sol} = r \cdot Min_{dry}/di \cdot \Phi_{per} \cdot dt \tag{3.2}$$

In this case Min_{dry} (mol) is the sum of minerals present in the dry sub-cell and Φ_{per} (-) is the porosity in the permeated sub-cell. As a result, the permeated sub-cell grows while the dry sub-cell shrinks. Only if a cell is fully permeated, a permeability >0 is assigned to it, so that fluid flow and transport of chemical species can take place. The chemical reactions resulting from transport and interchange are determined in the final calculation step (Figure 3.2) that is further described in the following section.

3.2.4 Chemical Reactions

If solution is transferred into a cell due to the interchange process (Figure 3.4), it is first mixed with the pre-existing solution in that cell by means of the PHREEQC simulation module. Thereafter, the occurring chemical reactions in each cell are calculated, using the updated rock compositions after the interchange (Section 3.2.3). Based on our previous results (Steding et al. 2020), it is valid to assume that salt rock and saline solution quickly reach thermodynamic equilibrium. Therefore, within each permeated (sub-) cell all minerals are added to the solution and both are equilibrated by using the keywords 'Reaction' and 'Equilibrium Phases' in PHREEQC. The resulting solution and rock composition as well as fluid density are calculated using PHREEQC; viscosity is calculated according to Laliberté (2007; 2009). Porosity and permeability are updated in each cell following the chemical calculations. For this purpose, the volume of the minerals is determined according to Table 3.1 to calculate its relation

to the cell volume. It may occur that the precipitated minerals exceed the available volume within the respective cell (Xie et al. 2011). In such cases, the cell porosity is set to zero, while potential excess solution is neglected. If the total mineral volume is smaller than the cell volume, and the solution volume does not correspond to the volumetric difference, its amount is adjusted accordingly. This ensures that the pore space is always completely permeated, whereby the resulting errors in the mass balance are recorded. If the water in a permeated cell is fully consumed by the chemical reactions, the cell dries out. In case of a previously partly permeated cell, the minerals from the dry and the (formerly) permeated sub-cell are combined to form the updated dry rock composition. A porosity-permeability relationship (Equation 3.3) introduced by Xie et al. (2011) is applied.

$$k_f = 1.12 \cdot 10^{-8} \cdot \Phi^{5.25} \tag{3.3}$$

3.2.5 Example Case of a Carnallite-Bearing Potash Seam

For the application example, leaching processes in a carnallite-bearing potash seam were simulated. Carnallitite is one of the most commonly occurring potash salts worldwide; besides carnallite ($KMgCl_3 \cdot 6\,H_2O$) and halite (NaCl) it contains also sylvite (KCl) and partly kieserite ($MgSO_4 \cdot H_2O$) as well as anhydrite ($CaSO_4$). The chemical processes resulting from the contact with NaCl-saturated solution are well documented (among others) by Koch and Vogel (1980). The authors consider vertical fault zones as main cause for the reaction initiation (Figure 3.1a). Close to these, a porous matrix of leached halite is formed, followed by a sylvinitic zone which may also contain kainite. They state that both zones show an increased porosity compared to the original potash seam. At further distance follows the dry, carnallite-bearing potash salt, which does not belong to the leaching zone anymore. According to Koch and Vogel (1980), the mineralogical boundaries between these three zones are often asymmetric, with the leaching being more pronounced close to the hanging wall of the potash seam (Figure 3.1). However, in horizontal direction, the leaching zone geometry is symmetric (Figure 3.1), so that 2D models are applied in the present study, making use of this symmetry to reduce the computational time.

Table 3.1: Potash salt mineral densities and dissolution properties.

Mineral	Density (kg/m^3)	Reaction equation (dissolution)	log K
Carnallite	1,600	$1\,KMgCl_3 \cdot 6\,H_2O \longrightarrow 3\,Cl^- + 6\,H_2O + 1\,K^+ + 1\,Mg^{2+}$	4.33
Halite	2,170	$1\,NaCl \longrightarrow 1\,Cl^- + 1\,Na^+$	1.586
Sylvite	1,990	$1\,KCl \longrightarrow 1\,Cl^- + 1\,K^+$	0.915

The aforementioned coupled reactive transport model was used to reproduce the formation of leaching zones. With regard to the rock composition, the main components carnallite, halite and sylvite with densities and dissolution properties according

to Table 3.1 were taken into account. By their dissolution, the quaternary system $NaCl-KCl-MgCl_2-H_2O$ was formed. The main overall reaction was the conversion of carnallite into sylvite and potash brine associated with the precipitation of halite (Equation 3.4):

$$KMgCl_3 \cdot 6\,H_2O + \text{brine}\,(NaCl) \longrightarrow KCl + NaCl\,(\text{brine}) + \text{brine}\,(MgCl_2, KCl, NaCl) \tag{3.4}$$

The reactive transport model applied was designed with a height of 2 m, based on the general thickness of potash seams in Germany, and a width of 5 m, and was discretized by 101 x 41 cells (Figure 3.6). In its initial state, the entire model consisted of dry, homogeneous carnallitite with a porosity of 0.1%. The left boundary represented a fault zone with a continuous inflow of fresh NaCl solution and formed the starting point of the leaching process within the carnallite-bearing potash seam. For that reason, the cells at the left boundary contained 1% halite, while the porosity was 99%, filled with a NaCl solution that was saturated with respect to halite. A Dirichlet boundary condition was used to keep the solution composition. Transport and interchange with adjacent cells were enabled, but precipitation was not permitted in these cells. Instead, it was assumed that all minerals were immediately transported out of these cells by the fluid flow present in the fault zone. This corresponded to a high exchange rate within the fault zone and, therefore, represented one of the most critical cases in nature with regard to its hazard potential (Höntzsch and Zeibig 2014). All the other model boundaries were considered to be impermeable. A pre-defined pressure gradient was not applied.

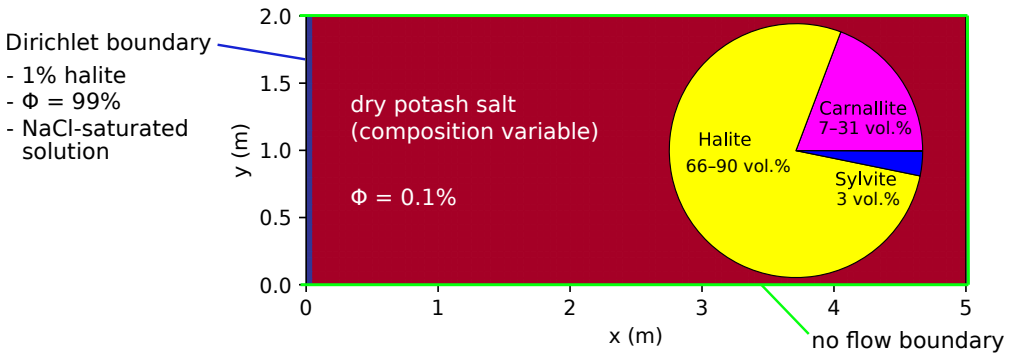

Figure 3.6: Initial and boundary conditions: the inflow region is prescribed by a Dirichlet boundary (blue line); all other boundaries are impermeable (green lines); the models are initialized with dry, homogeneous rock of varying mineral contents (following the scenario description).

The species diffusion coefficients in brines depend on the composition of the solution (Felmy and Weare 1991). However, since leaching zones generally represent advection-dominated systems, all diffusion coefficients were assumed to be equal and constant in the present study for reasons of simplicity. Based on the investigations of Yuan-Hui and Gregory (1974), an average value of $D_f = 1.5 \cdot 10^{-9}\,m^2/s$ was used

for all four transported species. Fluid compressibility was set to $c_f = 4.6 \cdot 10^{-10}$ 1/Pa and the simulation was undertaken at isothermal conditions at a temperature of 25°C. Dissolution rates of carnallitite were not available; however, it is known that they vary depending on rock and solution compositions (Durie and Jessen 1964; Hoppe and Winkler 1974; Röhr 1981). For this reason, a sensitivity analysis for dissolution rates of $r = 10^{-3}$ cm/s to 10^{-6} cm/s was performed. Furthermore, the carnallite content of the potash seam was varied between 5 wt.% and 25 wt.%, corresponding to 7 vol.% to 31 vol.% (Figure 3.6), to investigate the resulting flow velocities due to strongly changing porosities in the leaching zone. The sylvite content was always set to 3 wt.%, while the rest of the potash seam consisted of halite with a corresponding content between 72 wt.% and 92 wt.%.

3.3 Results

Shapes and growth rates of leaching zones differed significantly, depending on carnallite content and dissolution rates. The evolution over time on the basis of the permeated rock volume is presented in Figure 3.7. Simulations were terminated when the leaching zone had (nearly) reached the right model boundary or the permeated rock volume did no longer change considerably. The results show that for the same dissolution rate, the leaching zone growth was faster with increasing carnallite content: the permeated rock volume for a 25 wt.% carnallite content was always three to six times larger than that for a 5 wt.% carnallite content. Furthermore, it was noticeable that the leaching zone growth was almost linear and comparably slow for a dissolution rate of 10^{-6} cm/s (Figure 3.7a). After 10 years, only 0.8-2.5 m^3 of salt rock (depending on the carnallite content) were permeated, while the affected volume was 1.8 m^3 to >6 m^3 for higher dissolution rates. If the dissolution rate was above 10^{-6} cm/s, the curves were quite similar for identical carnallite contents, especially if these were below 15 wt.% (Figure 3.7b-d). In contrast to the permeated rock volume evolution for a dissolution rate of 10^{-6} cm/s, the curves flattened over time for higher dissolution rates, i.e., the growth rate of the leaching zone stagnated. This development could be particularly observed for high carnallite contents and becomes more pronounced with increasing dissolution rates. For example, in case of 25 wt.% carnallite and a dissolution rate of 10^{-3} cm/s (Figure 3.7d), the permeated rock volume within the first year was still as high or higher than for a dissolution rate of 10^{-4}-10^{-6} cm/s (Figure 3.7b,c). However, after 2-2.5 years the permeated rock volume was smaller than for the lower rates due to the more pronounced flattening of the curve. Assuming a constant further development, the permeated rock volume would even be smaller than that for a dissolution rate of 10^{-6} cm/s and a carnallite content of 25 wt.% after 20-25 years (Figure 3.7a).

In general, two different shapes of the leaching zone could be observed in the present simulations. The first exhibited a vertical, planar dissolution front, where the leaching zone expanded uniformly across the entire potash seam thickness. The second one

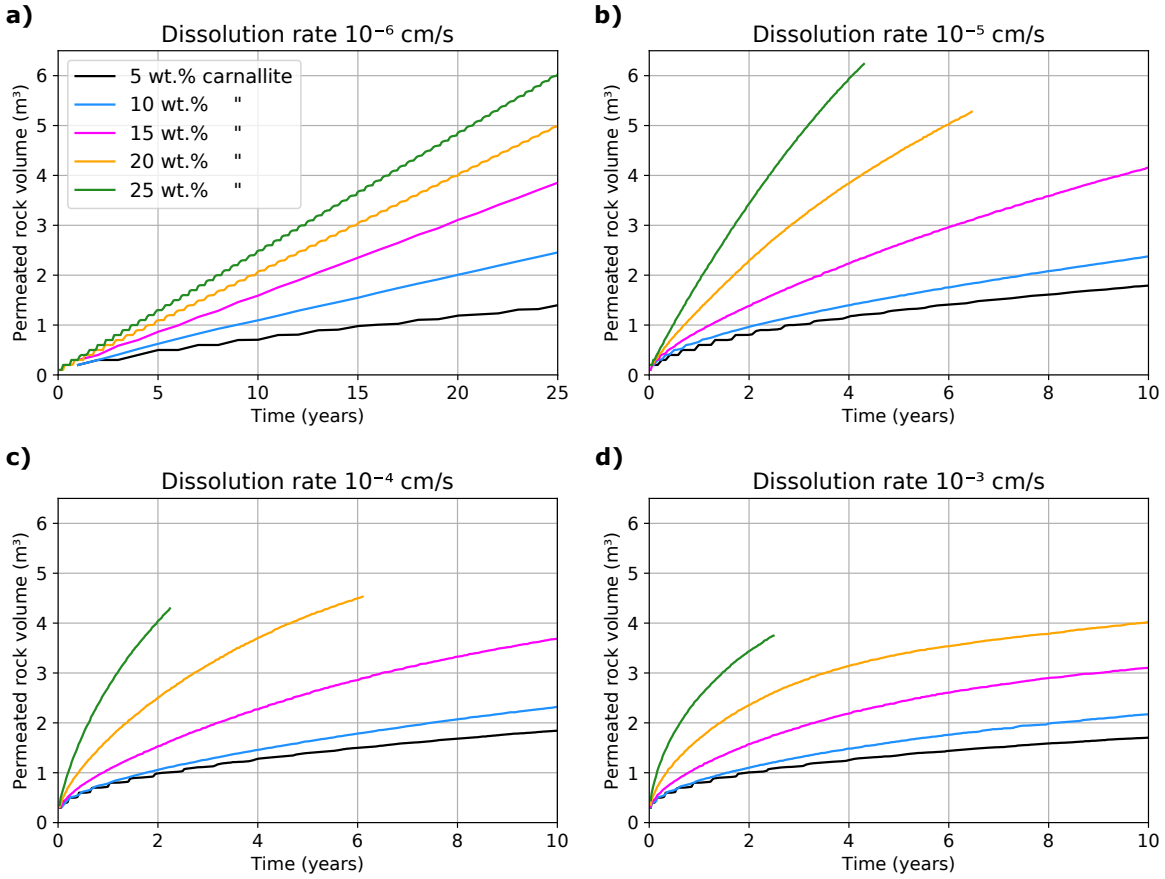

Figure 3.7: Comparison of the permeated rock volume over time for different dissolution rates (a-d) and carnallite contents (line color) of the modeled potash seam. Curves that end before a simulation time of 10 years indicate the leaching zone arrival at the right model boundary.

shows a funnel-type shape, where only the upper half of the potash seam was being permeated. A slow leaching zone growth was usually associated with a planar dissolution front, while a fast growing leaching zone often penetrated the potash seam preferentially close to the hanging wall. The Péclet (Pe) and Damköhler (Da) numbers (Equations 3.5-3.7) were determined to improve the process understanding and to establish criteria that facilitate a leaching zone classification. These numbers provide information about the ratio between advection and diffusion rate and between transport velocity and dissolution rate, respectively.

$$Pe = v \cdot l / D_f \tag{3.5}$$

$$Da = r / v \quad (\text{if Pe} > 2) \tag{3.6}$$

$$Da = r \cdot l / (2 \cdot D_f) \quad (\text{if Pe} < 2) \tag{3.7}$$

The flow velocity v corresponds to the advection rate and is spatially and temporally variable. D_f is the diffusion coefficient and l is the characteristic length over which

diffusion occurs in the model. The characteristic length was best described by using the current width of the leaching zone, since the NaCl solution at the left model boundary and the highly saturated potash brine at the dissolution front introduced a concentration gradient which was mainly horizontal. The Damköhler number, which describes the ratio of the dissolution rate to the transport velocity, depends on the Péclet number. In an advection-dominated system with Pe > 2, the transport velocity corresponds to the advection velocity v, whereas in a diffusion-dominated system with Pe < 2 it corresponds to the diffusion rate $2 \cdot D_f / l$. Therefore, Pe and Da were calculated individually for each cell based on the local flow velocity v and individual horizontal characteristic length l. Then, the median for all permeated cells was determined in order to derive an indicator for the entire system in addition to the median for the cells along the dissolution front.

The Péclet and Damköhler numbers allowed for a systematic classification of the different scenarios shown in Table 3.2. A Péclet number Pe < 2 indicated that the system was diffusion-dominated during the entire simulation period, while Pe > 2 indicated a permanently advection-dominated system. The term Pe sinking < 2 meant that the system was advection-dominated in the beginning, but became diffusion-dominated over time. If the dominating transport process changed more than once, the system was called Pe alternating. In case of the Damköhler number, Da < 1 indicated that the system is permanently reaction-dominated, while Da > 1 represented a permanently transport-dominated system. Da rising > 1 meant that the system was reaction-dominated in the beginning, but became transport-dominated over time. The results showed that most systems were dominated by transport either right from the beginning or at least in the long run. Only for a dissolution rate of 10^{-6} cm/s and more than 15 wt.% carnallite content, the system was permanently reaction-dominated. Regarding transport, diffusion permanently dominated if the carnallite content was 5 wt.%. Otherwise, the system was usually advection-dominated in the beginning, while in the long run diffusion dominated. Only for a dissolution rate of 10^{-6} cm/s and a carnallite content of more than 10 wt.%, the system was permanently dominated by advection. For a dissolution rate of 10^{-6} cm/s and 10 wt.% carnallite, both transport processes alternated.

The classification based on Pe and Da (Table 3.2) correlated with different shapes and mineralogies of the leaching zone. Figures 3.8 and 3.9 show the Mg^{2+} concentration distribution and mineralogy for two reaction-dominated systems where Pe was permanently below and above two, respectively. The Mg^{2+} concentration represents the fluid density and the saturation of the solution with respect to the potash salts carnallite and sylvite. While the NaCl solution at the left boundary, which did not contain any Mg^{2+}, was maximally undersaturated with respect to sylvite and carnallite and showed a density of 1,201 kg/m^3, saturation and density increased with increasing Mg^{2+} concentration. First, the solution was saturated with respect to sylvite, and from about 85 g/l Mg^{2+} (at 25°C) on also with respect to carnallite. Thereafter, the solution

Table 3.2: Classification of the scenarios into diffusion-dominated (Pe $<$ 2) or advection-dominated (Pe $>$ 2) and reaction-dominated (Da $<$ 1) or transport-dominated (Da $>$ 1) systems as well as hybrid forms (Pe alternating, Pe sinks $<$ 2, Da rises $>$ 1).

Dissolution rate (cm/s)	Amount of carnallite (wt.%)				
	5%	10%	15%	20%	25%
10^{-3}	Pe $<$ 2 Da $>$ 1	Pe sinks $<$ 2 Da $>$ 1	Pe sinks $<$ 2 Da $>$ 1	Pe sinks $<$ 2 Da $>$ 1	Pe sinks $<$ 2 Da $>$ 1
10^{-4}	Pe $<$ 2 Da $>$ 1	Pe sinks $<$ 2 Da $>$ 1	Pe sinks $<$ 2 Da $>$ 1	Pe sinks $<$ 2 Da $>$ 1	Pe sinks $<$ 2 Da $>$ 1
10^{-5}	Pe $<$ 2 Da $>$ 1	Pe sinks $<$ 2 Da $>$ 1	Pe sinks $<$ 2 Da rises $>$ 1	Pe sinks $<$ 2 Da rises $>$ 1	Pe sinks $<$ 2 Da rises $>$ 1
10^{-6}	Pe $<$ 2 Da rises $>$ 1	Pe alternating Da rises $>$ 1	Pe $>$ 2 Da rises $>$ 1	Pe $>$ 2 Da $<$ 1	Pe $>$ 2 Da $<$ 1

was in equilibrium with the carnallite-bearing potash seam and showed a density of 1,273 kg/m^3. Figures 3.8 and 3.9 show that in a reaction-dominated system this kind of solution (blue) was only present within the partly permeated cells at the dissolution front where transport was not considered. Within the fully permeated leaching zone, saturation and fluid density were very low with a maximum concentration of 25 g/l Mg^{2+}. In the diffusion-dominated system (Figure 3.8a), the concentrations were generally slightly lower compared to the advection-dominated system (Figure 3.9a), and the growth of the leaching zone was considerably slower (Figure 3.7a). Moreover, the concentration gradient within the fully permeated area of the diffusion-dominated system was exclusively horizontal, whereas it was predominantly vertical in the advection-dominated system. The latter resulted in a stronger concentration gradient between fully and partly permeated cells at the dissolution front within the upper half of the potash seam (Figure 3.9a). The flow field shows that the solution moved from the inflow region towards the dissolution front close to the hanging wall, from where it flowed down and returned to the inflow region close to the footwall (Figure 3.9a). The observed flow pattern corresponds to a typical convective flow system. Flow velocities close to the dissolution front were $1 \cdot 10^{-7}$ m/s to $2.4 \cdot 10^{-7}$ m/s (in the diffusion-dominated system $1 \cdot 10^{-9}$ m/s to $2 \cdot 10^{-9}$ m/s). Saturation with respect to sylvite was not reached at any point, resulting in the absence of a sylvinitic zone (Figures 3.8b and 3.9b). Instead, only halite was found with a volume fraction slightly higher than that in the initially dry rock, suggesting that the mineral precipitated evenly throughout the entire leaching zone. Therefore, a system that was reaction-dominated from the beginning always showed a vertical and planar dissolution front, whereby the permeated rock consisted entirely of halite.

In contrast to reaction-dominated systems, transport-dominated systems showed very different leaching zone shapes, depending on whether advection or diffusion governed the transport. Figures 3.10 and 3.11 show the Mg^{2+} concentration distribution and the mineralogy for both cases. It is noticeable that high Mg^{2+} concentrations (>60 g/l) not only occurred within the partly permeated cells at the dissolution

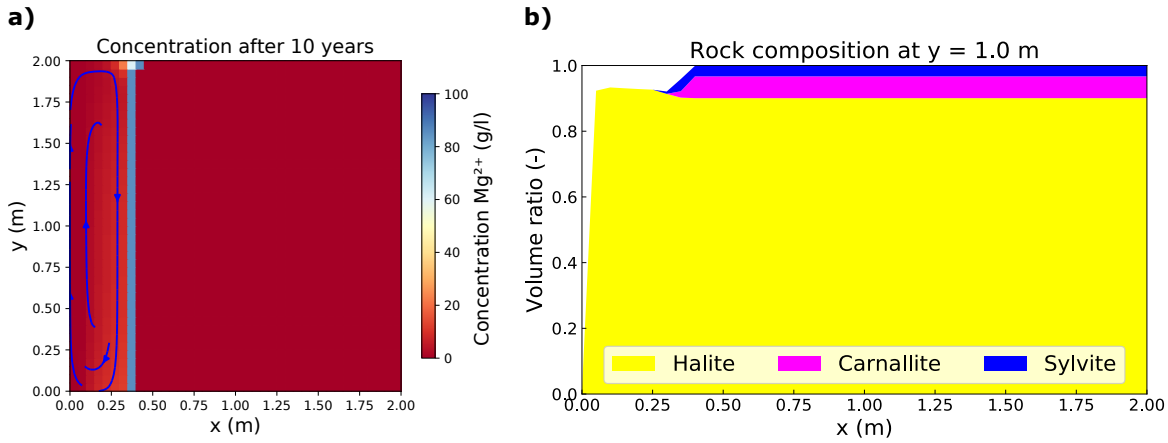

Figure 3.8: a) Mg^{2+} concentration distribution and b) mineralogy for a reaction- and diffusion-dominated system (scenario: dissolution rate 10^{-6} cm/s and 5 wt.% carnallite).

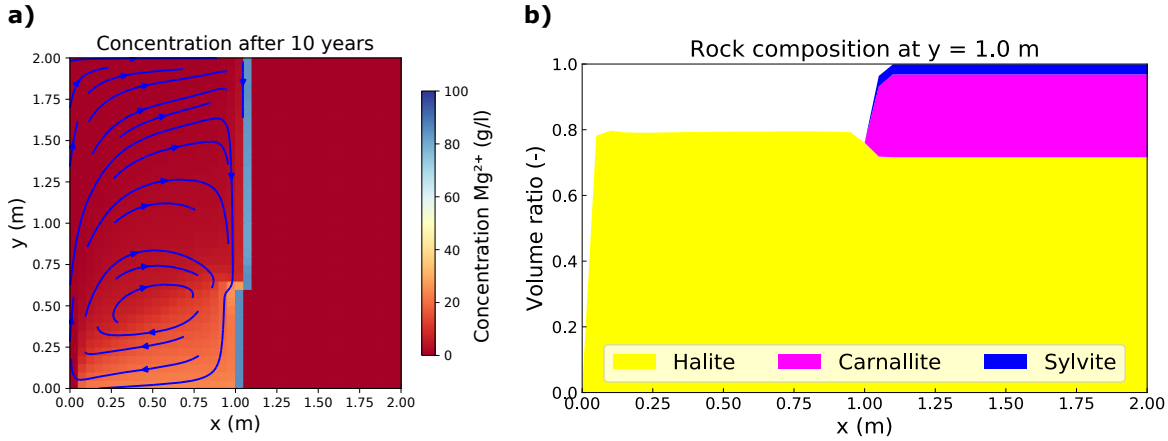

Figure 3.9: a) Mg^{2+} concentration distribution and b) mineralogy for a reaction- and advection-dominated system (scenario: dissolution rate 10^{-6} cm/s and 20 wt.% carnallite).

front but within the entire right and lower half of the leaching zone, respectively. In the case of the diffusion-dominated system (Figure 3.10a), the concentration gradient was still horizontal as shown in Figure 3.8a, but the concentrations within the leaching zone covered the entire range from 0-85 g/l, and its growth was faster than in the reaction-dominated case. With a maximum of $1 \cdot 10^{-9}$ m/s, flow velocities were very low. The dissolution front was still almost planar. However, a sylvinitic zone was now established in front of it, covering more than half of the leaching zone (Figure 3.10b). The sylvite content within this area was higher than in the initially dry rock. Between the sylvinitic zone and the inflow region, the rock matrix consisted exclusively of halite. It should be noted that the halite content slowly increased towards the inflow region, i.e., the porosity decreased there.

In an advection-dominated system (Figure 3.11), a concentration gradient in horizontal and vertical direction occurred, resulting in a highly undersaturated solution only in the upper left region of the potash seam. The shape of the leaching zone corresponded to a funnel that ends approximately halfway up the seam. While the

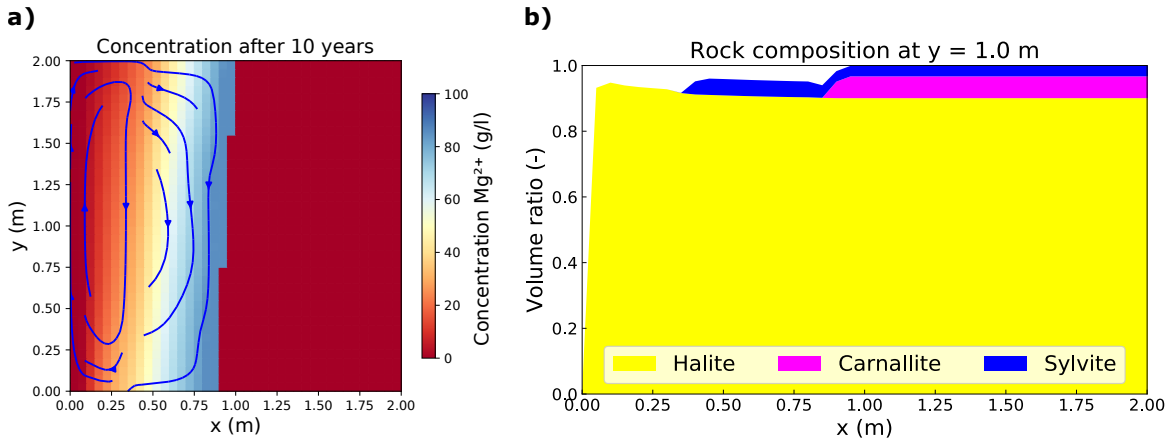

Figure 3.10: a) Mg^{2+} concentration distribution and b) mineralogy for a transport- and diffusion-dominated system (scenario: dissolution rate 10^{-5} cm/s and 5 wt.% carnallite).

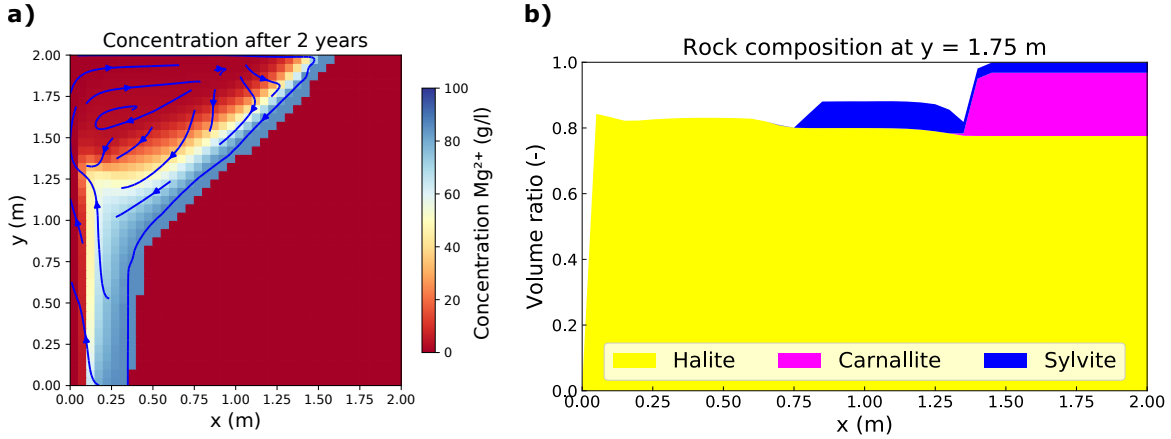

Figure 3.11: a) Mg^{2+} concentration distribution and b) mineralogy for a transport- and advection-dominated system (scenario: dissolution rate 10^{-4} cm/s and 15 wt.% carnallite).

dissolution front hardly moved forward at all and remained planar in the lower half of the seam, the width of the leaching zone increased evenly in the upper half and reached its maximum at the hanging wall (Figure 3.11a). A zone with significantly increased sylvite and slightly increased halite contents compared to the initial salt rock existed left to the dissolution front (Figure 3.11b). Figure 3.12 shows that their widths varied with height, whereby the sylvinitic zone corresponds to the yellow area with a porosity of approximately 15%. According to this, the zone reached its maximum width at a height of about 1.5 m, corresponding to the midway of the funnel. Below 1.5 m, its width decreased due to the funnel shape, while the leaching zone became wider above with the sylvinitic zone getting narrower, as a halite zone (20-25% porosity) of increasing thickness formed between it and the inflow region. Particularly at lower dissolution rates, its width increased much more towards the hanging wall than the width of the funnel did (Figure 3.12b). It was also noticeable, with increasing dissolution rates, that the funnel shape penetrated deeper into the potash seam and at the same time ended at a slightly higher location (Figure 3.12a). Thus, shape and mineralogy of the

leaching zone varied slightly, depending on the dissolution rate and carnallite content. In principle, however, transport- and advection-dominated systems always resulted in a funnel shape, where the dissolution processes were limited to the upper half of the potash seam.

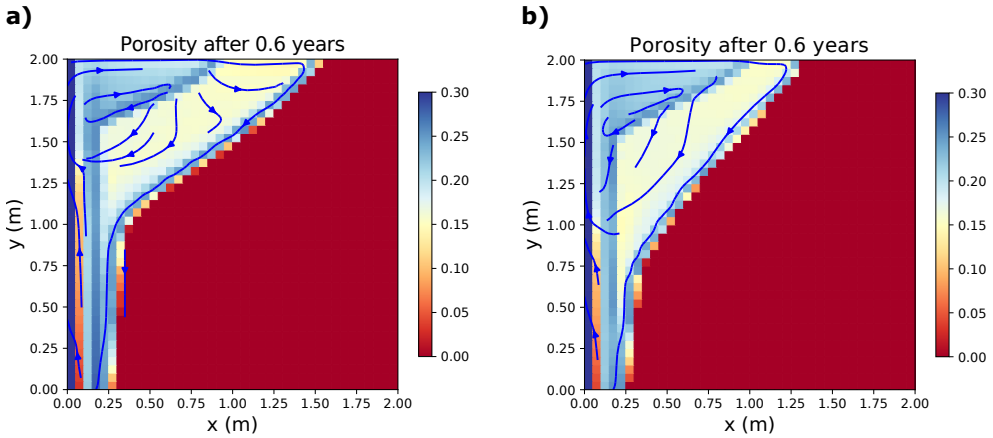

Figure 3.12: Porosity distribution in a transport- and advection-dominated system with 20 wt.% carnallite and a dissolution rate of a) 10^{-3} cm/s and b) 10^{-4} cm/s.

The flow within transport- and advection-dominated systems was mainly limited to the upper part of the potash seam, where dissolution processes took place (Figures 3.11a and 3.12). Again, a convective flow could be observed close to the hanging wall, where undersaturated solution flowed from the inflow region towards the dissolution front, down and then back towards the inflow region within the lower part of the funnel. The flow velocities varied depending on the carnallite content of the original rock: the higher its carnallite content, the higher the porosity and permeability of the later leaching zone, and thus the flow velocity of the solution. In case of 15 wt.% carnallite content, flow velocity was between 10^{-7} m/s and 10^{-8} m/s within the upper part of the potash seam, while it was around 10^{-7} m/s for 20 wt.% and even 10^{-6} m/s for 25 wt.% carnallite content. This resulted in a significantly faster growth of the leaching zone (Figure 3.7). Compared to a reaction- and advection-dominated system (Figure 3.9), the flow velocities were similar for a given porosity, but the leaching zone growth was much faster.

The porosity distributions in Figure 3.12 also show that precipitation occurred immediately next to the inflow region, reducing the porosity to almost zero, especially within the lower half of the potash seam. Accordingly, the solution exchange between the inflow region and the leaching zone was significantly restricted. The precipitations consisted entirely of halite, which was repeatedly supersaturated within this area. In the long run, the inflow of undersaturated solution and the outflow of saturated potash brine was thus only possible via the upper 0.5-1 m of the inflow region, since a flow barrier was formed by mineral precipitation. This phenomenon was also present in transport- and diffusion-dominated systems, but the precipitations were almost evenly distributed along the entire height and less pronounced with the porosity next to the

inflow region being only slightly reduced (Figure 3.10b). Barrier formation was not observed in reaction-dominated systems (Figures 3.8b and 3.9b).

Most of the calculated scenarios represent hybrid forms of the four cases described above (Table 3.2). For example, no system was permanently reaction- and diffusion-dominated. Scenarios with a dissolution rate of 10^{-6} cm/s and a carnallite content of 5-10 wt.% fell into that category for the first 10-15 years; after that, Da rose above one and the system became transport-dominated. As a result, the dissolution front remained almost planar, but the solution became more saturated with respect to sylvite and carnallite creating a sylvinitic zone (Figure 3.10b) and a barrier immediately next to the inflow region. The latter was limited to the lower half of the potash seam and its porosity decreased continuously towards the footwall. Whether the growth of the leaching zone would be affected by this in the long run was not clear since simulation times of 100 years showed only a slight inclination of the boundary between halitic and sylvinitic zone. In the scenario with 10 wt.% carnallite, Pe additionally alternated around two, i.e., advection gained influence, which was associated with a stronger barrier formation within the lower potash seam area as well as with a significant inclination of the dissolution front and the mineralogical boundary between halitic and sylvinitic zone (Figure 3.13b). At a medium porosity (15 wt.% carnallite), the system was already permanently advection-dominated; however, Da would only exceed 1 after about 10 years and would remain between 1 and 2 in the long run (permanently below 1 at the dissolution front). As a result, an (inclined) sylvinitic zone and a slightly inclined dissolution front were only formed within the lower part of the potash seam as shown in Figure 3.13b. For a dissolution rate of 10^{-6} cm/s and 20-25 wt.% carnallite, the system was permanently reaction- and advection-dominated as shown in Figure 3.9. Scenarios with a dissolution rate of 10^{-6} cm/s were thus always reaction-dominated at the beginning. Over time, Da increased, but a transport-dominated system only developed at low to medium porosities. Since diffusion was typically stronger than advection in these cases, the dissolution front tended to remain planar. Cases with an inclined dissolution front, as shown in Figure 3.13c, were the exception at very low dissolution rates.

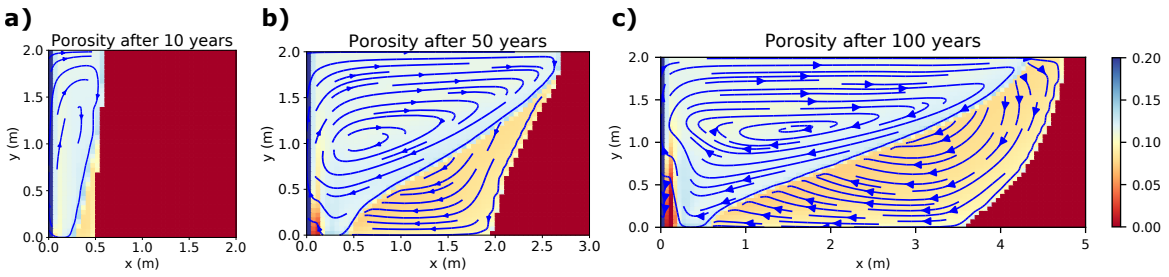

Figure 3.13: Porosity distribution within an a) initially reaction- and diffusion-dominated system; b,c) in the long run transport-dominated and with an increasing influence of advection (scenario: dissolution rate 10^{-6} cm/s and 10 wt.% carnallite).

Scenarios with a dissolution rate above 10^{-6} cm/s were usually dominated by transport, independent of maximum porosity (Table 3.2). Only in case of a dissolution rate of 10^{-5} cm/s and 15-25 wt.% carnallite (high porosity), a planar dissolution front was present at the beginning without or only a partially existing sylvinitic zone (Figure 3.14a), which was characteristic for a reaction-dominated system (Figures 3.8 and 3.9). However, Da exceeded the threshold value of one after a short period of time in all these scenarios. Since high porosities were present, the systems were all advection-dominated at the beginning. Accordingly, the dissolution front quickly became inclined and a funnel shape was formed, which, however, did not end at half the thickness of the potash seam but extended down to the footwall (Figure 3.14b,c). In addition, the inclination was not uniform as in systems that were dominated by advection and transport right from the beginning (Figures 3.11a and 3.12), and the sylvinitic zone did not extend to the hanging wall. On the other hand, the typical barrier formation within the lower potash seam area next to the inflow region could be observed here as well. The height of the barrier increased with simulation time (Figure 3.14), inhibiting the exchange of solutions between leaching zone and inflow region. Especially at the dissolution front, Pe and flow velocities decreased significantly within the lower potash seam area.

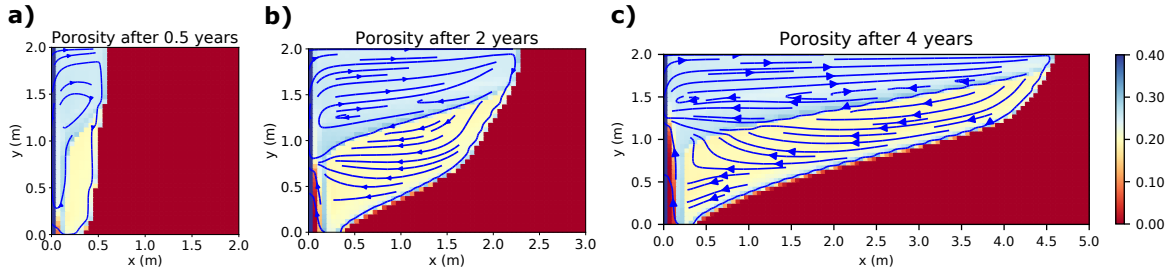

Figure 3.14: Porosity distribution within an a) initially reaction- and advection-dominated system; b,c) in the long run transport-dominated and with an increasing influence of diffusion (scenario: dissolution rate 10^{-5} cm/s and 25 wt.% carnallite).

All other scenarios with dissolution rates above 10^{-6} cm/s were permanently transport-dominated. Diffusion dominated the transport if porosity was low (5 wt.% carnallite) (Table 3.2), resulting in a leaching zone geometry as presented in Figure 3.10. In this case, the growth rate hardly differed for varying dissolution rates (Figure 3.7b-d). If the porosity was slightly higher (10 wt.% carnallite), advection dominated at the beginning and the leaching zone developed a funnel shape, which was about two to three times wider at the hanging wall than at the footwall. The higher the dissolution rate, the more pronounced the funnel shape became; however, the barrier next to the inflow region also extended further upwards. After a few years, Pe regressed below two, and in case of high dissolution rates the dissolution front received a curved funnel shape similar to that in Figure 3.14c. In case of lower dissolution rates (10^{-5} cm/s), the dissolution front was steeper and more similar to that in Figure 3.13c. The sylvinitic zone was present throughout the entire seam thickness and covered the

whole leaching zone behind the barrier, while it made up about 40% of its width at the hanging wall. The higher the barrier extended into the potash seam, the more the leaching zone growth rate was reduced. Finally, diffusion replaced advection as the main transport mechanism. If porosities were medium to high (>10 wt.% carnallite) and the dissolution rate was above 10^{-5} cm/s, the system was always transport-dominated with diffusion exceeding advection in the long run. During the first months or years, high Pe numbers facilitated the formation of a funnel shape according to Figures 3.11a and 3.12, which ended at a height of 0.5-1 m. However, this was also associated with the formation of a flow barrier. Especially if the dissolution rate was 10^{-3} cm/s, the exchange of solutions was quickly inhibited up to a height of more than 1 m and Pe regressed below 2 at the dissolution front, while it remained above 2 for several years in the overall system. As a result, the dissolution front developed in a curved funnel shape (Figure 3.15) and the growth rate decreased while the lower part of the potash seam remained unaffected. The higher the porosity, the faster and deeper the leaching zone could penetrate into the potash seam before diffusion prevailed (Figure 3.15b). A sylvinitic zone was always present for this hybrid form and reached its maximum width slightly below the upper end of the barrier, which was constantly growing with time and may completely prevent the exchange of solutions in the long run.

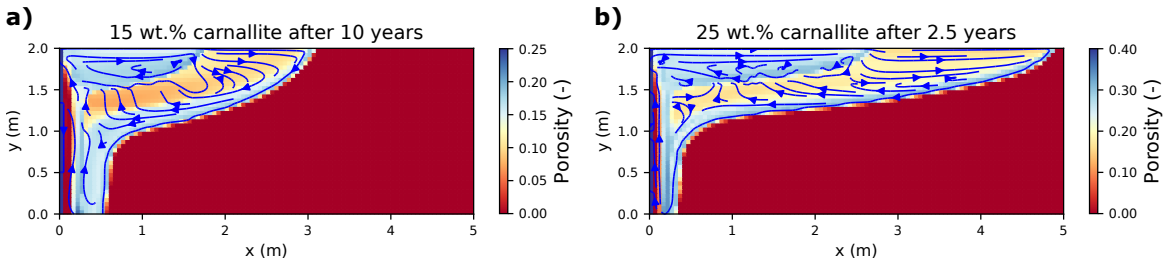

Figure 3.15: Porosity distribution in an initially transport- and advection-dominated system, in the long run diffusion-dominated (scenario: dissolution rate 10^{-3} cm/s, carnallite content a) 15 wt.% and b) 25 wt.%).

3.4 Discussion

The simulation results show that a fundamental distinction must be made between reaction-dominated and transport-dominated systems as well as between diffusion-dominated and advection-dominated systems with regard to the formation of leaching zones within potash seams. Depending on which of the four potential combinations is given, differences in mineralogy as well as in spatial and temporal leaching zone growth will occur. A classification is feasible using the Péclet and Damköhler numbers. The scenario analyses have shown that Pe mainly depends on the amount of carnallite within the potash seam, which is completely dissolved once it comes into contact with undersaturated solution, and thus determines the resulting porosity of the leaching zone. In contrast, Da mainly depends on the dissolution rate of the initially dry rock (Table 3.2).

Assuming the inflow of a NaCl-saturated solution, the fluid in reaction-dominated systems (Da $<$ 1) is neither saturated with respect to carnallite nor with respect to sylvite along the entire dissolution front (Figures 3.8a and 3.9a). This state requires a very low dissolution rate in combination with a minimum porosity, so that the dissolution rate determines the growth rate of the leaching zone. Since the dissolution rate is constant in space and time, a planar dissolution front is formed moving slowly but steadily forward. This results in a matrix of leached halite, with a porosity determined by the volume fraction of the dissolved minerals carnallite and sylvite, reduced by a few percent due to halite precipitation. Since higher porosities correspond to a larger contact area between solution and dry rock, the growth is faster for higher carnallite contents despite identical dissolution rates (Figure 3.7a). The porosity within the leaching zone is homogeneous, whereby a sylvinitic zone does not exist due to the low saturation (Figures 3.8b and 3.9b). Despite only small differences in concentration and fluid density, density-driven flow is established, inducing a mostly vertical concentration gradient in advection-dominated systems (Pe $>$ 2). On the contrary, convection hardly has any influence and the concentration gradient is horizontal in diffusion-dominated systems (Pe $<$ 2). In both cases, the low saturation of the solution with regard to potash salt is not sufficient to create halite precipitation next to the inflow region. Therefore, barrier formation is not observed and leaching zone growth is linear even for longer time periods (Figure 3.7a). However, it must be questioned whether the assumption of thermodynamic equilibrium in a reaction-dominated system is sufficiently accurate. On the other hand, scenario analyses and available field investigations (Koch and Vogel 1980; Steding et al. 2020) show that most systems are dominated by transport and that the assumption of thermodynamic equilibrium is generally reasonable in nature.

In transport-dominated systems (Da $>$ 1), the ratio between advection and diffusion is much more decisive. If the system is diffusion-dominated (Pe $<$ 2), the horizontal concentration gradient causes a uniform transport across the entire seam thickness, and thus a planar dissolution front (Figure 3.10a). Here, the saturations are much higher than in reaction-dominated systems, with sylvinite saturation reached after about 40% of the distance to the dissolution front, resulting in the formation of a wide sylvinitic zone (Figure 3.10b). Its porosity is always slightly lower than that of the halitic zone; however, the latter shows a decrease in porosity especially near the inflow region and the footwall. The halite precipitation occurring there can presumably be attributed to the influx of NaCl solution. Its contact with potash salt naturally leads to halite supersaturation (Koch and Vogel 1980), what can also be expected if it is mixed with potash brine. Due to the weak but nevertheless existing convection, the saturation with respect to potash salts is slightly higher within the lower potash seam area, and hence more precipitation occurs here (Figure 3.10a). Since diffusion-dominated systems require low porosities, even a few percent of additional halite can form a flow barrier. A reduction of the growth rate can be observed over time, but this is mainly due to the

increasing distance between the inflow region and the dissolution front, which causes a decrease in the diffusion rate. In systems dominated by transport and diffusion, the diffusion coefficient plays an important role in the evolution of the leaching zone, and the assumption of a uniform and constant value for all transported species is a strong simplification. However, most approaches to calculate diffusion coefficients depending on the brine composition are not validated for multicomponent systems with high salinities (Anderko and Lencka 1998; Tosca et al. 2011), especially if NaCl is not the main component (Felmy and Weare 1991). Due to the very low porosities within these systems (Table 3.2) and the very slow leaching zone growth (Figure 3.7), the risk potential to mining operations is rather low and uncertainties in temporal scaling are acceptable.

For transport- and advection-dominated systems (Pe $>$ 2), a significant flow barrier formation can be observed, which increasingly impedes the inflow of new NaCl solution, and thus slows down the growth of the leaching zone (Figures 3.12 and 3.15). This is on the one hand due to the full saturation of the solution with respect to potash salts at the dissolution front, and on the other hand due to a much stronger density-driven flow, which forces the saturated solution to flow towards the lower part of the potash seam and the inflow region, creating particularly strong concentration gradients next to it (Figure 3.11a). As a result of the flow barrier formation, the flow velocity decreases sharply and the transport becomes increasingly diffusion-dominated. Although the leaching zone growth rate for this case is by far the fastest in the beginning, it is conceivable that in the long run reaction-dominated systems will expand further, since barrier formation will not impede or even stop the growing process (Table 3.2, Figure 3.7). Another characteristic of transport- and advection-dominated systems is the funnel shape of the leaching zone, which also results from convective flow (Figures 3.11a and 3.12). It causes the solution, which is undersaturated with respect to potash salts, to arrive first at the upper part of the dissolution front, leading to maximum dissolution effects in this area. On its flow towards the model bottom, the solution becomes more saturated until finally rock is not dissolved anymore. The higher the dissolution rate, the earlier this state is reached. Hence, the funnel shape is more concentrated in the upper part of the potash seam and the underlying part that remains unaffected is more pronounced at higher dissolution rates. Within the latter, only the first 25-50 cm next to the inflow region are permeated at the beginning, since convective flow needs to develop first. Later, this area is located behind the halite barrier and contains saturated potash brine and sylvinite. Even within the funnel, the solution is mostly sufficiently saturated to create a sylvinitic zone. However, near the hanging wall its width decreases due to the inflow of NaCl solution.

The simulation results reveal a high qualitative agreement with the field studies by Koch and Vogel (1980), which deal with the formation of sylvinitic alteration zones within carnallite-bearing potash seams. As in the present models, the point of leaching zone initiation is a fault zone that enables the intrusion of saline solutions from the

underlying bedrock. The observed sequence of leached halite, followed by a particularly sylvite-rich alteration zone and finally the unaffected potash seam can be reproduced and explained by using the presented models (Figures 3.10b and 3.11b). The special case without the development of a sylvinitic zone is also mentioned by Koch and Vogel (1980) and associated with large fluid inflow rates. No statements are made about the shape and the dimensions of this special type of leaching zone, so that a comparison with the simulation results achieved for reaction-dominated systems (Figures 3.8 and 3.9) is not feasible. On the other hand, leaching zones with a sylvinitic zone are usually described by Koch and Vogel (1980) as being several meters wide and showing a clear inclination of the mineralogical boundaries as well as a preferential leaching near the hanging wall, which corresponds very well with the present findings. Many field investigations do not show any leaching within the lower half of the potash seam, resulting in leaching zone shapes as shown in Figure 3.15. The occurrence of narrower leaching zones is explained by a low or relatively short solution inflow. The simulation results further suggest that growth comes to a standstill if a lack of solution supply occurs; however, the main cause for this is not a lack of ascending solution but the precipitation of halite which leads to flow barrier formation. Whether this also occurs in nature is not described by Koch and Vogel (1980). In the present simulations, high concentration gradients are responsible for halite precipitation, whereby especially an increase in Mg^{2+} concentration induces a strong reduction of the halite solubility. It is conceivable that the assumption of a constant solution composition at the model boundary causes or at least artificially intensifies this phenomenon. The assumption of constant, uniform diffusion coefficients may also falsify concentrations and saturation within this area. However, the observations of Koch and Vogel (1980) basically support the simulation results regarding the mineralogy and shape of the leaching zones.

The simulated leaching zone shapes have been observed on the laboratory scale as well. For example, caverns with a nearly planar dissolution front were documented by Field et al. (2019), whereby nearly saturated NaCl solution was pumped through rock salt samples in vertical direction. On the other hand, caverns with more funnel-like shapes as shown in Figures 3.11a and 3.12 were observed when artificial seawater was used as leaching solution. The growth rate of the funnel-shaped caverns was significantly higher, although the pumping rate was the same. According to Field et al. (2019), the higher growth rate and the decreasing cavern width along the flow path are mainly due to an increase in saturation and the resulting decrease in the dissolution rates. For almost saturated NaCl solutions, this effect is smaller, with the cavern width hardly changing along the flow path. On the other hand, Gechter et al. (2008) and Weisbrod et al. (2012) observed funnel-shaped caverns as well when pumping water horizontally through rock salt samples and explained this shape by density-driven flow. Consequently, the different cavern shapes in Field et al. (2019) could also result from different Pe or Da numbers. The caverns generated at laboratory-scale conditions are cavities with presumably turbulent flow conditions, with diffusion

playing only a minor role in species transport. The high dissolution rates in case of seawater are consistent with transport-dominated systems, and thus with the funnel shape (Figure 3.12), which was observed by Gechter et al. (2008) as well for highly undersaturated solutions. Conversely, highly saturated solutions reduce the dissolution rate according to Field et al. (2019), what is consistent with a reaction-dominated system and the resulting planar dissolution front (Figures 3.8a and 3.9a).

The results of the scenario analysis indicate that usually hybrid forms of the cases discussed above can be found in situ (Figures 3.13, 3.14 and 3.15). The classification highly depends on the flow velocity and therefore on the porosity-permeability relationship. Only a few relationships are available for salt rock with medium or high porosities (Müller-Lyda et al. 1999; Spangenberg et al. 1998; Xie et al. 2011). However, these relationships were derived from crushed rock salt samples that were compacted by mechanical loading. In the medium to long run, deformations in rock salt reduce the effective pore space (Munson 1997) but the main porosity changes in leaching zones result from dissolution and precipitation processes. Several approaches are available to describe the effect of chemical reactions on permeability (Zarrouk and Sullivan 2001), but future investigations for leached potash salt are necessary to reduce the model uncertainty. The same accounts for the dissolution rate of varying potash salt compositions. Taking the different solubilities and saturation indices of minerals into account may result in a more selective dissolution process and different leaching zone shapes. However, laboratory data allowing for more precise calculations are so far only partially available.

The scenario analysis and the comparison with Koch and Vogel (1980) indicate that most leaching zones in nature represent transport-dominated systems which are advection-dominated in the beginning and diffusion-dominated in the long run. The reactive transport model can be used for a qualitative description of their shape as well as for a quantitative description of their mineralogy. The good agreement with literature data qualitatively confirms both, while for a fully quantitative model validation further investigations on laboratory and field scale are required.

3.5 Conclusions and Outlook

The reactive transport model developed and presented here enables the temporal and spatial reproduction of the formation of leaching zones for the first time. The scenario analyses for a carnallite-bearing potash seam show that growth rate, resulting shape and mineralogy mainly depend on the fluid flow velocity governed by density-driven flow, which can be classified by the Péclet and Damköhler number. In principle, four cases need to be distinguished: (1) reaction- and diffusion-dominated ($Da < 1$ and $Pe < 2$); (2) reaction- and advection-dominated ($Da < 1$ and $Pe > 2$), (3) transport- and diffusion-dominated ($Da > 1$ and $Pe < 2$) and (4) transport- and advection-dominated

systems (Da $>$ 1 and Pe $>$ 2). Only in the latter case, density-driven flow has a significant influence.

The first two cases occur if the dissolution rate is very low, impeding highly saturated solution at the dissolution front. The leaching zone growth proceeds slowly and evenly across the entire seam thickness and neither a sylvinitic zone nor a flow barrier are formed. At low porosities, diffusion dominates (case 1), while at high porosities advection prevails (case 2). The scenario analyses reveal that reaction- and diffusion-dominated systems usually become transport-dominated over time (Da rises $>$ 1) resulting in the formation of a sylvinitic zone, while the dissolution front remains planar. At dissolution rates $>10^{-6}$ cm/s, the system is generally transport-dominated. Below 10% porosity, advection has almost no influence (case 3) and the dissolution front remains planar; however, a sylvinitic zone and a weak fluid flow barrier with slightly reduced porosities are formed. The latter consists of halite which is precipitated near the inflow region, and thus inhibits the in- and outflow of solution from the leaching zone. At porosities $\geq$10%, density-driven flow gains influence and a funnel-shaped, rapidly growing leaching zone including a sylvinitic zone develops, while the lower half of the potash seam remains practically unaffected (case 4). This is the most common case in the scenario analyses. Due to the rapid barrier formation starting at the footwall, in- and outflow of solution diminish and flow velocity decreases over time. As a result, the system becomes diffusion-dominated (Pe sinks $<$ 2) and the growth of the leaching zone stagnates after a few years, especially in case of very high dissolution rates.

Available laboratory and field data support the simulation results. Dissolution experiments with water (Gechter et al. 2008; Weisbrod et al. 2012), seawater (Field et al. 2019) and almost saturated NaCl solution (Field et al. 2019) on rock salt samples also yielded nearly planar dissolution fronts for low dissolution rates (NaCl solution), and a funnel-shaped cavern for high dissolution rates (water, seawater). Natural leaching zones within carnallite-bearing potash seams often show the same inclined shape of the dissolution front as well as the same proportions and mineralogy that the present models yield for initially transport- and advection-dominated systems (Figure 3.15) (Koch and Vogel 1980). The reaction-dominated cases (1) and (2) provide an explanation for the formation of leaching zones described by Koch and Vogel (1980), where a sylvinitic zone does not occur. However, more detailed laboratory and field studies are required to further validate the present models.

Regarding the hazard potential to subsurface mining operations, case (4) is most critical in the short term since the leaching zone expands over several meters within the potash seam in only a few years. However, as soon as the flow barrier inhibits solution exchange, the leaching zone represents a closed system that remains stable over time and can therefore be safely controlled. On the contrary, in case (1) and (2) the slow expansion continues over long periods of time without a decrease in growth rate. Additionally, the entire potash seam is affected instead of only the upper half and

the porosity is higher compared to transport-dominated systems since no sylvinitic zone occurs. Higher porosities reduce the mechanical stability of the halite matrix and raise the amount of brine that could leak out of it. Accordingly, reaction- and advection-dominated systems (case 2) may cause a higher hazard potential in the long term.

In the next step, it is planned to apply the model presented here to potash seams that also contain kieserite ($MgSO_4 \cdot H_2O$) and anhydrite ($CaSO_4$), which are two other important potash salts. Due to the resulting hexary system, which additionally contains Ca^{2+} and ${SO_4}^{2-}$, a series of additional secondary minerals has to be expected, which will probably lead to the formation of more complex transition zones (Steding et al. 2020). To control mass balance errors due to differences between the volume of the pore and the solution within a cell, it is planned to include source and/or sink terms in future source code developments. Furthermore, heterogeneities in the composition of the potash seams will be taken into account, as these can have a strong influence on the shape of leaching zones (Field et al. 2019; Koch and Vogel 1980). It is also planned to adapt the model in order to include saturation-dependent dissolution rates. In doing so, the formation of leaching zones and cavernous structures within potash seams can be investigated in further detail in order to quantify their long-term behavior and to assess their hazard potential.

4 | How Insoluble Inclusions and Intersecting Layers Affect the Leaching Process within Potash Seams

Abstract

Potash seams are a valuable resource containing several economically interesting, but also highly soluble minerals. In the presence of water, uncontrolled leaching can occur, endangering subsurface mining operations. In the present study, the influence of insoluble inclusions and intersecting layers on leaching zone evolution was examined by means of a reactive transport model. For that purpose, a scenario analysis was carried out, considering different rock distributions within a carnallite-bearing potash seam. The results show that reaction-dominated systems are not affected by heterogeneities at all, whereas transport-dominated systems exhibit a faster advance in homogeneous rock compositions. In return, the ratio of permeated rock in vertical direction is higher in heterogeneous systems. Literature data indicate that most natural potash systems are transport-dominated. Accordingly, insoluble inclusions and intersecting layers can usually be seen as beneficial with regard to reducing hazard potential as long as the mechanical stability of leaching zones is maintained. Thereby, the distribution of insoluble areas is of minor impact unless an inclined, intersecting layer occurs that accelerates leaching zone growth in one direction. Moreover, it is found that the saturation dependency of dissolution rates increases the growth rate in the long term, and therefore must be considered in risk assessments.

4.1 Introduction

The role of potash seams within salt deposits can be viewed from different perspectives: on the one hand, they are a valuable resource that has been mined for many decades; on the other hand, they represent potential risks for technical caverns and subsurface waste repositories (Warren 2017). However, both perspectives consider the uncontrolled leaching of potash seams as highly critical. Whether water contact is enabled by geological fault zones or mining activities: in both cases, the increased solubility of potash salt causes a preferential expansion of leaching zones, jeopardizing the integrity and mechanical stability of mines or technical caverns (Boys 1993; Keime et al. 2012; Mengel et al. 2012; Prugger and Prugger 1991). In order to assess the hazard potential of leaching zones in potash seams, their evolution has to be described in space and time.

Steding et al. (2021b) developed a reactive transport model complemented by the 'interchange approach' to reproduce the complex interplay between chemical reactions and density-driven transport of species within potash seams. The authors showed that leaching zones can be classified into four different groups based on the Péclet (Pe) and Damköhler (Da) numbers, which indicate if a system is dominated by reactions (Da < 1) or transport (Da > 1), and if species transport is dominated by diffusion (Pe < 2) or advection (Pe > 2). However, only homogeneous potash seams have been investigated thus far. Studies on technical cavern construction in rock salt reveal that inclusions or intersecting layers of insoluble materials, such as mudstone, gypsum or sandstone, lead to highly irregular cavern shapes (Jinlong et al. 2020; Li et al. 2018; Thoms and Gehle 1999). Furthermore, inclined layers can cause an asymmetric expansion of leaching zones (Fokker 1995). To investigate if similar phenomena occur within potash seams, heterogeneous rock distributions need to be examined. In addition, mineralogical heterogeneity and the associated variations in dissolution rate need to be taken into account, because these can significantly influence dissolution structure, especially at high Péclet numbers (Liu et al. 2017; Wei et al. 2019).

For this purpose, the reactive transport model presented by Steding et al. (2021b) was extended by mineral-specific, saturation-dependent dissolution rates, and a scenario analysis under density-driven flow conditions was performed. Thereby, six generic mineral distributions were investigated, with insoluble areas ranging from several small inclusions to one continuous layer. The main objective was to determine the influence of insoluble layers and inclusions on the evolution and hazard potential of leaching zones within potash seams, and if a risk assessment based on the Pe and Da numbers is still feasible.

4.2 Materials and Methods

The concept of the applied reactive transport model is shown in Figure 4.1. Each simulation time step starts with the solution of the partial differential equations for the fluid flow and transport of chemical species using the TRANsport Simulation Environment (TRANSE) (Kempka 2020). TRANSE is coupled with the geochemical reaction module PHREEQC (Parkhurst and Appelo 2013), applied in combination with the THEREDA database (Altmaier et al. 2011). In the second calculation step, PHREEQC is used to update fluid densities and mineral saturations following transport. After that, the 'interchange' step is performed, which describes the dissolution of minerals from (nearly) dry into permeated cells and allows the dissolution front to progress (Steding et al. 2021b). The terms 'dry' and 'permeated' are used in view of the fluid saturation in the pore space, whereas the term 'saturated' refers to the chemical equilibration of the solution with respect to salt minerals. In the final calculation step, the chemical reactions resulting from transport and interchange are determined using PHREEQC. Thereby, thermodynamic equilibrium is assumed within each cell. The

updated concentrations and fluid properties, such as density and viscosity, are then transferred back to TRANSE to calculate flow and transport in the next simulation time step (Figure 4.1). More details on this procedure are presented in Steding et al. (2021b). The interchange of minerals and solution has been extended in the present study and will be described in detail in the following subsection.

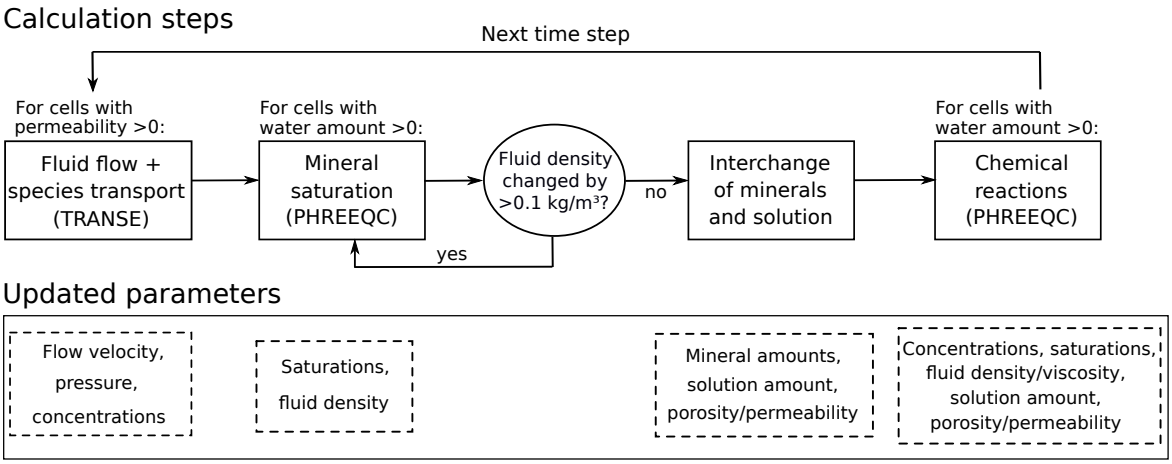

Figure 4.1: Flow sheet of the coupled reactive transport model: calculations undertaken at each simulation time step and associated output parameters (modified from Steding et al. (2021b)).

4.2.1 Extended Interchange Approach

In Steding et al. (2021b), constant dissolution rates were used to calculate the interchange of salt minerals. However, it is known that close to equilibrium, the dissolution rates decrease considerably (Durie and Jessen 1964; Palandri and Kharaka 2004; Röhr 1981). Based on the results of Alkattan et al. (1997), a linear saturation dependency is assumed:

$$rate = k_{max} \cdot (1 - \Omega) \quad \text{with } \Omega = Q/K = 10^{SI} \tag{4.1}$$

where k_{max} (cm/s) is the dissolution rate in an infinitely dilute solution. Q is the activity product and K the equilibrium constant. The saturation index SI (-) results from log(Q/K). Leaching zones can contain several primary and secondary minerals that differ in maximum dissolution rate k_{max} as well as in saturation state (Steding et al. 2020); therefore, an average dissolution rate for the potash seam (Figure 4.2a) is not applicable here. Instead, the dissolution rate according to Equation 4.1 and the amount of minerals dissolved into an adjacent cell Min_{sol} (mol) need to be calculated individually for each mineral (Figure 4.2b). Thereby, $rate$ (cm/s) always refers to the saturation state of the solution into which the mineral is dissolved. Between Cell A and Cell B, the amount of interchanged mineral n can be calculated with Equation 4.2:

$$Min_{sol,n} = rate_n \cdot Min_{A,n}/di \cdot (\Phi_B - \Phi_A)/(1 - \Phi_A) \cdot dt \tag{4.2}$$

The amount of mineral n present in Cell A, $Min_{A,n}$ (mol), divided by the cell diameter perpendicular to the dissolution front di (cm) gives the affected amount of mineral n if the width of 1 cm is dissolved from Cell A. To take into account the contact area between the rock in Cell A and the solution in Cell B, this amount is multiplied with the porosity difference between both cells ($\Phi_B - \Phi_A$) and divided by the volume fraction of the rock in Cell A ($1 - \Phi_A$). If $\Phi_A \geq \Phi_B$, the interchange is zero, i.e., minerals can only be dissolved into adjacent cells with higher porosity. dt (s) is the length of the simulation time step. If the solution in Cell B is already saturated with respect to n, $rate_n$ becomes zero and the mineral is not dissolved. The interchange takes place at each interface between two cells within the model. The volumes of all minerals dissolved at one interface are cumulated to determine the amount of solution that is transferred in return to keep the volume of both cells constant (Figure 4.2).

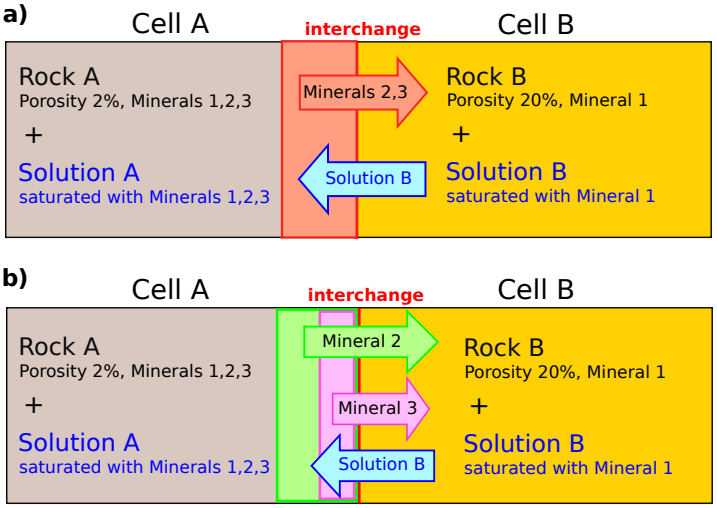

Figure 4.2: Sketch of the interchange approach with a) constant and b) variable dissolution rates. A defined amount of each mineral according to Equation 4.2 is dissolved from a cell with low porosity (Cell A) into an adjacent cell with higher porosity (Cell B). These amounts are cumulated, and the solution is transferred into the cell with lower porosity to fill the newly formed pore space (modified from Steding et al. (2021b)).

At the dissolution front, the interchange approach enables originally dry cells to receive solution for the first time from an adjacent cell (Figure 4.3a). The solution needs to be undersaturated with at least one of the minerals from the dry rock; otherwise, no interchange takes place. Newly permeated cells are divided into a permeated and a dry sub-cell to avoid immediate drying out due to high solid-fluid-ratios (Figure 4.3b). In cases of constant dissolution rates, all minerals in the permeated part were assumed to be in equilibrium with the solution of the cell, whereas minerals in the dry part were not considered in the subsequent calculation of chemical reactions (Steding et al. 2021b). However, as shown in Figure 4.3a, the varying dissolution rates challenge the identification of a clear borderline between dry and permeated or equilibrated and non-equilibrated parts, respectively. It can be seen that Mineral 2 has the highest dissolution rate, and therefore limits the region of increased porosity where mineral solution occurs (green). Within this region, it is reasonable to equilibrate the

solution with regard to Mineral 2. However, Mineral 3 has a lower dissolution rate, and can therefore only be equilibrated with the solution in the pink subregion. Following this reasoning, one would end up with an additional subregion for each mineral, which is of course not practical. Instead, the permeated part within each cell is split up into minerals that are in equilibrium with the solution (equilibrated minerals Min_{eq}) and such that are not (non-equilibrated minerals Min_{neq}; Figure 4.3b). Thereby, the volume of the permeated part V_{per} is determined by the most soluble mineral (Mineral 2, green area). Outside of this area, the salt rock is still dry and the composition Min_{dry} corresponds to the originally unaffected potash seam. In contrast, minerals within the permeated area V_{per} are surrounded by solution, whereby it is not yet in equilibrium with all minerals. Minerals that remain undissolved during the interchange due to their lower dissolution rates (Mineral 1 and parts of Mineral 3 within the green area, Figure 4.3a) are assigned to the non-equilibrated minerals Min_{neq}. In contrast, precipitations from Solution B belong to the minerals equilibrated with the solution Min_{eq}.

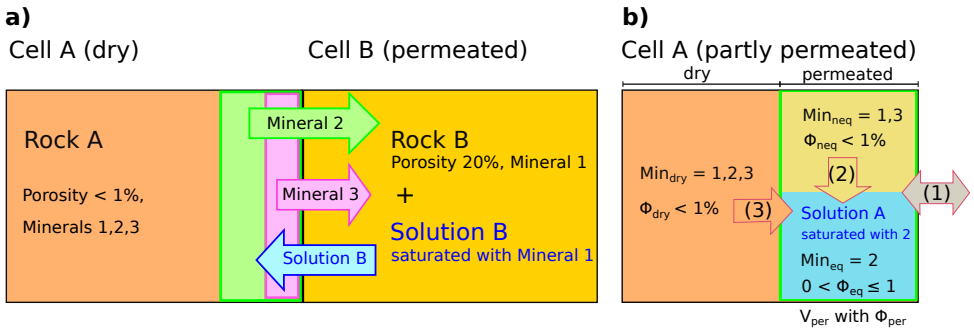

Figure 4.3: Sketch of the interchange at the dissolution front a) resulting in a partly permeated cell b). The permeated part V_{per} contains minerals Min_{eq} that are in equilibrium with Solution A and minerals Min_{neq} that are not. In addition to interchange with adjacent cells (1), the internal dissolution of non-equilibrated minerals (2) and dry minerals (3) is considered following Equations 4.2, 4.4 and 4.5 (modified from Steding et al. (2021b)).

In the case of partly permeated cells, three different types of dissolution can occur (Figure 4.3b): the first one is interchange with the (fully permeated) adjacent cells according to Equation 4.2. For this, all three mineral compositions Min_{dry}, Min_{eq} and Min_{neq}, are added together to determine Min_A. Φ_A is the average porosity of the cell calculated from the volume of Min_A related to the cell volume. If the partly permeated cell shows a higher average porosity than the fully permeated one, the interchange of minerals is possible in the reverse direction as well. The dissolved amount of each mineral is split among Min_{dry}, Min_{eq} and Min_{neq}, according to their contribution to the total amount of this mineral. The solution transferred in return is mixed with the pre-existing solution in the permeated part. The chemical reactions resulting from the mixing and the following equilibration with Min_{eq} are determined after the interchange (Figure 4.1).

In addition to the interchange, internal dissolution processes within cells containing dry (Min_{dry}) or non-equilibrated (Min_{neq}) minerals need to be taken into account (Figure 4.3b). The interface area between a dry part and the adjacent permeated part(s) is assumed to be constant over time. At the beginning, when the cell is completely dry, the adjacent permeated area is the neighbor cell and dry minerals can only be dissolved via interchange. Accordingly, the interface area is the interface between both cells, which is the cell width multiplied by its height. As V_{per} increases, Min_{dry} makes up a smaller part of the total mineral amount within the partly permeated cell and its interchange amount decreases. At the same time, the interface area between the dry and permeated parts within the partly permeated cell increases, enhancing the internal dissolution of dry minerals. To account for that, the permeation state of the cell S_{per} (-) is calculated referring to the volume of the permeated part V_{per} in relation to the cell volume V_{cell}:

$$S_{per} = V_{per}/V_{cell} \tag{4.3}$$

The higher S_{per}, the more of the dry rock is dissolved into the solution of its own cell (by internal dissolution) instead of the adjacent cell (by interchange). Equation 4.4 is used to determine the amount of mineral n dissolved from Min_{dry} into the solution within the permeated part:

$$Min_{sol,dry,n} = rate_n \cdot Min_{dry,n}/\big(di \cdot (1 - S_{per})\big) \cdot \Phi_{per} \cdot S_{per} \cdot dt \tag{4.4}$$

Generally, Equation 4.4 is identical to Equation 4.2, but multiplied by the permeation state S_{per}. $rate$ is calculated from the saturation state within the partly permeated cell using Equation 4.1. In order to determine the affected amount of mineral n if a width of 1 cm of the dry part is dissolved, the present amount, $Min_{dry,n}$ (mol), is divided by the diameter of the dry part perpendicular to the dissolution front. Therefore, the cell diameter di (cm) is now multiplied by the volume ratio of the dry part $(1-S_{per})$. The porosity within the dry part is nearly zero, simplifying the term $(\Phi_B-\Phi_A)/(1-\Phi_A)$ in Equation 4.2 to Φ_B, which equals the average porosity of the permeated part Φ_{per}. The dissolved amount of each mineral $Min_{sol,dry}$ is added to Min_{eq}. The same applies to precipitations resulting from the equilibration after the interchange (Figure 4.1). Similar to the interchange of dry minerals, the highest dissolution rate according to Equation 4.1 determines the volume that is newly added to the permeated part V_{per} (Figure 4.3). For minerals with lower dissolution rates, the difference between the amount within this volume and the dissolved amount is added to Min_{neq}.

Finally, the internal dissolution of non-equilibrated minerals (Min_{neq}) has to be taken into account (Figure 4.3b). These minerals belong to the permeated part of a cell and are already surrounded by solution. However, when the area is permeated for the first time, their dissolution rate is too low to dissolve all minerals. Basically, there are two possible reasons for this: either the maximum dissolution rate k_{max} is (much)

lower than that of the other minerals, or the solution is already (nearly) saturated with these. In the latter case, one could add them to Min_{eq} without changing the solution or rock composition of the permeated part. However, the solution composition changes over time, and originally saturated minerals may become undersaturated. In this case, an immediate equilibration could induce errors because the lower dissolution rates would be neglected. To account for the variation of dissolution rates, Min_{neq} is added stepwise to the solution. The dissolved amount $Min_{sol,neq}$ (mol) of each mineral is determined by Equation 4.5:

$$\begin{aligned} Min_{sol,neq,n} &= rate_n \cdot Min_{neq,n}/V_{neq} \cdot contact\_area \cdot dt \\ &= rate_n \cdot Min_{neq,n}/V_{neq} \cdot factor \cdot di \cdot 1\text{m} \cdot \Phi_{eq} \cdot S_{per} \cdot dt \end{aligned} \tag{4.5}$$

The rate law is similar to those used for interchange (Equation 4.2) and the internal dissolution of dry minerals (Equation 4.4). Again, $rate$ (cm/s) is calculated from the saturation state within the partly permeated cell according to Equation 4.1. Min_{neq} (mol) divided by the volume of the non-equilibrated minerals V_{neq} (cm^3) and multiplied by the contact area between non-equilibrated minerals and solution (cm^2) gives the amount of mineral n if a width of 1 cm of the non-equilibrated minerals is dissolved. V_{neq} is calculated from the mineral amounts and densities in Min_{neq}, neglecting small porosities. However, the contact area between non-equilibrated minerals and solution is hard to determine, because the pore structure and spatial arrangement of the different minerals in the original rock are unknown. Therefore, a variable called $factor$ (-) is introduced. If it is set to 1, a rectangular contact area similar to that between Min_{dry} and the solution (Equation 4.4) is assumed. This can be seen as a minimum value. If precipitations do not block the access to Min_{neq}, the contact area to the solution flowing between the non-equilibrated minerals should be several times higher. Therefore, it can make sense to simplify the approach and to directly add Min_{neq} to Min_{eq}. In this case, it is assumed that the contact area is large enough to immediately equilibrate minerals and solution within an originally dry volume as soon as the first mineral has been dissolved from it. However, this is only realistic if the maximum mineral dissolution rates do not vary by several orders of magnitude. Furthermore, the first mineral dissolved should make up more than a few vol.% of the dry rock in order to create a sufficiently large contact area. If this is not the case, the internal dissolution of non-equilibrated minerals has to be considered. For some minerals, this may take much longer than the permeation of the cell, i.e., fully permeated cells can still contain non-equilibrated minerals (Figure 4.4). For the interchange according to Equation 4.2, Min_{eq} and Min_{neq} are added up to determine Min_A and Φ_A is defined as the average porosity of equilibrated and non-equilibrated areas.

Generally, it is assumed that minerals belonging to Min_{eq} are first dissolved if an undersaturation occurs. As a result, the interchange or internal dissolution of minerals present in Min_{eq} is not possible. Chemical reactions resulting from the processes de-

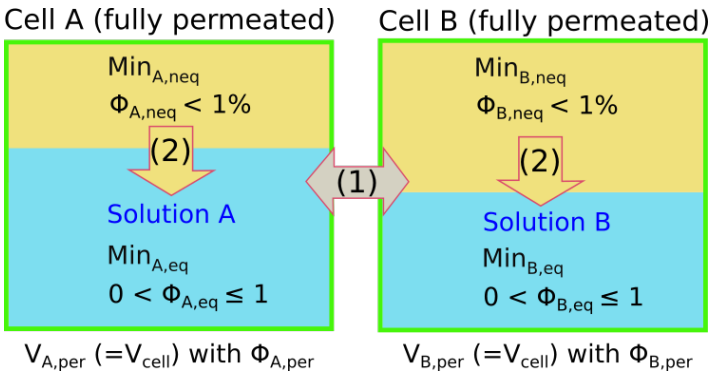

Figure 4.4: Fully permeated cells can still contain non-equilibrated minerals due to their lower dissolution rates. Internal dissolution (2) within a cell reduces the amount of non-equilibrated minerals; additionally they are considered for interchange (1). The average porosity of the permeated part Φ_{per} corresponds to the average porosity of the cell and is used for interchange as well as for flow and transport calculations.

scribed above are determined in the final calculation step of the simulation (Figure 4.1). Thereby, thermodynamic equilibrium is assumed in every cell. The average porosity of the cell is always used in the flow and transport simulation step.

4.2.2 Scenario Analysis

In order to study the influence of heterogeneities, leaching processes in a carnallite-bearing potash seam containing insoluble layers or inclusions were simulated. Carnallitite is a very common, globally occurring potash salt whose leaching behavior was studied for homogeneous rock compositions by Steding et al. (2021b). It was found that transport- and advection-dominated systems (Da $>$ 1 and Pe $>$ 2) are most common and also most critical in the short term with regard to hazard potentials, whereas reaction- and advection-dominated systems (Da $<$ 1 and Pe $>$ 2) become more critical in the long term. Both cases were investigated in this study to identify possible differences in the effect of heterogeneities.

According to Steding et al. (2021b), 25 wt.% carnallite is a sufficiently high ratio to produce Pe $>$ 2 and low enough to ensure that Darcy flow is still maintained. Therefore, a carnallite-bearing potash seam composition of 25 wt.% carnallite ($KMgCl_3 \cdot 6\,H_2O$), 72 wt.% halite (NaCl) and 3 wt.% sylvite (KCl) was applied in all scenarios, corresponding to the volume fractions shown in Figure 4.5. Mineral densities and dissolution properties are provided in Table 4.1. The dissolution rate k_{max} strongly depends on the hydrodynamic boundary conditions: it increases with flow velocity (Yang et al. 2017) and reaches values under turbulent flow conditions that are at least one order of magnitude higher than that for laminar flow (Alkattan et al. 1997; Durie and Jessen 1964). This is due to most salt minerals showing transport-controlled dissolution behavior, i.e., k_{max} is controlled by the thickness of the diffusive boundary layer at the mineral surface (Alkattan et al. 1997; De Baere et al. 2016; Hoppe and Winkler 1974). The boundary layer thickness, and consequently k_{max}, depend on the flow velocity, diffusion coefficients and surface roughness (Ahoulou et al. 2020; Dreybrodt and Buh-

mann 1991; Dutka et al. 2020; Raines and Dewers 1997). Based on the values of Röhr (1981), an average k_{max} of $5 \cdot 10^{-4}$ cm/s was applied to all three minerals in Table 4.1. However, this is an upper value because it refers to convection in open cavities. It can be expected that convection within a porous leaching zone results in smaller flow velocities, and therefore in smaller dissolution rates. Accordingly, a second k_{max} of $5 \cdot 10^{-6}$ cm/s was taken into account to ensure that both transport- (Da $>$ 1) and reaction-dominated (Da $<$ 1) systems are investigated (Steding et al. 2021b).

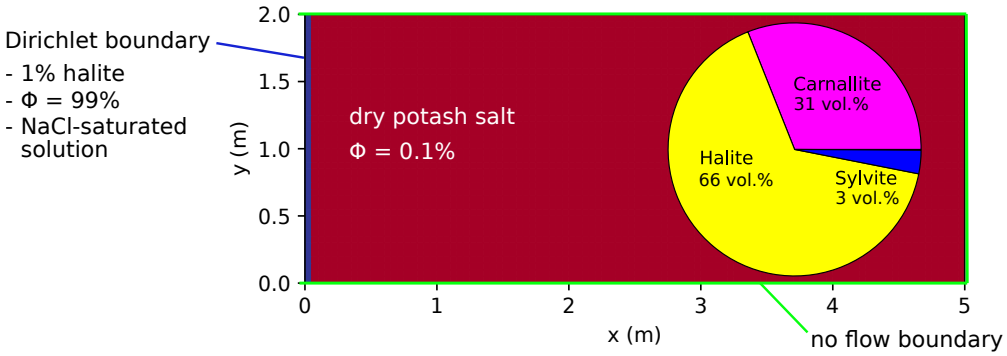

Figure 4.5: Initial and boundary conditions: the inflow region is prescribed by a Dirichlet boundary (blue line); all other boundaries are impermeable (green lines); the models are initialized as dry with homogeneous potash salt (red, mineralogical composition shown) and halite inclusions according to Figure 4.6 (modified from Steding et al. (2021b)).

Table 4.1: Potash salt mineral densities and dissolution properties (modified from Steding et al. (2021b)).

Mineral	Density (kg/m^3)	Reaction equation (dissolution)	Log K
Carnallite	1,600	$KMgCl_3 \cdot 6\,H_2O \longrightarrow 3\,Cl^- + 6\,H_2O + K^+ + Mg^{2+}$	4.33
Halite	2,170	$NaCl \longrightarrow Cl^- + Na^+$	1.586
Sylvite	1,990	$KCl \longrightarrow Cl^- + K^+$	0.915

The 2D model height was 2 m, representing the typical thickness of potash seams in Germany, whereas the model width was 5 m with a discretization of 101 x 41 cells (Figure 4.5). At the start of the simulation, the entire model consisted of dry potash salt with a porosity of 0.1%. Natural caverns and leaching zones are commonly formed in the vicinity of tectonic fault systems which enable fluid migration (Höntzsch and Zeibig 2014). Due to the fact that the ascending solution has to cross several rock salt layers before it reaches the potash seam, it is usually NaCl-saturated. To represent such a fault zone, a Dirichlet boundary was used (Figure 4.5). It maintains a constant solution composition and porosity at the left model boundary, assuming a high fluid and mineral exchange rate within the fault zone. The other boundaries were considered as impermeable without any pre-defined pressure gradient applied. The 2D model made use of the horizontally symmetric expansion of leaching zones to be expected if a potash seam has the same composition in both horizontal directions. Seen from the fault zone, the starting point of the leaching process, only one direction was simulated by taking advantage of the symmetry to reduce the required computational time.

If carnallite-bearing potash seams come into contact with NaCl-saturated brine, carnallite is always dissolved first, triggering the precipitation of sylvite and halite (Koch and Vogel 1980). Equation 4.6 gives the overall reaction:

$$\mathrm{KMgCl_3 \cdot 6\,H_2O + brine\,(NaCl) \longrightarrow KCl + NaCl\,(brine) + brine\,(MgCl_2, KCl, NaCl)} \tag{4.6}$$

In contrast, halite is not dissolved from the potash seam (Koch and Vogel 1980; Steding et al. 2021b), resulting in areas of pure halite (further referred to as halitic areas), acting as barriers to fluid flow. To investigate their influence on leaching zone evolution and hazard potentials, six generic rock distributions were considered. As shown in Figure 4.6, the first three represented a potash seam (red) with intersecting layers of halite (grey). These layers were 30 cm thick and showed inclinations of 0° or ±10°, respectively (Figure 4.6a-c). To ensure that boundary conditions are comparable, the layers always started at the same height at the center of the fault zone. In the other three cases, the potash seam contained halite inclusions ranging from 10 cm x 10 cm (Figure 4.6d) to nearly continuous, horizontal layers (Figure 4.6f). Their distribution was created with GSTools (Müller and Schüler 2021), using correlation lengths of 2:1, 17:0.5 and 34:1 in the horizontal direction. In all six cases, the halitic area made up between 13% and 15% of the potash seam and the surrounding potash salt was homogeneous with the composition shown in Figure 4.5. For comparison, an additional case without any halitic areas was considered.

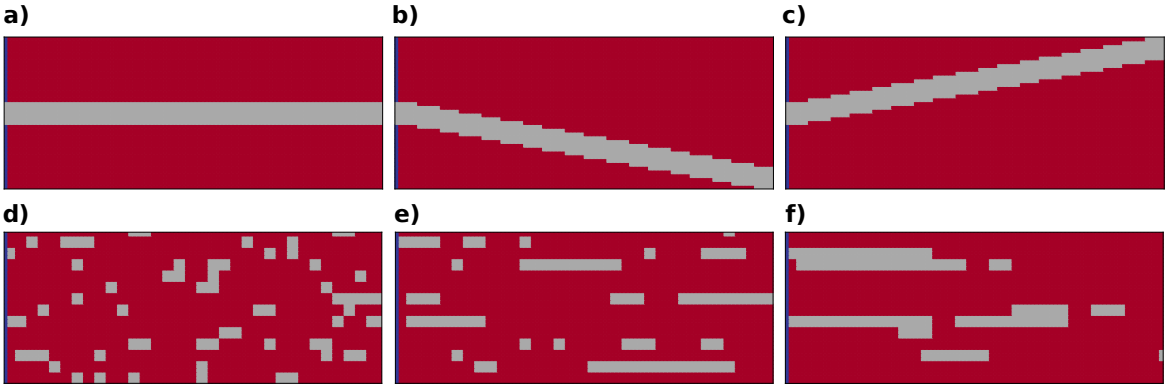

Figure 4.6: Heterogeneous rock distributions examined: The homogeneous potash salt (red) shown in Figure 4.5 is veined by layers with a) 0°, b) +10°, c) −10° inclination or inclusions of pure halite with correlation lengths of d) 2:1, e) 17:0.5 and f) 34:1 that make up 13-15% of the potash seam.

For flow and transport calculations, the porosity-permeability relationship presented by Xie et al. (2011) was applied. Carnallite is dissolved first and makes up >30% of the rock volume; therefore, a relatively large contact area between the solution and remaining minerals, sylvite and halite, can be assumed. Both minerals show the same maximum dissolution rate k_{max} as carnallite, facilitating a quick equilibration in the case of undersaturations. Therefore, non-equilibrated minerals were neglected in this study. Instead, sylvite and halite were immediately added to the equilibrated part

Min_{eq} as soon as the carnallite in their surroundings was dissolved. The diffusion coefficients of all four transported species Na^+ , Cl^-, K^+ and Mg^{2+} were assumed to be equal and constant: an average value of $D_f = 1.5 \cdot 10^{-9}\,m^2/s$ was chosen based on the study by Yuan-Hui and Gregory (1974). The fluid compressibility was set to $c_f = 4.6 \cdot 10^{-10}\,1/Pa$. Temperature differences are negligible for a model height of 2 m; therefore, all simulations were undertaken at isothermal conditions at a temperature of 25°C. Accordingly, the density-driven convective flow exclusively occurred due to dissolution and precipitation processes. The formation of leaching zones was simulated until the right model boundary was reached by the reaction front.

4.3 Results

4.3.1 Leaching Zone Growth

Figure 4.7 shows the evolution of the ratio between permeated and total rock volume (halitic areas not included). In cases of low dissolution rates ($k_{max} = 5 \cdot 10^{-6}\,cm/s$), the leaching zone growth was nearly linear (Figure 4.7a,b). For all rock distributions, it took 13-14 years for the simulations to meet the stop criterion with 96% of the (non-halitic) rock being permeated. Only in the case of +10° inclination, the growth rate started to decrease after approximately six years (Figure 4.7a), with only 85% of the rock being permeated at the end. Halite inclusions led to a less regular growth rate compared to the homogeneous case, but large deviations from linear growth were not observed (Figure 4.7b).

In cases of high dissolution rates ($k_{max} = 5 \cdot 10^{-4}\,cm/s$), the differences between rock distributions increase (Figure 4.7c,d). Along a homogeneous potash seam, the leaching zone expands to the right model boundary in two years, showing only a slight decrease in growth rate. However, only 50% of the rock become permeated, whereas the other half is not affected. In contrast, heterogeneous potash seams show permeation ratios of 59% to 72%, taking up to 3.6 years until the right model boundary is reached. Intersecting halite layers result in different evolutions depending on the inclination (Figure 4.7c). In cases of a 0° inclination, the permeation speed is slightly faster than for the homogeneous case, but the stop criterion is only met when 72% of the rock is permeated. Therefore, it takes 3.6 years instead of the 2 years in the homogenous case. In the case of a +10° inclination, the leaching zone growth is slower and only 60% of the rock is permeated within the same time period. An inclination of −10° (Figure 4.6c) causes the highest permeation speed, with 2.6 years required to reach a 67% permeation or the right model boundary. Potash seams with halite inclusions show a very similar permeation speed compared to homogeneous ones (Figure 4.7d). However, because 66% to 70% of the (soluble) rock is permeated (instead of 50%), it takes the reaction front almost twice as long to arrive at the right model boundary. Accordingly, heterogeneities slow down the leaching zone growth in horizontal direction by a factor of 1.25 to 1.8 in cases of high dissolution rates.

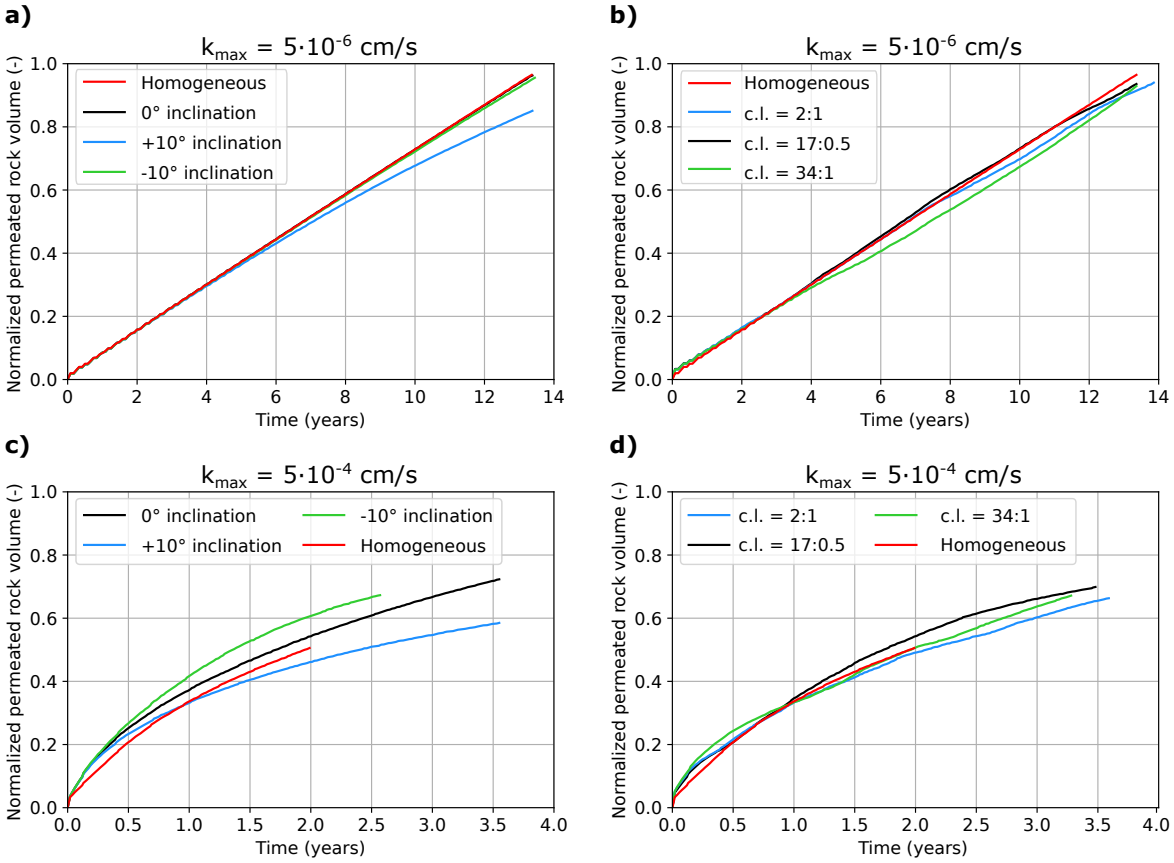

Figure 4.7: Ratio between permeated and total (soluble) rock volume over time for a), c) an intersecting halite layer and b), d) halite inclusions (c.l., correlation length) compared to the homogeneous case.

4.3.2 Péclet and Damköhler Numbers

In order to determine whether the systems are transport- or reaction-dominated, and if the transport is dominated by advection or diffusion, the dimensionless parameters of Péclet (Pe) and Damköhler (Da) can be used, allowing for a classification into four different cases which show different temporal and spatial evolutions of the leaching zone (Steding et al. 2021b). The Péclet number is determined from the flow velocity v, the diffusion coefficient D_f and the characteristic length l, following Equation 4.7. Pe has to be calculated individually for each cell, because v varies in space (and time). l is approximated with the current width of the leaching zone, which varies over time in the vertical direction.

$$Pe = v \cdot l / D_f \tag{4.7}$$

To determine if the system was dominated by advection (Pe $>$ 2) or diffusion (Pe $<$ 2), the median of all permeated cells was determined. All homogeneous and heterogeneous scenarios showed a median Péclet number which was clearly above two over the entire modeling period, i.e., all systems were advection-dominated. This means that diffusion was negligible as a transport process within the leaching zone, and the

Damköhler number, which is defined as the ratio between reaction rate and transport velocity, could be calculated from the flow velocity v according to Equation 4.8. To calculate the reaction rate of each mineral, Equation 4.1 was used, considering the saturations of the inflowing solution. The studies of Field et al. (2019) indicate that at the same flow velocity, low saturations cause transport-dominated systems (Da $>$ 1), whereas high saturations result in reaction-dominated systems (Da $<$ 1). The solution at the left boundary was NaCl-saturated; therefore, the reaction rate for halite was zero. In the cases of sylvite and carnallite, *rate* corresponds to k_{max} because the inflowing solution is highly undersaturated with respect to both minerals. The transport velocity corresponds to the flow velocity calculated by TRANSE.

$$Da = \text{reaction rate / transport velocity} = k_{max}/v \quad (\text{if Pe} > 2) \tag{4.8}$$

A Damköhler number for the system can be derived from k_{max} and the median of all flow velocities within the permeated area. The latter is divided into upper and lower halves in cases of intersecting halite layers. Figure 4.8 shows that the median always ranges between 10^{-6} m/s and 10^{-8} m/s. This means that for $k_{max} = 5{\cdot}10^{-4}$ cm/s, Da is always above one, whereas for $k_{max} = 5{\cdot}10^{-6}$ cm/s, Da falls below one if the flow velocity is above $5 \cdot 10^{-8}$ m/s. In the case of homogeneous potash seams, this holds true during the first 2 years of simulation (Figure 4.8a,b). After that, the decrease in flow velocity results in a Damköhler number slightly above one, eventually equaling 1.4. If the potash seam is intersected by a horizontal halite layer, it takes 3 years to reach Da = 1 because the average flow velocity is slightly higher at the beginning (Figure 4.8a). Later, its decrease is stronger; thus, Da = 1.4 is eventually reached as well. Similar evolutions can be observed within the upper half of the potash seam if the intersecting halite layer is inclined. However, after 7-8 years, the flow velocity decrease becomes faster and Da becomes higher. On the other hand, flow velocities within the lower half are constantly lower for a $+10°$ inclination and constantly higher for a $-10°$ inclination. In the latter case, Da rises above one only after 13 years. In the case of halite inclusions, it partly takes more than 2 years to reach Da = 1, e.g., for the 17:0.5 distribution, and the evolution of the average flow velocity is less regular, resulting in several crossings of Da = 1 over time, e.g., for the 34:1 distribution (Figure 4.8b). However, the overall evolution of flow velocities is relatively similar to the homogeneous case.

In contrast, $k_{max} = 5 \cdot 10^{-4}$ cm/s leads to larger deviations in flow velocity (Figure 4.8c,d). Thereby, heterogeneous potash seams generally show smaller flow velocities than homogeneous ones. In the case of a horizontal, intersecting layer, both halves show the same decrease in flow velocity over time, and after 2 years, the flow velocity amounts to approximately 50% of that in the homogeneous case (Figure 4.8c). The same evolution can be seen within the upper half of potash seams with intersecting layers at $\pm 10°$ inclination. After 3.6 years, the flow velocities have decreased to $1.5 \cdot 10^{-8}$ m/s, which represents only 20% of the final flow velocity in the homogeneous case. However, for a $-10°$ inclination, the velocity decrease is reduced after 2 years, and the right

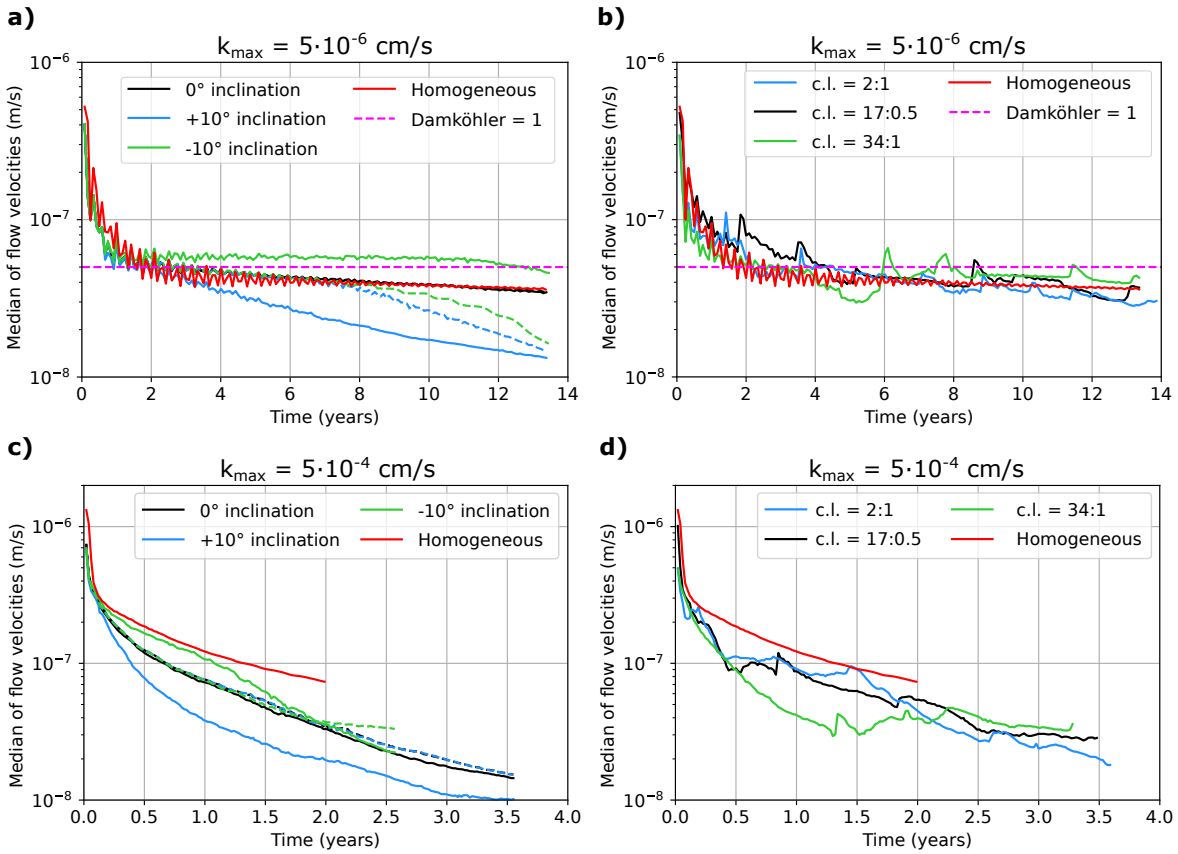

Figure 4.8: Median of flow velocities over time for a), c) an intersecting halite layer (solid line, below layer; dotted line, above layer) and b), d) halite inclusions (c.l., correlation length) compared to the homogeneous case.

model boundary is reached after only 2.6 years. Within the lower half of the potash seam, the average flow velocity is smaller compared to the upper half if the inclination of the intersecting layer is $+10°$. In contrast, it is generally higher in cases of $-10°$ inclination. Thus, flow velocities within the lower half show an increased dependency on inclination. Heterogeneous potash seams with halite inclusions also show a clear trend towards flow velocity decreases over time (Figure 4.8d). However, phases of increase occur as well - especially for 34:1 distribution - which cannot be observed for homogeneous potash seams or intersecting layers.

4.3.3 Leaching Zone Evolution for Low Dissolution Rates (Da ≈ 1)

To evaluate the shift from reaction- (Da < 1) to transport-dominated (Da > 1) systems in the case of $k_{max} = 5 \cdot 10^{-6}$ cm/s, the distribution of Mg^{2+} after different time periods is shown in Figure 4.9. The Mg^{2+} concentration is a useful indicator for fluid density and saturation: an absence of Mg^{2+} usually represents a NaCl solution with a density of 1,200 kg/m^3, whereas a solution with >85 g/l Mg^{2+} (at 25°C) has a density of >1,270 kg/m^3 and is fully saturated with respect to halite, sylvite and carnallite. In cases of homogeneous potash seams (Figure 4.9), the solution is highly undersaturated with regard to sylvite and carnallite along the entire dissolution front during the first

two years. Accordingly, both minerals are fully dissolved and only halite remains. In contrast to halitic areas, the rock is fully permeated and porosity is high (≈30%) within these zones (further referred to as halite zones). The dissolution front is planar during that time, whereas concentration and density gradients are comparatively low. However, the Mg^{2+} concentration at the bottom increases, and after 2 years, when Da = 1 is reached, the dissolution of sylvite and carnallite is significantly reduced at the lower end of the dissolution front. As a result, a sylvinitic zone, consisting of halite and sylvite (Figure 4.9d,e), is formed next to it and an inclination of the dissolution front occurs. Over time, its upper end moves upwards (Figure 4.9b,c) and the sylvinitic zone with lower porosity grows. Additionally, a small barrier is formed next to the lower end of the inflow due to the precipitation of halite (Figure 4.9d).

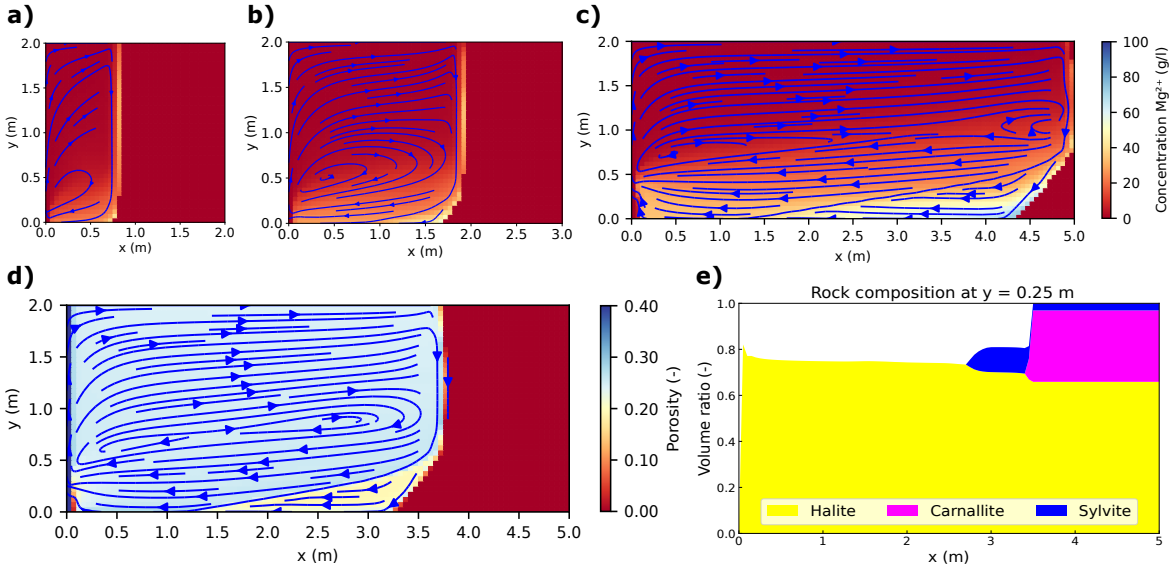

Figure 4.9: Convection cell of a system shifted from a reaction- to a transport-dominated one: Mg^{2+} concentration distribution after simulation times of a) 2 years, b) 5 years and c) 13.4 years; d) porosity distribution and e) mineralogical composition after 10 years for a homogeneous potash seam and $k_{max} = 5 \cdot 10^{-6}$ cm/s.

In cases of halite inclusions, the leaching zone evolution is basically similar to the homogeneous case. However, the more often the dissolution front is disturbed by inclusions, the more irregular it becomes (Figure 4.10a-c). The same applies to the sylvinitic zone within the lower area. Apart from that, sylvinitic zones now also occur above or behind inclusions and are often re-dissolved as soon as the flow regime changes and local Mg^{2+} concentrations decrease. A slower growth rate, which is usually associated with a sylvinitic zone next to the dissolution front, can now be observed within the upper area as well (Figure 4.10c). Generally, the convection cell is increasingly divided into smaller sub-cells, the broader the inclusions are. However, with regard to the shape and penetration depth of the leaching zone, differences compared to the homogeneous case are negligible.

In the case of an intersecting, insoluble halite layer, the system is split up into two convection cells that evolve independently of each other. In the case of a horizontal

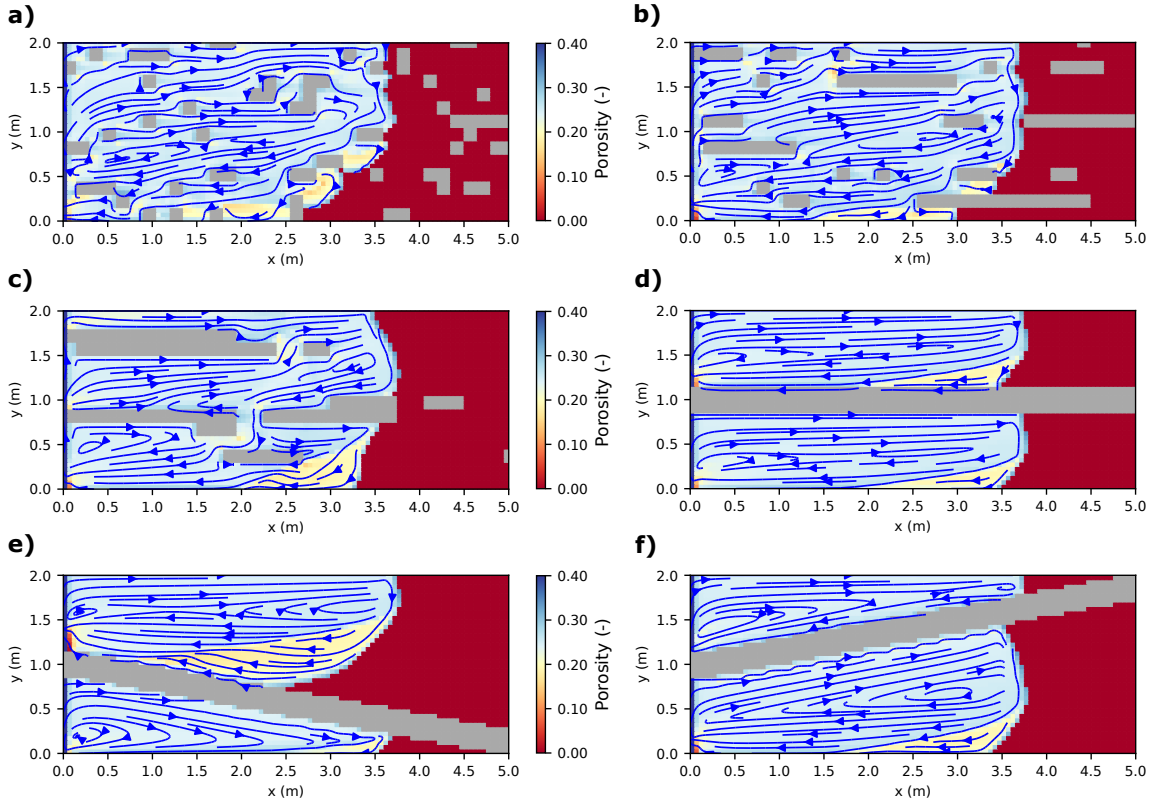

Figure 4.10: Porosity distribution after a simulation time of 10 years for heterogeneous potash seams with halitic inclusions for the distributions a) 2:1, b) 17:0.5, c) 34:1 and intersecting layers with d) 0°, e) +10°, f) −10° inclination and $k_{max} = 5 \cdot 10^{-6}$ cm/s.

layer (Figure 4.10d), both convection cells show nearly the same evolution compared to the homogeneous case (Figure 4.9). Although the sylvinitic zone is formed slightly later - after about 3 years instead of 2 years - it quickly covers a larger part of the dissolution front: after 10 years, approximately 50% of it, compared to 30% in the homogeneous case (Figures 4.9 and 4.10d). However, the penetration depth at the upper end of the dissolution front is approximately the same. In contrast, the convection cells develop differently after some years if the intersecting layers are inclined (Figure 4.10e,f). Although the upper halves show similar flow velocities as in case of a horizontal layer during the first 7-8 years (Figure 4.8a), the sylvinitic zone is formed earlier and grows faster if the height increases (Figure 4.10e), whereas it does not occur at all if the height decreases (Figure 4.10f). The same applies to the formation of the barrier next to the inflow. On the other hand, an increasing height within the lower half results in the same sylvinitic zone and barrier formation, as in the case of a horizontal layer (Figure 4.10d,f), although flow velocities are higher and it takes 13 years to reach Da = 1 (Figure 4.8a). If the height within the lower half decreases, the sylvinitic zone starts forming after about 2.5 years, but grows relatively slow. After 10.5 years, it completely covers the dissolution front (Figure 4.10e), although it is only 1 m wide and 0.2 m high. From that point in time, the growth rate of the lower half is reduced, whereas flow velocities already show a significant decrease after 3 years (Figure 4.8a).

In all other cases, the maximum penetration depth is the same within the upper and lower layer and the right model boundary is reached after 13.4 years.

4.3.4 Leaching Zone Evolution for High Dissolution Rates (Da > 1)

For $k_{max} = 5 \cdot 10^{-4}$ cm/s, the Damköhler number is clearly above one during the entire simulation time and a funnel-shaped leaching zone is formed, showing preferential dissolution within the upper half of the potash seam (Figure 4.11). Its width decreases nearly linearly from the top to the bottom. The lower part of the potash seam is not dissolved, resulting in an increased flattening of the dissolution front over time. As indicated in Figure 4.7c,d, the expansion becomes slower over time: although the leaching zone penetrates 3 m deep into the seam in the first year, it proceeds only two more meters within the second year. The precipitation of halite next to the left model boundary leads to the formation of a flow barrier within the lower half of the potash seam. Close to the entire dissolution front, a sylvinitic zone is formed (Figure 4.11a, yellow). Its maximum width in the horizontal direction is reached at the height of the barrier top. Basically, two different solution compositions exist within the leaching zone. The first one contains almost no Mg^{2+} and can be found within the halite zone (Figure 4.11a, blue), whereas the second one shows Mg^{2+} concentrations of >70 g/l and is present within the sylvinitic zone (Figure 4.11a, yellow). The border reaches from the upper end of the dissolution front to the top of the barrier and represents an area with large concentration gradients. Thus, there is a large density gradient at the border as well, representing the driving force of the free convection. Figure 4.11a shows that above this border, fluid flow proceeds mainly from left to right, whereas below it, the (highly saturated) solution is moving from the dissolution front back towards the left boundary.

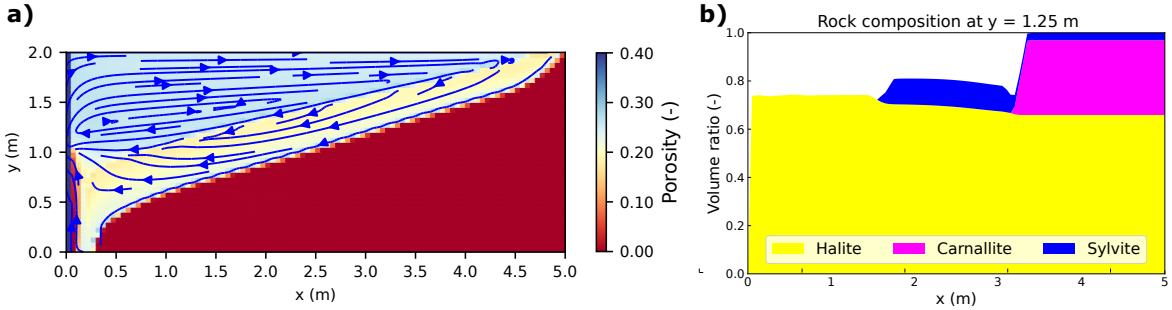

Figure 4.11: Convection cell of a fully transport-dominated system: a) porosity distribution and b) mineralogical composition after a simulation time of 2 years for a homogeneous potash seam and $k_{max} = 5 \cdot 10^{-4}$ cm/s.

In cases of small and medium-sized halite inclusions, the flow field becomes less regular but still shows one main convection cell with undersaturated inflowing solution, mainly present within the upper-left area of the leaching zone, and highly saturated outflowing solution along the dissolution front and within the lower area (Figure 4.12a,b). Accordingly, the shape of the sylvinitic zone and barrier remains basically similar to

the homogeneous case. However, zones containing only halite now also occur within the lower half of the leaching zone behind the barrier. In return, wide sylvinitic zones can occur in the upper half, especially above inclusions (Figure 4.12b). Neither the inclination of the dissolution front nor of the border between the halite and sylvinitic zone is linear anymore, and the lower end of the dissolution front is about 1 m away from the inflow compared to 0.25 m in the homogeneous case (Figures 4.11a and 4.12a,b). For broader inclusions, the flow field shows three smaller convection cells after 10 years, with each having its own barrier at the left (Figure 4.12c). The same applies to the sylvinitic zone. The dissolution front is subdivided into 3-4 sections with different penetration depths. Thereby, the upper one shows lower dissolution rates than the one below, leading to a recess at 1.6 m height. However, this phenomenon quickly disappears as soon as the upper half of the dissolution front is not subdivided anymore, and the flow regime changes accordingly. Between large inclusions, the flow is not disturbed and the dissolution front as well as the borders between halite and sylvinitic zones are nearly as regular as in the homogeneous case (Figure 4.11a). However, the overall inclination of the dissolution front is much steeper. As a result, the same permeation speed leads to smaller penetration depths within the upper part of the potash seam after 2 years, but higher permeation ratios at the end for all cases of halite inclusions (Figure 4.7d). Here, the right model boundary is reached after 3.3 years (34:1) to 3.6 years (2:1).

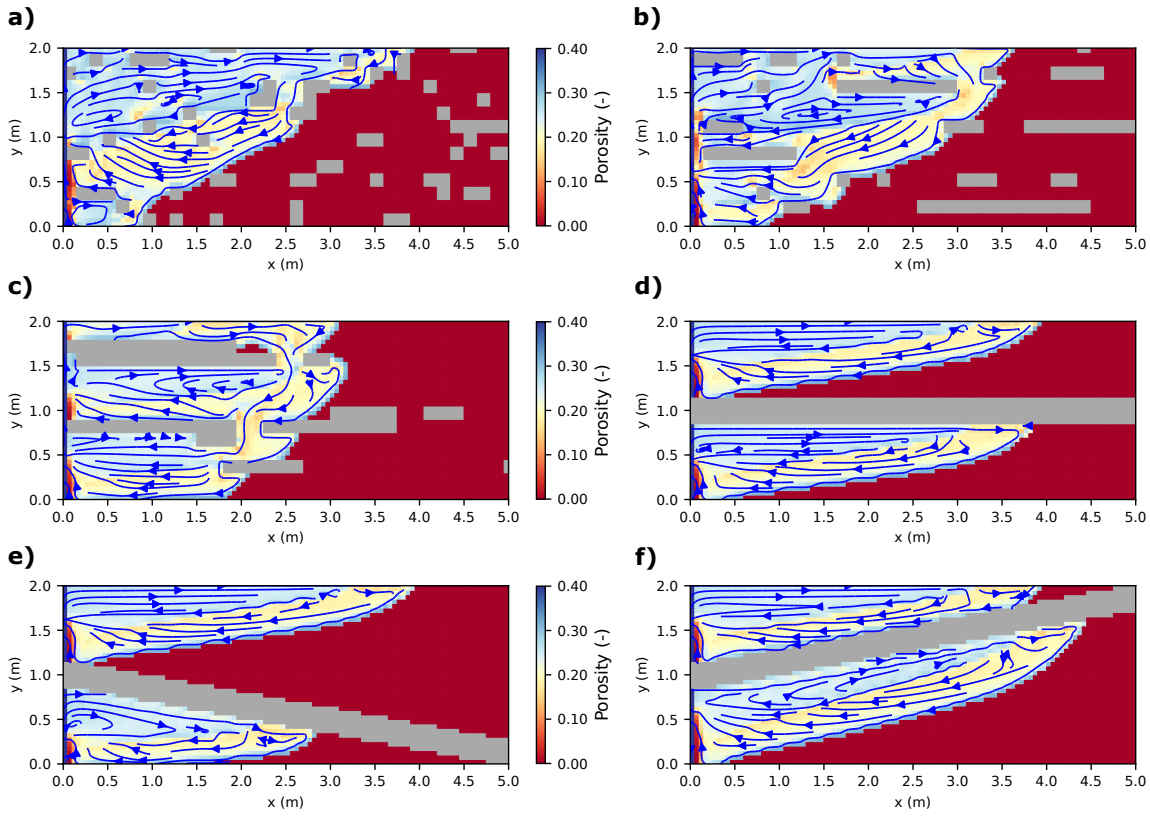

Figure 4.12: Porosity distribution after a simulation time of 2 years for heterogeneous potash seams with halitic inclusions for distributions of a) 2:1, b) 17:0.5, c) 34:1 and intersecting layers with d) 0°, e) +10°, f) −10° inclination and $k_{max} = 5 \cdot 10^{-4}$ cm/s.

The leaching zones above intersecting layers show nearly similar evolutions in penetration depth regardless of the inclination (Figure 4.12d-f). If the height is constant or increases, shape and flow velocities evolve similarly (Figures 4.12d,e and 4.8d), whereas in cases of decreasing height, the dissolution front follows the intersecting layer (Figure 4.12f) and the penetration speed slightly decreases as the height falls below 0.25 m. Compared to the homogeneous case, the width of the leaching zone shows a lower decrease within the upper half and a greater decrease within the lower half, resulting in higher permeation ratios (Figure 4.7c). Only if the height increases, a large area of undissolved potash salt is maintained between the intersecting layer and the upper leaching zone, leading to an overall permeation ratio of 59% (compared to >70% for 0° and −10° inclination) at the end of the simulation time (Figures 4.7c and 4.12e). After 2 years, the barrier covers about half of the upper in- and outflow region and the right model boundary is reached after 3.5 years. However, in the case of a −10° inclination, the lower leaching zone grows faster than the upper one (Figure 4.12f). Thus, the right model boundary is already reached after 2.6 years. In contrast, the +10° inclination results in smaller growth rates within the lower half (Figure 4.12e). Generally, layers with increasing height grow faster, whereas layers with decreasing height show higher permeation ratios (Figure 4.12e,f). Compared to the homogeneous case, sylvinitic zones (yellow) are slightly broader at the upper end of the dissolution front in all cases of intersecting layers.

4.4 Discussion

The results show that the influence of insoluble inclusions and intersecting layers strongly depends on the dissolution rate of the soluble minerals. In cases of low dissolution rates ($k_{max} = 5 \cdot 10^{-6}$ cm/s), the evolution of the leaching zone is only slightly affected (Figures 4.7a,b and 4.10), although local and average flow velocities are significantly changed (Figure 4.8a,b). In contrast, heterogeneities lead to a reduction in penetration depth (Figure 4.12) and higher permeation ratios (Figure 4.7c,d) if dissolution rates are high ($k_{max} = 5 \cdot 10^{-4}$ cm/s). These differences can be explained by a distinction between reaction-dominated and transport-dominated systems. A fully reaction-dominated system (Da $\ll 1$) is given if the effective dissolution rates of sylvite and carnallite according to Equation 4.1 correspond to the maximum dissolution rate, i.e., if their saturation only shows a very slight increase along the dissolution front. In this case, the dissolution front is planar and neither local nor overall changes in flow velocity affect the growth rate of the leaching zone: it is entirely controlled by the reaction speed. This case is given for $k_{max} = 5 \cdot 10^{-6}$ cm/s at the start of the simulation. However, after some years, the saturations along the dissolution front become high enough to significantly reduce the dissolution rate of sylvite and carnallite, making the system only partly reaction-dominated (Da ≈ 1). The reason for that can be a decrease in flow velocity or an increase in the length of the dissolution front. As a result, the

dissolution front becomes inclined and a sylvinitic zone as well as a barrier are formed (Figure 4.9). If the entire dissolution front is inclined and covered by a sylvinitic zone, the system is fully transport-dominated (Da $\gg 1$), as given for $k_{max} = 5 \cdot 10^{-4}$ cm/s. These systems are much more sensitive to changes in flow velocity. Therefore, they are much more affected by heterogeneities influencing both the local distribution and the average flow velocity (Figures 4.8, 4.10 and 4.12).

The Damköhler number is a useful indicator to determine if a system is dominated by reaction or transport (Oltéan et al. 2013; Steding et al. 2021b; Weisbrod et al. 2012). Generally, the simulation results show that an overall Da calculated from the average flow velocity and the saturation-dependent dissolution rate of the inflowing solution corresponds to the observed leaching zone shapes. In cases of $k_{max} = 5 \cdot 10^{-4}$ cm/s, Da $\gg 1$ is given and a funnel shape can be observed, including a barrier at the left and a sylvinitic zone along the entire dissolution front (Figure 4.11). These are typical indicators for a transport-dominated system (Steding et al. 2021b). In cases of $k_{max} = 5 \cdot 10^{-6}$ cm/s, the dissolution front is planar in the beginning when Da < 1, whereas it becomes inclined as Da rises above one, with a sylvinitic zone and barrier rising from the bottom (Figures 4.8a,b and 4.9a-c). However, insoluble inclusions make it more difficult to identify this point in time, because the average flow velocity evolves less regularly (Figure 4.8b) and strong local deviations occur, resulting in small sylvinitic zones near the inclusions and a more irregular dissolution front (Figure 4.10a-c). In cases of intersecting layers, Da has to be determined for each sub-system or convection cell, and if the layer is inclined, the time period in which Da rises above one does no longer correlate with the formation of sylvinitic zones and barriers (Figures 4.8a and 4.10d-f). From our point of view, the reason for this is a change in the length of the dissolution front: if it increases, higher saturations can be reached at the bottom without a change in flow velocity, and vice versa. All in all, the larger the heterogeneities are in size, the less appropriate an overall Damköhler number is to determine if the system is dominated by reactions or transport. Additionally, it has to be noted that complex systems containing several minerals can be reaction- and transport-dominated at the same time: if the maximum dissolution rate k_{max} or the saturations of the inflowing solution vary a lot for different minerals, some of them will show Da > 1, whereas others show Da < 1. Accordingly, the Damköhler number has to be calculated individually for each mineral and an internal contact area between equilibrated and non-equilibrated minerals has to be defined (Figure 4.4) to reproduce the formation of several dissolution fronts, as observed by Ahoulou et al. (2020). In this case, heterogeneities are expected to mainly influence the dissolution pattern of minerals with Da > 1.

Heterogeneities also affect the hazard potential of leaching zones by influencing the growth rate, shape and permeation ratio. In this context, higher growth rates are associated with faster expansion of the leaching zone and an increasing risk of mine flooding or integrity loss of a cavern. Higher permeation ratios or porosities also in-

crease the hazard potential because they result in a lower mechanical stability as well as larger solution amounts stored per meter leaching zone. The results show that for $\mathrm{Da} \gg 1$, insoluble inclusions mainly affect the shape: at the top, the dissolution front is progressing relatively slowly, whereas at the bottom, dissolution rates are higher compared to the homogeneous case (Figures 4.11 and 4.12a-c). As a result, the permeation speed is basically the same (Figure 4.7d), but the dissolution front is steeper, and it takes 1.65-1.8 times longer until the right model boundary is reached. It is important to note that the distribution of insoluble inclusions does not have a significant influence if their volume ratio is identical. Although broader inclusions increasingly split up the convection cell into smaller ones and lead to a more irregular average flow velocity, the overall evolution is always quite similar (Figures 4.7d, 4.8d and 4.12a-c). Thereby, the leaching zone growth in the horizontal direction is slower compared to the homogeneous case, but the permeation ratio is higher at the end of the simulation, which can become more critical with regard to mechanical stability. In the case of one continuous insoluble layer, the leaching zone consists of two independent convection cells, showing the same regular dissolution front, sylvinitic zone and barrier as in the homogeneous case. However, flow velocities and permeation speed are more similar to those of insoluble inclusions (Figures 4.7c, 4.8c and 4.12d). Inclined, intersecting layers particularly influence the flow velocity within the lower half (Figure 4.8c). Thereby, negative inclinations increase the flow velocity, resulting in faster leaching zone growth compared to the upper half (Figure 4.12f), and vice versa. The evolution of the upper half is basically not influenced (Figure 4.12e,f). However, the amount of undissolved potash rock is larger with increasing height, resulting in relatively small permeation ratios (Figure 4.7c). In summary, an intersecting layer with negative inclination is the most critical distribution of insoluble inclusions, leading to higher permeation ratios and only slightly smaller growth rates in the horizontal direction compared to the homogeneous case.

Field observations indicate that the formation of caverns and leaching zones in salt rock is usually dominated by transport. According to Koch and Vogel (1980), the upper half of a potash seam is often preferentially dissolved, and natural leaching zones within carnallitic rock are mostly divided into a halite zone near the inflow region and a sylvinitic zone close to the dissolution front. These observations agree with the results for a transport-dominated system ($k_{max} = 5 \cdot 10^{-4}\,\mathrm{cm/s}$) of homogeneous rock composition (Figure 4.11). In the case of intersecting layers from pure halite, Koch and Vogel (1980) assumed a split into several dissolution fronts with different penetration depths. A similar phenomenon has been observed in solution mining: if several insoluble layers cross the salt body, the resulting cavern shape resembles an inverted Christmas tree (Thoms and Gehle 1999). The same shape is described by Fokker (1995) for technical caverns crossing different (potash) salt layers. Furthermore, Fokker (1995) implies that inclined layers cause an asymmetric shape, whereby the growth rate is faster in the direction of upward-directed inclination. These descriptions all correspond to

the simulation results for a transport-dominated system with intersecting halite layers (Figure 4.12d-f). However, time frames for the evolution of natural leaching zones are not available. Regarding insoluble inclusions, laboratory experiments conducted by Gechter et al. (2008) and Field et al. (2019) confirm that the cavern shape becomes increasingly distorted, and notches occur at the dissolution front if insoluble lenses impede regular fluid flow (Figure 4.12a-c). Additionally, findings that inclusions do not reduce the amount of dissolved/permeated rock per time, but only its distribution (Figure 4.7d), are consistent (Gechter et al. 2008). Reaction-dominated systems with (nearly) planar dissolution fronts only occur if the inflowing solution is already highly saturated with respect to the present salt minerals (Field et al. 2019). In this case, significantly slower growth rates as well as an increased influence of rock fabric were observed. The first finding agrees with our simulation results (Figure 4.7), whereas the second one could not be reproduced (Figure 4.10a-c). Overall, there is a good correlation between literature data and model results regarding the influence of heterogeneities. However, temporal scaling is still uncertain, and more data are required for comprehensive quantitative model validation.

Finally, the results reveal how saturation-dependent dissolution rates affect barrier formation and leaching zone shape. In the case of fully reaction-dominated systems ($Da \ll 1$), there is no difference compared to constant dissolution rates because k_{max} is always reached. In contrast, transport-dominated systems show a more linear decrease in width from the top to the bottom, because the effective dissolution rate decreases along the dissolution front. Therefore, a longer distance is required until the solution is fully saturated and the transition from dissolved to undissolved sections of the potash seam is less sharp compared to constant dissolution rates (Steding et al. 2021b). Additionally, the barrier next to the inflow is smaller, resulting in a less decreasing flow velocity and growth rate over time. Thus, saturation-dependent dissolution rates lead to a wider extension, and therefore a higher hazard potential of the leaching zone in the long term. Furthermore, they intensify the coupling between chemical reactions and transport. Next to the dissolution front, where strong concentration gradients occur, changes in advection, diffusion or dispersion immediately affect the saturations, and therefore the effective dissolution rates. In return, the dissolved mineral amounts affect transport parameters such as brine density, viscosity and diffusion coefficients. An even stronger coupling would be achieved if k_{max} is treated as a function of flow velocities. Several studies indicate that for fast-dissolving minerals, such as most potash salts, the dissolution rate is controlled by the transport across a so-called diffusive boundary layer which is formed at the mineral-fluid interface (Alkattan et al. 1997; De Baere et al. 2016; Dutka et al. 2020). Thereby, higher fluid flow velocities induce a decrease in thickness of the boundary layer, and therefore higher dissolution rates of the minerals. As a result, k_{max} varies locally and heterogeneities may have a stronger effect. However, the approach uses input parameters, such as the reaction rate constant, which are currently not known for many potash minerals. Furthermore, knowledge about

the flow field at pore scale and the bulk concentrations outside the boundary layer are required (Molins et al. 2012). Both are hard to determine by continuum-scale models which cannot exactly reproduce the concentration distribution at the dissolution front. By using average saturations to calculate the dissolution rates, artificial mixing is always generated, influencing the leaching zone shape or the fluid flow path until full saturation is reached. Accordingly, a calibration of the model based on experimental data is crucial. Overall, the simulation results show that the saturation dependency of dissolution rates has a significant influence on the leaching zone evolution in cases of partly or fully transport-dominated systems (Da $\geq$ 1), and therefore needs to be considered when investigating further scenarios.

4.5 Conclusions

The scenario analysis for a generic potash seam has significantly improved the understanding of the influence of insoluble inclusions and intersecting layers on the evolution of leaching zones. It was shown that in the case of advection- and reaction-dominated systems (Pe $>$ 2 and Da $<$ 1), growth rate, shape and porosity of the leaching zone are basically identical in heterogeneous and homogeneous cases, meaning that heterogeneities can be neglected with regard to risk assessment. In advection- and transport-dominated systems (Pe $>$ 2 and Da $>$ 1), the amount of potash salt permeated over time is similar in both cases, but the shape of the leaching zones is different. As a result, the upper end of the dissolution front(s) moves forward 1.8 times slower in the heterogeneous case, regardless of the distribution of insoluble areas. Consequently, heterogeneities decrease the hazard potential. To account for this effect, only the volume ratio of insoluble minerals has to be known, representing a major advantage in practice because exact distributions are seldom known. Only in the case of intersecting layers with negative inclination, a smaller reduction in growth rate and an asymmetric expansion of the leaching zone need to be considered. Neglecting heterogeneities usually generates a safety margin in the overall assessment, unless the increase in permeation ratio endangers the mechanical stability of the leaching zone. If insoluble layers and/or large inclusions collapse, new fluid flow paths may be formed, significantly increasing leaching zone growth rates as well as hazard potentials.

Literature data indicate that most natural systems are transport-dominated. However, the Damköhler number needs to be calculated individually for each mineral and, in the case of intersecting layers, also for each separate leaching zone to reliably assess the influence of heterogeneities and to predict further leaching zone evolution. Heterogeneities, especially inclined intersecting layers, influence local and average fluid flow velocities; therefore, the validity of a global Damköhler number is reduced. Instead, the occurrence of funnel shapes, barriers and sylvinitic zones (in the case of carnallitic potash salt) should be used to determine if a system is dominated by reaction (Da $<$ 1) or transport (Da $>$ 1).

The extension of the reactive transport model by variable saturation-dependent dissolution rates has improved its accuracy with regard to the leaching zone shape, growth rate and barrier formation. It is shown that constant dissolution rates overestimate barrier formation, and therefore underestimate hazard potentials in the long term. In the next step, it is planned to not only distinguish between insoluble and highly soluble minerals, but to also include more slowly dissolving minerals such as anhydrite ($CaSO_4$) or kieserite ($MgSO_4 \cdot H_2O$) into the assessment by using individual maximum dissolution rates. In doing so, the effects of mineral heterogeneity can be investigated in further detail. However, for many secondary minerals occurring in these complex quinary or hexary systems, k_{max} is unknown. Furthermore, a dependency on the local flow velocity is expected to intensify the coupling between chemical reactions and transport. Therefore, laboratory and field measurement data are required to calibrate k_{max}. With these extensions, the reactive transport model can be principally applied to any study area for prediction of the preferential expansion of leaching zones along potash seams and assessment of their hazard potentials.

5 | Discussion in Terms of Thesis Objectives

Salt deposits host an important industrial raw material and provide storage capacities for energy and hazardous waste. Uncontrolled cavern evolution can seriously endanger each of these utilization types. If geological fault zones enable the contact with migrating groundwater, large natural cavern systems may evolve, leading to mine flooding, land subsidence or contaminant transport (Warren 2017). In the event that natural or technical caverns cross highly soluble potash seams, preferential expansion along them has to be expected, increasing the risk of stability or integrity loss (Höntzsch and Zeibig 2014). To facilitate a safe utilization of salt deposits, these risks need to be evaluated in advance, necessitating a localization of natural cavern systems as well as a comprehensive understanding of the coupled chemical and hydraulic processes that govern cavern formation.

In this dissertation, numerical simulations are applied to understand and reproduce the preferential expansion of caverns along potash seams. Thereby, water-rock interactions between saline solutions and potash rock are investigated first, using the geochemical reaction module PHREEQC (Parkhurst and Appelo 2013) in combination with the THEREDA database (Altmaier et al. 2011). By means of titration models and 1D models, the dissolution and precipitation behavior of various rock compositions is examined. For validation, results are compared with field data from a natural brine occurrence in a German potash mine. Subsequently, PHREEQC is coupled with the flow and transport code TRANSE (Kempka 2020), and a new approach called 'interchange' is added describing water-rock interactions at the solid-liquid interface. The resulting 2D reactive transport model is then used to study cavern evolution in space and time. Two scenario analyses are carried out based on a carnallite-bearing potash seam: firstly, the influence of varying carnallite contents and dissolution rates on cavern shape, growth rate and mineralogy is analyzed. Secondly, heterogeneous potash seams containing insoluble inclusions or intersecting layers are examined. Thereby, the interchange approach is extended by mineral-specific and saturation-dependent dissolution rates. Both studies focus on natural, density-driven convection, which is considered to be the main driving force in the formation of natural and technical caverns (Anderson and Kirkland 1980; Velema et al. 2010). Finally, the results are used to develop a classification scheme that enables a first assessment of the hazard potentials of cavernous structures.

Results of the geochemical reaction models show that the water-rock interactions within potash seams can generally be reproduced by assuming thermodynamic equilibrium. Field data from a cavernous structure in a German potash mine indicate that potash brines are saturated with respect to the minerals surrounding them unless forced convection occurs (Chapter 2). Thereby, brine and rock composition vary significantly

across the cavern: comparisons show that they cover the entire reaction path of the dry potash salt, with the solid-fluid-ratio increasing towards the unaffected rock. These observations correspond to previous field and laboratory experiments (Bach 2010; Bohn 2014; Herbert 2000). However, volume balances also reveal that already at an early stage of the reaction path, precipitated minerals use to have a larger volume than the previously dissolved ones, indicating that higher solid-fluid-ratios can not be reached because pores are fully clogged. To overcome this apparent contradiction, each transition line between regions of different porosity and mineralogy must be treated as dissolution front. In doing so, minerals can be dissolved into an adjacent region of higher porosity and lower saturation. Only then, dissolution fronts can progress and caverns are enabled to grow. For this purpose, the interchange approach is developed (Chapter 3). Because contact areas between regions of different porosity are small, it takes dissolution kinetics into account. Furthermore, the interchange approach is capable of considering multiple dissolution fronts and thus of reproducing even leaching zones with complex mineralogical compositions as they occur within potash seams.

Coupling the geochemical reaction models and the interchange approach explained above with a flow and transport code yields a reactive transport model that is able to describe the evolution of caverns within potash seams in space and time. According to the scenario analysis conducted in Chapter 3, results can be classified based on the dimensionless Péclet (Pe) and Damköhler (Da) numbers. The first one represents the ratio between advection and diffusion rate, providing information about the dominating transport mechanism. The second one represents the ratio between dissolution rate of the rock and transport velocity, providing information on whether cavern growth is controlled by reaction or transport rate. In case of fully advection-dominated systems ($Pe > 2$), the transport velocity equals the average flow velocity within the leaching zone, whereas in fully diffusion-dominated systems ($Pe < 2$), Da has to be calculated from the diffusion rate. In general, the dissolution rate, and therefore Da, must be determined individually for each mineral, taking the saturation state of the inflowing solution into account (Chapter 4). Furthermore, insoluble inclusions influence local as well as average flow velocities and thus reduce the validity of a global Da. In case of insoluble intersecting layers, Da needs to be calculated individually for each subsystem or convection cell, respectively. If layers are inclined, its validity decreases further, complicating a general classification. Nevertheless, simulation results from Chapters 3 and 4 have shown that in principle, a strong correlation exists between Pe and Da on the one hand, and shape, growth rate and mineralogical composition on the other. This finding is consistent with the results of previous studies on density-driven dissolution (Ahoulou et al. 2020; Oltéan et al. 2013). In general, four different types of leaching zones can be observed.

Transport- and advection-dominated systems ($Da > 1$ and $Pe > 2$) are characterized by a funnel shape, caused by density-driven convection. The undersaturated solution entering the leaching zone flows towards the hanging wall, leading to max-

imum dissolution rates in the upper part of the potash seam. Afterwards, it flows down along the dissolution front(s), with saturation and density increasing, whereas the dissolution rate(s) decrease and the leaching zone becomes narrower. Reaching the footwall of the potash seam, the solution is maximally saturated with respect to all the minerals where Da $>$ 1 is given. Large density gradients induce high flow velocities and thus very fast growth rates in the beginning. However, as the highly saturated potash brine flows back towards the inflow region, it mixes with entering NaCl solution, causing a precipitation of halite. As a result, a flow barrier is formed next to the lower part of the inflow region, reducing flow velocities and cavern growth in the long term. Although this phenomenon might be artificially intensified by the assumption of a constant solution composition at the model boundary, it matches the reaction path of carnallitic and kieseritic potash salt: in both cases, halite is precipitated as NaCl solution becomes more saturated with respect to potash minerals (Chapters 2 and 3). In case of insoluble inclusions or intersecting layers, the flow field is split up into several convection cells, with each of them showing a flow barrier next to the inflow (Chapter 4). Flow velocities and thus cavern growth are reduced to a varying extend, depending on the volume ratio of insoluble inclusions. However, distribution only has a minor impact unless an inclined, intersecting layer occurs. Compared to other types of leaching zones, transport- and advection-dominated systems grow much faster initially, showing a clear correlation between growth rate and height of the convection cell or potash seam, respectively.

Conversely, transport- and diffusion-dominated systems (Da $>$ 1 and Pe $<$ 2) evolve almost independently of density-driven convection. Instead, the concentration gradients between inflow region and dissolution front(s), where the solution is maximally saturated, are similar across the entire height. As a result, planar dissolution front(s) are formed, and brine and rock composition do not vary in vertical direction. Accordingly, growth rates are neither affected by potash seam thickness nor by local variations in flow velocity, e.g., due to heterogeneity. Barrier formation is much less pronounced and uniform across height, leading to more steady growth rates in the long term. However, as diffusive transport takes significantly longer compared to advection, leaching zone growth is generally slow. Over time, the increase in leaching zone width leads to a further reduction in diffusion and growth rate. For a quantitative description, variable diffusion coefficients depending on the brine composition need to be considered. However, most approaches are not validated for potash brines of high salinity (Anderko and Lencka 1998; Felmy and Weare 1991). Fully transport- and diffusion-dominated systems are often a long-term result of barrier formation in the case of originally transport- and advection-dominated systems. Furthermore, they can occur if potash seams contain large amounts of insoluble minerals or if the solution entering is already saturated with respect to most of the potash minerals. Both cases lead to low porosities ($<$10%) or flow velocities, respectively, making diffusion the dominating transport mechanism.

Besides that, porosities often decrease from the cavern center towards the unaffected rock, resulting in a partially advection- and partially diffusion-dominated system.

Fully reaction-dominated systems (Da $<$ 1) only occur if all minerals show low dissolution rates in relation to the average transport velocity. In diffusion-dominated systems (Pe $<$ 2), this is usually not conceivable since the transport velocity is too low. In contrast, advection-dominated systems (Pe $>$ 2) can reach very high transport velocities, e.g., due to forced convection. Besides that, reaction-dominated systems may occur if the solution entering is already highly saturated with respect to all fast-dissolving minerals from the potash seam. In any of these cases, the amount of minerals dissolved is so small that the saturation state of the solution is only slightly increased at the dissolution front(s), preventing any reduction in dissolution rate as well as any precipitation of secondary minerals. As a result, dissolution front(s) are planar and no barrier is formed next to the inflow region. Due to low dissolution rates, leaching zone growth is very slow but steady (Chapter 3). Insoluble inclusions and intersecting layers have a minor impact if Da $<$ 1, but they can change the shifting point towards a transport-dominated system (Da $>$ 1) by reducing the average flow velocity (Chapter 4). If this happens in an advection-dominated system (Pe $>$ 2), the dissolution front(s) become funnel-shaped (Chapter 3).

Regarding the mineralogical composition of leaching zones, the simulation results reveal clear differences between transport- (Da $>$ 1) and reaction-dominated (Da $<$ 1) systems. In the first case, large concentration gradients occur between the (upper) inflow region, where the solution is maximally undersaturated, and the unaffected rock, where the adjacent solution is maximally saturated. As a result, mineralogy and porosity strongly vary across the leaching zone. The results from Chapter 2 show that brine and rock composition generally follow the reaction path of the dry potash salt with the solid-fluid-ratio increasing towards the unaffected rock. As soon as the reaction path reaches a point where secondary minerals are precipitated, the porosity starts decreasing and a transition zone is formed between cavern center and unaffected potash seam. Its width depends on the concentration field: simulation results from Chapter 3 reveal that in case of funnel-shaped leaching zones (Da $>$ 1 and Pe $>$ 2), only a small transition zone exists near the hanging wall, because the inflowing solution is maximally undersaturated and only the first part of the reaction part is covered towards the unaffected rock. Close to the footwall, transition zones are small as well, because the leaching zone is generally narrower and the solution shows higher saturations, meaning that only the rear section of the reaction path is covered. The largest transition zones can be observed at medium height of the funnel, covering the entire reaction path and showing the most regular increase in solid-fluid-ratio between inflow region and unaffected rock. In case of transport- and diffusion-dominated systems (Da $>$ 1 and Pe $<$ 2), these transition zones are standard because concentrations evolve regularly between both ends and do not vary across potash seam thickness. Heterogeneities only affect the transition zones of funnel-shaped caverns, with lower flow velocities

increasing the local saturation and thus the precipitation of secondary minerals and vice versa. In case of insoluble inclusions, transition zones become less regular and occur preferably behind these, whereas insoluble intersecting layers lead to the evolution of an independent transition zone in each convection cell (Chapter 4). In sum, transition zones are quite pronounced in case of transport-dominated systems, containing all secondary minerals that occur along the reaction path.

In contrast, reaction-dominated systems (Da < 1) have such low dissolution rates that the point where additional secondary minerals besides halite are precipitated is not reached. Instead, all soluble minerals get fully dissolved at the same dissolution front. As a result, a homogeneous leaching zone is formed, containing solely minerals the encountering solution is already saturated with. Only if maximum dissolution rates vary widely, but still Da < 1 is given for all the minerals originally present, several planar dissolution fronts can theoretically evolve, leading to regions of different porosity and mineralogy between inflow region and unaffected rock as well. However, the more minerals have been dissolved from a region, the larger the contact area between solution and remaining minerals becomes. It is expected that this reduces or even compensates the effect of different maximum dissolution rates. Accordingly, transition zones usually do not occur in reaction-dominated systems.

Differences in leaching zone shape, growth rate and mineralogical composition are associated with different hazard potentials regarding the utilization of salt deposits. Thereby, fast growth rates are generally critical because the further leaching zones expand along potash seams, the higher is the risk of encountering a mine, a geological fault zone or an aquifer. In each of these cases, a dynamic outlet is created, enabling a significant increase in solution exchange, which in turn accelerates cavern growth. Experiences from potash mining have shown that the inflow of brine into mines is often small at the beginning, but if it can not be stopped, dissolution processes enlarge fluid flow paths and the inflow increases until the mine finally gets flooded (Herbert and Schwandt 2007; Prugger and Prugger 1991). In the vicinity of geological repositories, fast growing cavern systems reduce the width of rock barriers and increase the risk of contaminants being transported towards aquifers by means of advection (Mengel et al. 2012). In case of technical caverns, the quick preferential expansion along potash seams leads to more irregular cavern shapes and increases the risk of hydraulic connections between adjacent caverns (Thoms and Gehle 1999). In combination with high porosity, the mechanical stability of technical or natural cavern systems can be endangered as well. If they collapse, land subsidence and the formation of new fluid flow paths that give rise to even larger cavern systems are potential consequences (Boys 1993; Johnson 2008; Zhang et al. 2019). Accordingly, fast growth rates continuing over long periods of time and accompanied by a high porosity of the leaching zone cause the largest hazard potential.

The occurrence of transition zones can generally be seen as beneficial with regard to reducing hazard potentials. Secondary minerals such as kainite, leonite or recrys-

tallized halite are already known as indicators for the presence of water, and regions where they are encountered are usually not further mined (Boys 1993). The reactive transport model developed in this thesis offers the possiblity to determine composition and width of transition zones in greater detail. By calculating the distance between current working faces and cavern center based on brine and rock samples, the localization of cavernous structures can be improved. Furthermore, precise knowledge about the minerals forming transition zones allows for a detection of leaching zones at the earliest possible stage. In doing so, the risk of mine flooding is reduced.

The classification scheme described above allows for a first assessment of the hazard potentials of leaching zones within potash seams. If Pe and Da are known, conclusions can be drawn about the evolution of shape, growth rate and mineralogy. Thereby, transport- and advection-dominated systems ($Da > 1$ and $Pe > 2$) are considered as most critical in the short term as they expand very fast within the first few years (Chapters 3 and 4). However, if the potash seam is homogeneous, only the upper half is dissolved, and a transition zone with secondary minerals and lower porosity is formed, enabling a better localization. Due to the funnel shape of the leaching zone, it can be encountered first at the top of the potash seam. Nevertheless, exploration drilling may be better done at medium height as the thickness of the transition zone is expected to be the highest in this area. Heterogeneity in the form of insoluble inclusions and intersecting layers reduces the growth rate but also leads to less regular shapes. Furthermore, the permeation ratio of the potash seam is increased to significantly more than 50%. Thus, heterogeneity is only beneficial if the mechanical stability is maintained. In the long term, the system shifts towards transport- and diffusion-dominated ($Da > 1$ and $Pe < 2$) due to barrier formation, accompanied by a significant decrease in growth rate. This transformation is highly relevant with regard to risk assessment. In the case that barrier formation does not occur, transport- and advection-dominated systems can expand several tens of meters per decade, and would therefore represent the most critical case not only in the short term but also in the long term.

Transport- and diffusion-dominated systems ($Da > 1$ and $Pe < 2$) are considered as least critical regarding hazard potentials as they grow rather slow and show a relatively thick transition zone across the entire height (Chapter 3). Heterogeneity can be neglected as it does not affect shape or growth rate (Chapter 4). A disadvantage compared to transport- and advection-dominated systems is that the entire potash seam is permeated instead of just the upper half. However, since diffusion-dominated systems only occur in case of low porosity, the mechanical stability should be maintained. In contrast, reaction-dominated systems ($Da < 1$) do occur at high porosity as well, especially if advection dominates ($Pe > 2$), and a transition zone enabling localization is not formed. Growth rates are rather slow but very steady without a barrier being formed, and the potash seam is always entirely permeated. Heterogenities are of minor impact regarding shape and growth rate. Therefore, reaction- and advection-dominated systems ($Da < 1$ and $Pe > 2$) are considered as most critical in the long term.

Pe and Da can be determined by means of reactive transport simulations if the composition of the dry potash seam and the encountering solution are known. In turn, brine and rock samples can be used to draw conclusions about the classification, e.g., if the information on rock composition is insufficient. It is important to note that Pe and Da change over time and that heterogeneous rock compositions reduce their validity, especially in case of inclined, intersecting layers. Accordingly, a combination of reactive transport simulations and field measurements for calibration and validation is always necessary to predict the evolution of leaching zones and to assess their hazard potentials. Thereby, the simulation results for carnallite-bearing potash seams display a good agreement with the literature data available on cavern evolution in salt deposits (Chapter 3 and 4): the funnel shape and mineralogy calculated for transport- and advection-dominated systems correspond to the natural leaching zones described by Koch and Vogel (1980). Similar shapes have been observed for technical caverns (Fokker 1995; Thoms and Gehle 1999), indicating that $Da > 1$ and $Pe > 2$ is the most common case in nature. Conversely, reaction-dominated systems ($Da < 1$) provide an explanation for natural leaching zones without sylvinitic transition zones, which are mentioned by Koch and Vogel (1980) as well. The formation of independent subsystems showing different growth rates in case of insoluble intersecting layers matches the descriptions of all three studies. The findings that insoluble inclusions cause irregular dissolution fronts and do not reduce the amount of potash salt dissolved per time but only its distribution is confirmed by laboratory experiments for rock salt (Field et al. 2019; Gechter et al. 2008). In sum´, the results are qualitatively validated but for a comprehensive quantitative model validation, more data, especially on growth rates, are required.

The case study from Chapter 2 provides lots of data on leaching zone evolution, but the system is also highly complex. In particular, it contains varying amounts of kieserite and sylvite as well as anhydrite, leading to a hexary system with different reaction paths, depending on the ratio between the first two minerals. In contrast, the potash seams in Chapters 3 and 4 represent quaternary systems. As a result, transition zones with much more secondary minerals and strongly varying porosity are formed (Chapter 2). During the first two decades, brine and rock samples confirm the existence of a transition zone that covers the entire reaction path, meaning that the system must be mainly transport-dominated ($Da > 1$) during that period of time. However, since the dissolution rates between minerals vary by several orders of magnitude (Hoppe and Winkler 1974), it is conceivable that the system is partially reaction-dominated ($Da < 1$) as well. Moreover, the dominating transport mechanism is unclear, because the cavern shape is not exactly known. It is assumed that in the central cavern, the transport is advection-dominated ($Pe > 2$), whereas in the transition zone, it is mainly diffusion-dominated ($Pe < 2$) due to much lower porosities. This presumption is supported by the fact that after two decades, a borehole encountering the cavern only reduces the saturations within the central part. Presumably, the dy-

namic outflow does not affect transport processes within the transition zone, because diffusion is dominating, and saturations remain stable. In contrast, the central cavern represents an advection-dominated system, which is why higher flow velocities lead to a shift from transport- towards reaction-dominated, resulting in considerably lower saturations. However, systems with forced convection, as those caused by a dynamic outflow, have not been studied in detail so far. Overall, one can conclude that classifying the flow and transport conditions in hexary systems, such as the case study from Chapter 2, is much more challenging compared to quaternary systems, such as the carnallite-bearing potash seams in Chapters 3 and 4.

Hexary systems are also more complex with regard to reaction behavior. For example, large variations in porosity and flow velocity across the leaching zone are expected to considerably influence the dissolution rates (Alkattan et al. 1997; De Baere et al. 2016; Dutka et al. 2020). Thus, a dependency not only on saturation but also on Pe should be considered. Furthermore, brine samples from Chapter 2 showing supersaturation, particularly with regard to Ca-containing minerals, indicate that the assumption of thermodynamic equilibrium is not always accurate and that precipitation kinetics may have to be taken into account as well. However, for many secondary minerals that occur along the transition zone, dissolution kinetics are still unknown, not to mention their precipitation kinetics. Another difficulty regarding the hexary system from Chapter 2 is the fact that a solution can not be in equilibrium with kieserite and sylvite (at temperatures around 25°C), i.e., the reaction path continues until no water is left. Since PHREEQC (Parkhurst and Appelo 2013) shows convergence problems at very high solid-fluid-ratios, an extrapolation of reactions is necessary near the unaffected rock. This option has already been implemented so that in general, the reactive transport model is capable of simulating kieseritic potash seams as those in Chapter 2 as well. Nevertheless, due to the increased complexity, comprehensive data on growth rate, brine and rock composition are necessary to calibrate the model.

In sum, the first reactive transport model has been developed that is capable of reproducing preferential expansion of natural and technical caverns along potash seams in space and time. It is applicable to any potash salt and mineral distribution, provided that the resulting leaching zone represents a porous structure where Darcy flow is maintained. Once the model has been calibrated, thickness and composition of the transition zone can be determined, facilitating an optimization of the early detection systems currently existing in potash mining. Furthermore, a classification can be made based on Pe and Da, which allows conclusions to be drawn about cavern shape and growth rate and thus a first assessment of the hazard potentials.

6 | Conclusions and Outlook

Preferential expansion of natural or technical caverns along highly soluble potash seams is a considerable risk for salt mining, geological repositories and energy storage. Previous models are not capable of reproducing the complex interplay between chemical reactions and fluid flow. Hence, the first objective of the accomplished research is to systematically investigate the chemical reactions within different types of potash seams. Based on that, transition zones between the center of cavernous structures and unaffected salt rock can be described, facilitating the detection of natural caverns at the earliest possible stage. In this context, it is found in Chapter 2 that brine and rock composition can easily be determined by calculating the reaction path of the dry potash salt. To do so, geochemical reaction models are applied assuming thermodynamic equilibrium. Results can be transferred to the spatial scale, with the solid-fluid-ratio increasing towards the unaffected rock. In case of kieseritic potash seams, which contain all six major components of seawater, complex transition zones consisting of various mineralogical regions are formed. The exact composition mainly depends on the ratio between kieserite and sylvite. In contrast, potash seams with less components, e.g., carnallitic ones, may only show one mineralogical region of intermediate porosity (Chapters 3 and 4). In general, the porosity is always decreasing from the central cavern towards the unaffected rock. Comparing the simulation results with field measurements enables to draw conclusions about the current position along the transition zone and therefore facilitates a better localization of natural caverns.

Referring to the second objective in Chapter 1.3, geochemical reaction models are subsequently coupled with a flow and transport code and complemented by an newly developed approach called ‘interchange’. The result is a reactive transport model suitable to describe the expansion of caverns along potash seams in space and time. From the scenario analyses in Chapters 3 and 4, a classification scheme is derived, based on the dimensionless Péclet (Pe) and Damköhler (Da) numbers. Generally, four different cases of leaching zone evolution are distinguished (with the initial growth rate tending upwards from case 1 to 4):

1. dominated by reactions ($Da < 1$) and diffusion ($Pe < 2$)
2. dominated by reactions ($Da < 1$) and advection ($Pe > 2$)
3. dominated by transport ($Da > 1$) and diffusion ($Pe < 2$)
4. dominated by transport ($Da > 1$) and advection ($Pe > 2$)

Reaction-dominated systems (cases 1 and 2) are associated with low dissolution rates, resulting in a slow but steady cavern growth that proceeds evenly across the entire seam

thickness and only weakly depends on the Péclet number (Figure 6.1a,b). In contrast, transport-dominated systems (cases 3 and 4) are associated with relatively high dissolution rates and the dominating transport mechanism is of great importance. Thereby, small porosity causes diffusion to prevail (case 3), resulting in cavern shapes and growth rates comparable to those of reaction-dominated systems (Figure 6.1c). In the case of high porosity (>10%), advection is the dominating transport mechanism and density-driven convection gains substantial influence (case 4). Hence, funnel-shaped caverns evolve and growth rates are significantly faster at the beginning (Figure 6.1d). However, strong concentration gradients also cause the precipitation of halite next to the lower inflow region, leading to the formation of a barrier, which impedes solution exchange after a few years. Consequently, these systems generally shift towards transport- and diffusion-dominated (case 3) over time, associated with a significant decrease in growth rate (Figure 6.1d). A transition zone is only formed in case of transport-dominated systems, whereas reaction-dominated systems usually show a homogeneous leaching zone, where all minerals the inflowing solution is undersaturated with are fully dissolved (Figure 6.1). It can be stated that Da and Pe depend on the composition of the dry potash seam as well as on the solution encountering it. These framework conditions determine dissolution rate and transport velocity, which in turn control shape, growth rate and mineralogical composition of the leaching zone.

With regard to the third objective of this thesis, it is shown that insoluble inclusions and intersecting layers only need to be considered in case of transport- and advection-dominated systems (case 4). Close to the hanging wall, they cause caverns to advance more slowly, whereas close to the footwall, more potash salt is dissolved. Consequently, the cavern shape changes, depending on the distribution of insoluble inclusions: while broad inclusions lead to a steeper dissolution front, intersecting layers cause the evolution of several smaller funnel-shaped caverns. Inclined intersecting layers result in asymmetric cavern shapes, with one half advancing considerably faster than the other. However, except for the latter case, the reduction in growth rate is always similar. It only depends on the volume ratio of insoluble inclusions and not on their distribution. Heterogeneous rock distributions complicate a classification, because the convection cell is disturbed or split up into several ones. Thus, using an average flow velocity is not sufficient anymore, and especially the resulting shifting points ($Da = 1$ and $Pe = 2$) must be interpreted with caution. Instead, the occurrence of transition zones and barriers should be used to determine if a system is dominated by reaction or transport. Regarding variations in dissolution rate, it is important to note that Da has to be calculated individually for each mineral, considering its maximum solubility as well as the saturation state of the inflowing solution.

Combining all of these findings finally allows for an assessment of the hazard potentials of cavernous structures, which is also part of the second objective in Chapter 1.3. Thereby, fast and stable growth rates in combination with high porosities and a missing transition zone can be seen as the most critical case: the cavern contains a large

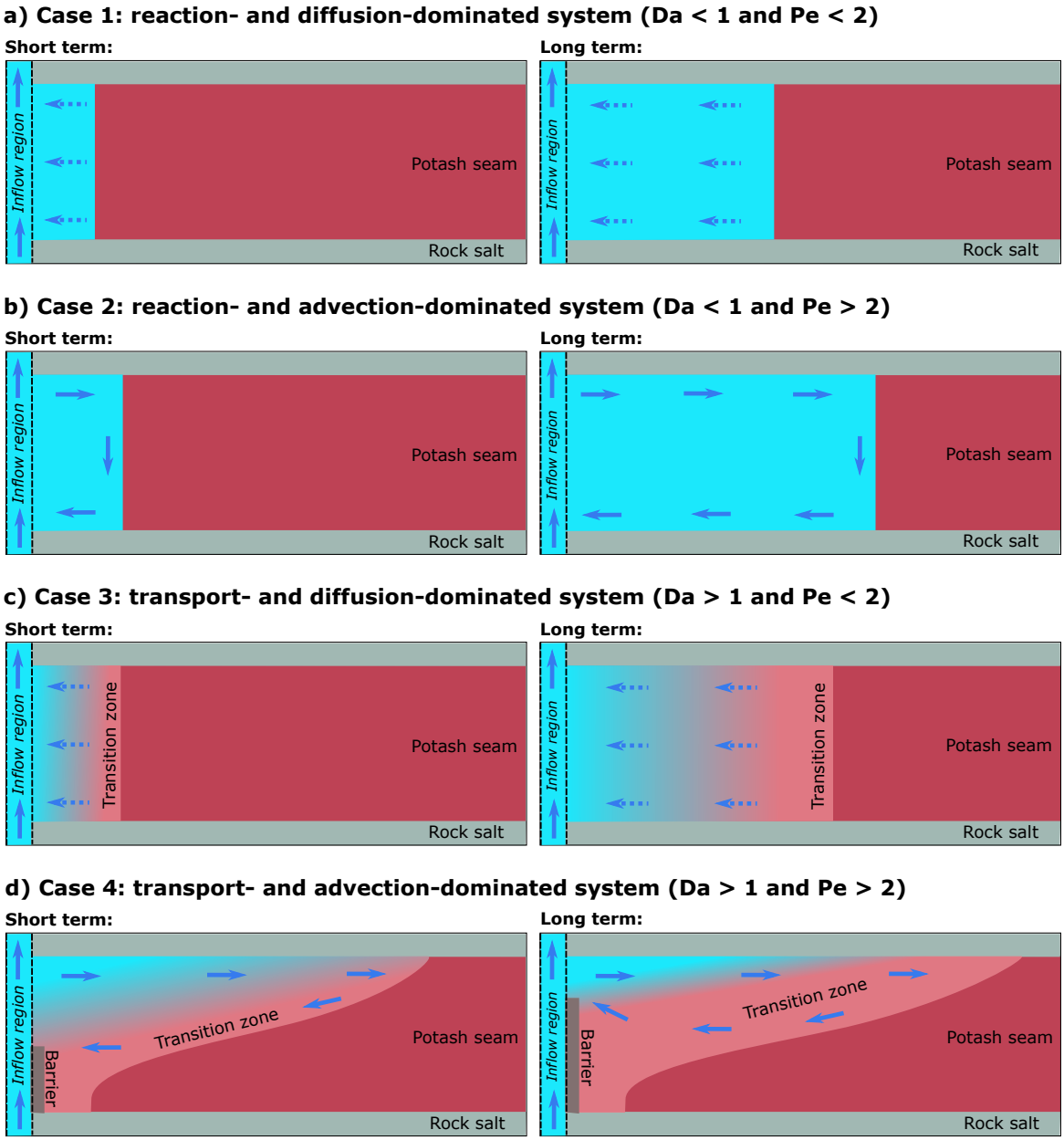

Figure 6.1: Overview of the four different cases of cavern evolution and their hazard potentials. Reaction- and advection-dominated systems are considered as most critical in the long term (b), whereas transport- and advection-dominated systems are more critical in the short term (d).

amount of brine, its mechanical stability is rather low, and the risk of encountering a mine, a geological fault zone or an aquifer sooner or later is relatively high, whereas a localization based on rock and brine samples from the transition zone is not possible. Transport- and advection-dominated systems (case 4) can penetrate several meters deep into a potash seam within only a few years and are therefore considered as most critical in the short term (Figure 6.1d). However, only the upper half of the seam is dissolved, and after the first few years, cavern growth nearly stops due to barrier formation. Furthermore, a transition zone with lower porosity is formed, facilitating an early detection of the cavern. Insoluble inclusions or intersecting layers reduce growth rate and hazard potential as well. To account for this effect, only their volume ratio has to

be known. Neglecting them generates a safety margin in the overall assessment as long as the mechanical stability of the leaching zone is given. In contrast, the collapse of insoluble layers or inclusions can create new fluid flow paths or even cavities associated with a significant increase in growth rates and hazard potentials. Reaction-dominated systems show constant growth rates over long periods of time, and transition zones do not exist (Figure 6.1a,b). Thereby, advection-dominated systems are associated with higher porosity and growth rates than diffusion-dominated ones. Accordingly, case 2 is considered as most critical with regard to long-term expansion, mechanical stability as well as detectability (Figure 6.1b). Generally, the scenario analyses in Chapters 3 and 4 as well as the case study in Chapter 2 indicate that most systems in nature represent a mixture of the four cases described above. Particularly in case of heterogeneous rock compositions as well as potash seams containing all six major components of seawater, Pe and Da vary in space, time and between minerals. For such complex systems, an assessment of the hazard potentials is only feasible if extensive field data are available for calibration and validation. The reactive transport model presented in this thesis provides a reliable basis for doing so.

For a more comprehensive risk assessment, stability of the rock matrix has to be taken into account. Thus, the reactive transport model must be coupled to a mechanical model that is able to describe partly dissolved potash seams. However, since previous models focus on rock salt, this requires extensive laboratory experiments and presumably the development of new constitutive laws. Additional laboratory and field data are also necessary to properly describe the relationship between porosity and permeability. Moreover, there is a need to learn more about the dissolution kinetics within potash seams: first, for many secondary minerals occurring in quinary and hexary systems, dissolution rates are still not available. Second, it is still unclear how they generally depend on the local flow velocity. Both questions need to be addressed by performing dissolution experiments for different minerals under various flow conditions. Additionally, field measurements are required in order to calibrate reactive transport models. Once this has been done, the evolution of caverns and transition zones within any potash seam can be reproduced in space and time. Thereby, the following scenarios should be analyzed as they frequently occur in practice:

- potash seams consisting of minerals with greatly differing maximum dissolution rates
- heterogeneous potash seams consisting of several layers that principally contain the same minerals but in varying proportions
- boreholes encountering a natural cavern leading to massive outflow and thus to forced convection

Finally, the reactive transport model presented here might be extended or embedded into a larger system, comprising rock salt layers and fault zones or technical caverns as

well. In doing so, the boundary conditions at the inflow region of a potash seam can be determined more precisely. Since this area is not accessible for field investigations, only simulations can provide information about the circumstances that are necessary to produce large cavernous structures. The results are not only useful with regard to cavern localization and risk assessment, but may also enable to develop and evaluate strategies that prevent preferential expansion along potash seams (Deppe and Pippig 2002; Keime et al. 2012; Ziegenbalg 2012).

References

Ahoulou A. W. A., Tinet A., Oltéan C. and Golfier F. (2020): Experimental Insights Into the Interplay Between Buoyancy, Convection, and Dissolution Reaction. *Journal of Geophysical Research: Solid Earth* 125 (11), 1–18. doi: 10.1029/2020JB020854.

Alkattan M., Oelkers E. H., Dandurand J.-L. and Schott J. (1997): Experimental studies of halite dissolution kinetics, 1 The effect of saturation state and the presence of trace metals. *Chemical Geology* 137 (3-4), 201–219. doi: 10.1016/S0009-2541(96)00164-7.

Altmaier M., Brendler V., Bube C., Neck V., Marquardt C., Moog H. C., Richter A., Scharge T., Voigt W., Wilhelm S., Wilms T. and Wollmann G. (2011): *THEREDA - Thermodynamische Referenz-Datenbasis*. Tech. rep. Braunschweig, Germany: Gesellschaft für Anlagen- und Reaktorsicherheit (GRS), p. 864. url: https://www.grs.de/content/grs-265-thereda-thermodynamische-referenzdatenbasis-abschlussbericht (accessed on 03 August 2021)

Anderko A. and Lencka M. M. (1998): Modeling Self-diffusion in Multicomponent Aqueous Electrolyte Systems in Wide Concentration Ranges. *Industrial Engineering Chemistry Research* 37 (7), 2878–2888. doi: 10.1021/ie980001o.

Anderson R. Y. and Kirkland D. W. (1980): Dissolution of salt deposits by brine density flow. *Geology* 8 (2), 66–69. doi: 10.1130/0091-7613(1980)8<66:DOSDBB>2.0.CO;2.

Bach J. (2010): Untersuchung der lösekinetischen Vorgänge beim Ersaufen der Staßfurter Kaligruben. *Erkennen, analysieren, bewerten und prognostizieren der zukünftigen Entwicklung der Bergbaufolgeschäden: Exkursionsführer und Veröffentlichungen der Deutschen Gesellschaft für Geowissenschaften 244*, ed. by J. Gerardi. Staßfurt, Germany, p. 18.

Baumert B. (1953): Die Laugenspeicher in den Schichten des Zechsteins und ihre Gefahren für den Salzbergbau. *Zeitschrift der Deutschen Geologischen Gesellschaft* 105, 729–733.

Bérest P., Bergues J., Brouard B., Durup J. and Guerber B. (2001): A salt cavern abandonment test. *International Journal of Rock Mechanics and Mining Sciences* 38 (3), 357–368. doi: 10.1016/S1365-1609(01)00004-1.

Bethke C. M. (2007): Geochemical and Biogeochemical Reaction Modeling. 2nd ed. Cambridge, UK: Cambridge University Press, p. 564. doi: 10.1017/CBO9780511619670.

Bohn A. (2014): Hydrogeochemische Analyse und Modellierung von Lösungs- und Reaktionsprozessen im Salinar- und Deckgebirge am Staßfurter Sattel. Ph.D. thesis, Brandenburg University of Technology, Cottbus, p. 185. url: https://opus4.kobv.de/opus4-btu/frontdoor/index/index/docId/2862 (accessed on 14 May 2019)

Bolen W. (2021): *Mineral Commodity Summaries - Salt*. Tech. rep. U.S. Geological Survey.

Boys C. (1993): A Geological Approach to Potash Mining Problems in Saskatchewan, Canada. *Exploration and Mining Geology* 2 (2), 129–138.

Braitsch O. (1971): Salt Deposits Their Origin and Composition. Berlin / Heidelberg, Germany: Springer Berlin Heidelberg. doi: 10.1007/978-3-642-65083-3.

Campos de Orellana A. (1996): Pressure solution creep and non-associated plasticity in the mechanical behavior of potash mine openings. *International Journal of Rock Mechanics and Mining Sciences Geomechanics Abstracts* 33 (4), 347–370. doi: 10.1016/0148-9062(95)00075-5.

Cyran K. (2020): Insight into a shape of salt storage caverns. *Archives of Mining Sciences* 65 (2), 363–398. doi: 10.24425/ams.2020.133198.

De Baere B., Molins S., Mayer K. U. and François R. (2016): Determination of mineral dissolution regimes using flow-through time-resolved analysis (FT-TRA) and numerical simulation. *Chemical Geology* 430, 1–12. doi: 10.1016/j.chemgeo.2016.03.014.

Debure M., Lassin A., Marty N. C., Claret F., Virgone A., Calassou S. and Gaucher E. C. (2019): Thermodynamic evidence of giant salt deposit formation by serpentinization: an alternative mechanism to solar evaporation. *Scientific Reports* 9 (1), 11720. doi: 10.1038/s41598-019-48138-9.

Deppe S. and Pippig M. (2002): Erkundung und Maßnahmen zur Beherrschung der Salzlösungzuflüsse im Grubenfeld Merkers. *Kali und Steinsalz* 2, 40–49.

Diersch H.-J. and Kolditz O. (2002): Variable-density flow and transport in porous media: approaches and challenges. *Advances in Water Resources* 25 (8-12), 899–944. doi: 10.1016/S0309-1708(02)00063-5.

Dijk P. E. and Berkowitz B. (2000): Buoyancy-driven dissolution enhancement in rock fractures. *Geology* 28 (11), 1051–1054. doi: 10.1130/0091-7613(2000)28<1051:BDEIRF>2.0.CO;2.

Dreybrodt W. and Buhmann D. (1991): A mass transfer model for dissolution and precipitation of calcite from solutions in turbulent motion. *Chemical Geology* 90, 107–122. doi: 10.1016/0009-2541(91)90037-R.

Durie R. and Jessen F. (1964): Mechanism of the Dissolution of Salt in the Formation of Underground Salt Cavities. *Society of Petroleum Engineers Journal* 4, 183–190. doi: 10.2118/678-PA.

Dutka F., Starchenko V., Osselin F., Magni S., Szymczak P. and Ladd A. J. (2020): Time-dependent shapes of a dissolving mineral grain: Comparisons of simulations with microfluidic experiments. *Chemical Geology* 540, 119459. doi: 10.1016/j.chemgeo.2019.119459.

Edler D. (2010): The status of modeling software for salt cavern leaching, identification of some unsolved problems and investigation of few of their aspects. *Underground Storage of CO2 and Energy*. Ed. by M. Hou, H. Xie and J. Yoon. London, UK: Taylor Francis Group.

Elsner H. (2016): *Salze in Deutschland*. Tech. rep. Bundesanstalt für Geowissenschaften und Rohstoffe (BGR).

Felmy A. R. and Weare J. H. (1991): Calculation of multicomponent ionic diffusion from zero to high concentration: I. The system Na-K-Ca-Mg-Cl-SO4-H2O at 25°C. *Geochimica et Cosmochimica Acta* 55 (1), 113–131. doi: 10.1016/0016-7037(91)90405-T.

Field L. P., Milodowski A. E., Evans D., Palumbo-Roe B., Hall M. R., Marriott A. L., Barlow T. and Devez A. (2019): Determining constraints imposed by salt fabrics on the morphology of solution-mined energy storage cavities, through dissolution experiments using brine and seawater in halite. *Quarterly Journal of Engineering Geology and Hydrogeology* 52 (2), 240–254. doi: 10.1144/qjegh2018-072.

Fokker P. (1995): The behaviour of salt and salt caverns. Ph.D. thesis, TU Delft, p. 143. url: http://repository.tudelft.nl/view/ir/uuid:6847f8e4-3b09-4787-be02-bcce9f0eed06/ (accessed on 17 September 2021)

Gasanzade F., Pfeiffer W. T., Witte F., Tuschy I. and Bauer S. (2021): Subsurface renewable energy storage capacity for hydrogen, methane and compressed air – A performance assessment study from the North German Basin. *Renewable and Sustainable Energy Reviews* 149, 111422. doi: 10.1016/j.rser.2021.111422.

Gechter D., Huggenberger P., Ackerer P. and Waber H. N. (2008): Genesis and shape of natural solution cavities within salt deposits. *Water Resources Research* 44 (11), 1–18. doi: 10.1029/2007WR006753.

Gimm W. and Meyer H. (1968): Hydrologische Gefahren. *Kali- und Steinsalzbergbau*. Ed. by W. Gimm. Bd. 1. Leipzig, Germany: VEB Deutscher Verlag für Grundstoffindustrie, pp. 429–496.

Graf T. and Therrien R. (2007): Coupled thermohaline groundwater flow and single-species reactive solute transport in fractured porous media. *Advances in Water Resources* 30 (4), 742–771. doi: 10.1016/j.advwatres.2006.07.001.

Harvie C. E., Møller N. and Weare J. H. (1984): The prediction of mineral solubilities in natural waters: The Na-K-Mg-Ca-H-Cl-SO4-OH-HCO3-CO3-CO2-H2O system to high ionic strengths at 25°C. *Geochimica et Cosmochimica Acta* 48 (4), 723–751. doi: 10.1016/0016-7037(84)90098-X.

Harvie C. E. and Weare J. H. (1980): The prediction of mineral solubilities in natural waters: the Na-K-Mg-Ca-Cl-SO4-H2O system from zero to high concentration at 25° C. *Geochimica et Cosmochimica Acta* 44 (7), 981–997. doi: 10.1016/0016-7037(80)90287-2.

Herbert A. W., Jackson C. P. and Lever D. A. (1988): Coupled groundwater flow and solute transport with fluid density strongly dependent upon concentration. *Water Resources Research* 24 (10), 1781–1795. doi: 10.1029/WR024i010p01781.

Herbert H.-J. (2000): Zur Geochemie und geochemischen Modellierung hochsalinarer Lösungen. Stuttgart, Germany: Schweizerbart, p. 377.

Herbert H.-J. and Schwandt A. (2007): *Salzlösungszuflüsse im Salzbergbau Mitteldeutschlands*. Tech. rep. Köln, Germany: Gesellschaft für Anlagen- und Reaktorsicherheit (GRS), p. 198. url: https://www.grs.de/sites/default/files/pdf/GRS-226d.pdf (accessed on 10 January 2020)

Höntzsch S. and Zeibig S. (2014): Geogenic caverns in rock salt formations - a key to the understanding of genetic processes and the awareness of hazard potential. *GeoFrankfurt 2014*, Frankfurt a.M., Germany: Schweizerbart.

Hoppe H. and Winkler F. (1974): Beitrag zur Lösekinetik von Mineralien der Kaliindustrie. *Wiss. Zeitschrift Techn. Hochsch. Chem. Leuna-Merseburg* 16 (1), 23–28.

Hou Z. (2003): Mechanical and hydraulic behavior of rock salt in the excavation disturbed zone around underground facilities. *International Journal of Rock Mechanics and Mining Sciences* 40 (5), 725–738. DOI: 10.1016/S1365-1609(03)00064-9.

Husband W. H. W. and Ozsahin S. (1967): Rates of dissolution of potash ore. *The Canadian Journal of Chemical Engineering* 45 (4), 234–237. DOI: 10.1002/cjce.5450450410.

IAEA (2020): *Design Principles and Approaches for Radioactive Waste Repositories*. Tech. rep. Vienna: International Atomic Energy Agency.

Jänecke E. (1912): Eine graphische Darstellung der Gewichtsverhältnisse bei den ozeanen Salzablagerungen. *Kali* 6, 255–258.

Jasinski S. (2021): *Mineral Commodity Summaries - Potash*. Tech. rep. U.S. Geological Survey.

Jinlong L., Wenjie X., Jianjing Z., Wei L., Xilin S. and Chunhe Y. (2020): Modeling the mining of energy storage salt caverns using a structural dynamic mesh. *Energy* 193, 116730. DOI: 10.1016/j.energy.2019.116730.

Johnson K. S. (2008): Evaporite-karst problems and studies in the USA. *Environmental Geology* 53 (5), 937–943. DOI: 10.1007/s00254-007-0716-8.

Karsten O. (1954): Lösungsgeschwindigkeit von Natriumchlorid, Kaliumchlorid und Kieserit in Wasser und in wässerigen Lösungen. *Zeitschrift für anorganische und allgemeine Chemie* 276, 247–266. DOI: 10.1002/zaac.19542760506.

Keime M., Charnavel Y., Lampe G. and Theylich H. (2012): Obstruction in a salt cavern : Solution is dissolution. *25th World Gas Conference*, Kuala Lumpur, Malaysia, p. 11.

Kempka T. (2020): Verification of a Python-based TRANsport Simulation Environment for density-driven fluid flow and coupled transport of heat and chemical species. *Advances in Geosciences* 54, 67–77. DOI: 10.5194/adgeo-54-67-2020.

Khaledi K., Mahmoudi E., Datcheva M. and Schanz T. (2016): Stability and serviceability of underground energy storage caverns in rock salt subjected to mechanical cyclic loading. *International Journal of Rock Mechanics and Mining Sciences* 86, 115–131. DOI: 10.1016/j.ijrmms.2016.04.010.

Koch K. and Vogel J. (1980): Zu den Beziehungen von Tektonik, Sylvinitbildung und Basaltintrusionen im Werra-Kaligebiet (DDR). Leipzig, Germany: VEB Deutscher Verlag für Grundstoffindustrie, p. 104.

Krupp R. E. (2005): Formation and chemical evolution of magnesium chloride brines by evaporite dissolution processes—Implications for evaporite geochemistry. *Geochimica et Cosmochimica Acta* 69 (17), 4283–4299. DOI: 10.1016/j.gca.2004.11.018.

Küchler H. (2014): Empirische Untersuchungen des Strömungsverhaltens beim indirekten Solverfahren von Kavernen. *Erdöl Erdgas Kohle* 130 (11), 434–439.

Kuhlman K. (2014): *Summary Results for Brine Migration Modeling Performed by LANL LBNL and SNL for the UFD Program*. Tech. rep. Albuquerque, NM, and Livermore, CA, USA: Sandia National Laboratories (SNL). DOI: 10.2172/1163122.

Laliberté M. (2007): Model for Calculating the Viscosity of Aqueous Solutions. *Journal of Chemical Engineering Data* 52 (2), 321–335. DOI: 10.1021/je0604075.

Laliberté M. (2009): A Model for Calculating the Heat Capacity of Aqueous Solutions, with Updated Density and Viscosity Data. *Journal of Chemical Engineering Data* 54 (6), 1725–1760. DOI: 10.1021/je8008123.

Laouafa F., Guo J., Quintard M. and Luo H. (2015): Numerical modelling of salt leaching-dissolution process. *49th US Rock Mechanics / Geomechanics Symposium 2015*, San Francisco, California, USA: ARMA, American Rock Mechanics Association. URL: https://hal-ineris.archives-ouvertes.fr/ineris-01855079.

Laouafa F., Guo J. and Quintard M. (2019): Modeling of salt and gypsum dissolution: applications, evaluation of geomechanical hazards. *European Journal of Environmental and Civil Engineering* 25 (8), 1405–1426. DOI: 10.1080/19648189.2019.1579758.

LBEG (2021): *Erdöl und Erdgas in der Bundesrepublik Deutschland 2020*. Tech. rep. Hannover, Germany: Landesamt für Bergbau, Energie und Geologie, p. 49. URL: https://www.lbeg.niedersachsen.de / erdoel - erdgas - jahresbericht / jahresbericht - erdoel - und - erdgas - in - der - bundesrepublik - deutschland-936.html (accessed on 10 September 2021)

Letcher T. M., ed. (2016): Storing Energy. Elsevier. DOI: 10.1016/C2014-0-04236-0.

Li J., Shi X., Yang C., Li Y., Wang T. and Ma H. (2018): Mathematical model of salt cavern leaching for gas storage in high-insoluble salt formations. *Scientific Reports* 8, 372. DOI: 10.1038/s41598-017-18546-w.

Liu M., Shabaninejad M. and Mostaghimi P. (2017): Impact of mineralogical heterogeneity on reactive transport modelling. *Computers and Geosciences* 104, 12–19. doi: 10.1016/j.cageo.2017.03.020.

Liu X., Yang X., Wang J., Li D., Li P. and Yang Z. (2016): A dynamic dissolution model of rock salt under gravity for different flow rates. *Arabian Journal of Geosciences* 9 (3), 226. doi: 10.1007/s12517-015-2254-0.

Luo J., Diersch H.-J. G. and Monninkhoff L. M. M. (2012): 3D Modeling of Saline Groundwater Flow and Transport in a Flooded Salt Mine in Stassfurt, Germany. *Mine Water and the Environment* 31 (2), 104–111. doi: 10.1007/s10230-012-0181-9.

Lux K.-H. (2005): Zum langfristigen Tragverhalten von verschlossenen solegefüllten Sazkavernen - ein neuer Ansatz zu physikalischer Modellierung und numerischer Simulation. Theoretische und laborative Grundlagen. *Erdöl Erdgas Kohle* 121 (11), 414–422.

Lux K.-H. and Eberth S. (2007): Fundamentals and first application of a new healing model for rock salt. *Conference on the Mechanical Behavior of Salt (Saltmech VI) - Understanding of THMC Processes in Salt*, ed. by Wallner, Lux, Minkley and H. Jr. Hannover, Germany: CRC Press/Balkema, pp. 129–138.

Lux K.-H., Wolters R. and Düsterloh U. (2015): Konsistente TH2M-gekoppelte multi-physikalische Simulationen zum Tragverhalten von Speicherkavernen im Salzsteingebirge während der Aussol-, der Betriebs- und der Stilllegungsphase sowie in der Nachverschlussphase. *Erdöl Erdgas Kohle* 131 (11), 428–437.

Mahmoudi E., Khaledi K., Blumenthal A. von, König D. and Schanz T. (2016): Concept for an integral approach to explore the behavior of rock salt caverns under thermo-mechanical cyclic loading in energy storage systems. *Environmental Earth Sciences* 75 (14), 1069. doi: 10.1007/s12665-016-5850-8.

Mao X, Prommer H, Barry D., Langevin C., Panteleit B. and Li L. (2006): Three-dimensional model for multi-component reactive transport with variable density groundwater flow. *Environmental Modelling Software* 21 (5), 615–628. doi: 10.1016/j.envsoft.2004.11.008.

Mengel K., Röhlig K.-J. and Geckeis H. (2012): Endlagerung radioaktiver Abfälle. *Chemie in unserer Zeit* 46 (4), 208–217. doi: 10.1002/ciuz.201200582.

Minkley W, Knauth M and Bruckner D (2013): Discontinuum-mechanical behaviour of salt rocks and the practical relevance for the integrity of salinar barriers. *47th US Rock Mechanics/Geomechanics Symposium*, San Francisco, CA, USA: American Rock Mechanics Association (ARMA), pp. 1522–1534.

Molins S., Trebotich D., Steefel C. I. and Shen C. (2012): An investigation of the effect of pore scale flow on average geochemical reaction rates using direct numerical simulation. *Water Resources Research* 48 (3), 1–11. doi: 10.1029/2011WR011404.

Monnin C. and Ramboz C. (1996): The anhydrite saturation index of the ponded brines and sediment pore waters of the Red Sea deeps. *Chemical Geology* 127, 141–159. doi: 10.1016/0009-2541(95)00069-0.

Müller S. and Schüler L. (2021): GeoStat-Framework/GSTools. doi: 10.5281/zenodo.1313628.

Müller-Lyda I., Birthler H. and Fein E. (1999): *Ableitung von Permeabilitäts-Porositätsrelationen für Salzgrus*. Tech. rep. Köln, Germany: Gesellschaft für Anlagen- und Reaktorsicherheit (GRS), p. 74.

Munson D. (1997): Constitutive model of creep in rock salt applied to underground room closure. *International Journal of Rock Mechanics and Mining Sciences* 34 (2), 233–247. doi: 10.1016/S0148-9062(96)00047-2.

Nazary Moghadam S., Nazokkar K., Chalaturnyk R. J. and Mirzabozorg H. (2015): Parametric assessment of salt cavern performance using a creep model describing dilatancy and failure. *International Journal of Rock Mechanics and Mining Sciences* 79, 250–267. doi: 10.1016/j.ijrmms.2015.06.012.

Olivella S, Carrera J, Gens A and Alonso E. E. (1994): Nonisothermal multiphase flow of brine and gas through saline media. *Transport in Porous Media* 15 (3), 271–293. doi: 10.1007/BF00613282.

Oltéan C., Golfier F. and Buès M. A. (2013): Numerical and experimental investigation of buoyancy-driven dissolution in vertical fracture. *Journal of Geophysical Research: Solid Earth* 118 (5), 2038–2048. doi: 10.1002/jgrb.50188.

Palandri J. L. and Kharaka Y. K. (2004): *A compilation of rate parameters of water-mineral interaction kinetics for application to geochemical modeling*. Tech. rep. Menlo Park, CA, USA: U.S. Geological Survey (USGS), p. 71. URL: https://pubs.usgs.gov/of/2004/1068/ (accessed on 12 June 2021)

Parkhurst D. L. and Appelo C. (2013): *Description of Input and Examples for PHREEQC Version 3 — A Computer Program for Speciation, Batch-Reaction, One-Dimensional Transport, and Inverse Geochemical Calculations*. Tech. rep. Reston, VA, USA. Chap. 43, p. 497. DOI: 10.3133/tm6A43.

Pitzer K. S. (1973): Thermodynamics of electrolytes. I. Theoretical basis and general equations. *The Journal of Physical Chemistry* 77 (2), 268–277. DOI: 10.1021/j100621a026.

Prugger F. F. and Prugger A. F. (1991): Water problems in Saskatchewan potash mining - what can be learned from them? *Canadian Institute of Mining Bulletin* 84 (945), 58–66.

Pudewills A (2012): Numerical simulation of coupled Thermo-Hydro-Mechanical processes in rock salt. *Mechanical Behavior of Salt VII*. Ed. by P. Bérest, M. Ghoreychi, F. Hadj-Hassen and M. Tijani. London, UK: CRC Press, pp. 115–122. DOI: 10.1201/b12041.

Raines M. A. and Dewers T. A. (1997): Mixed transport/reaction control of gypsum dissolution kinetics in aqueous solutions and initiation of gypsum karst. *Chemical Geology* 140 (1-2), 29–48. DOI: 10.1016/S0009-2541(97)00018-1.

Röhr H. (1981): Lösungsgeschwindigkeiten von Salzmineralen beim Ausspülen von Hohlräumen im Salz. *Kali und Steinsalz* 8 (4), 103–111.

Sdanowski A. (1958): Gesetzmäßigkeiten in der Kinetik der Salzauflösung. *Mineralogie, Geologie, Chemie und Technologie der Mineralsalze ozeanischen Ursprungs*. Berlin, Germany: Akademie Verlag Berlin, pp. 257–268. URL: http://digital.slub-dresden.de/id1677376767 (accessed on 01 August 2021)

Spangenberg E., Spangenberg U. and Heindorf C. (1998): An experimental study of transport properties of porous rock salt. *Physics and Chemistry of the Earth* 23 (3), 367–371. DOI: 10.1016/S0079-1946(98)00039-1.

Stadler S, Sültenfuss J, Holländer H., Bohn A, Jahnke C and Suckow A (2012): Isotopic and geochemical indicators for groundwater flow and multi-component mixing near disturbed salt anticlines. *Chemical Geology* 294-295, 226–242. DOI: 10.1016/j.chemgeo.2011.12.006.

Stauffer P., Harp D., Jordan A., Lu Z., Kelkar S., Kang Q., Cate J. T., Boukhalfa H., Labyed Y., Reimus P., Caporuscio F., Miller T. and Robinson B. (2013): *Coupled Model for Heat and Water Transport in a High Level Waste Repository in Salt*. Tech. rep. Washington DC, USA: U.S. Department of Energy, p. 136. URL: https://www.energy.gov/ne/downloads/coupled-model-heat-and-water-transport-high-level-waste-repository-salt (accessed on 13 July 2021)

Steding S., Kempka T. and Kühn M. (2021a): How Insoluble Inclusions and Intersecting Layers Affect the Leaching Process within Potash Seams. *Applied Sciences* 11 (19), 9314. DOI: 10.3390/app11199314.

Steding S., Kempka T., Zirkler A. and Kühn M. (2021b): Spatial and Temporal Evolution of Leaching Zones within Potash Seams Reproduced by Reactive Transport Simulations. *Water* 13 (2), 168. DOI: 10.3390/w13020168.

Steding S., Zirkler A. and Kühn M. (2020): Geochemical reaction models quantify the composition of transition zones between brine occurrence and unaffected salt rock. *Chemical Geology* 532, 119349. DOI: 10.1016/j.chemgeo.2019.119349.

Steefel C. I., Appelo C. A. J., Arora B., Jacques D., Kalbacher T., Kolditz O., Lagneau V., Lichtner P. C., Mayer K. U., Meeussen J. C. L., Molins S., Moulton D., Shao H., Šimůnek J., Spycher N., Yabusaki S. B. and Yeh G. T. (2015): Reactive transport codes for subsurface environmental simulation. *Computational Geosciences* 19 (3), 445–478. DOI: 10.1007/s10596-014-9443-x.

Stiller M., Yechieli Y. and Gavrieli I. (2016): Rates of halite dissolution in natural brines: Dead Sea solutions as a case study. *Chemical Geology* 447, 161–172. DOI: 10.1016/j.chemgeo.2016.10.023.

Thoms R. and Gehle R. (1999): Non-halites and fluids in salt formations, and effects on cavern storage operations. *Third National Conference, Geo-Engineering for Underground Facilities*, ed. by G. Fernandez and R. Bauer. Vol. 90. Urbana, IL, USA: American Society of Civil Engineers (ASCE), pp. 780–796.

Tosca N. J., McLennan S. M., Lamb M. P. and Grotzinger J. P. (2011): Physicochemical properties of concentrated Martian surface waters. *Journal of Geophysical Research* 116, E05004. DOI: 10.1029/2010JE003700.

Velema R., Bullen J., Visser J. and Bruining J. (2010): Magnesium from Solution Mining of Bischofite Layers and Carnallite Layers. *ECMOR XII - 12th European Conference on the Mathematics of Oil Recovery*, Oxford, UK: European Association of Geoscientists Engineers, p. 20. doi: 10.3997/2214-4609.20145026.

Voigt W. (2015): What we know and still not know about oceanic salts. *Pure and Applied Chemistry* 87 (11-12), 1099–1126. doi: 10.1515/pac-2015-0606.

Wan J., Peng T., Shen R. and Jurado M. J. (2019): Numerical model and program development of TWH salt cavern construction for UGS. *Journal of Petroleum Science and Engineering* 179, 930–940. doi: 10.1016/j.petrol.2019.04.028.

Wang T., Yang C., Ma H., Daemen J. and Wu H. (2015): Safety evaluation of gas storage caverns located close to a tectonic fault. *Journal of Natural Gas Science and Engineering* 23, 281–293. doi: 10.1016/j.jngse.2015.02.005.

Warren J. K. (2017): Salt usually seals, but sometimes leaks: Implications for mine and cavern stabilities in the short and long term. *Earth-Science Reviews* 165, 302–341. doi: 10.1016/j.earscirev.2016.11.008.

Wei W., Varavei A., Sanaei A. and Sepehrnoori K. (2019): Geochemical Modeling of Wormhole Propagation in Carbonate Acidizing Considering Mineralogy Heterogeneity. *SPE Journal* 24 (05), 2163–2181. doi: 10.2118/195593-PA.

Weisbrod N., Alon-Mordish C., Konen E. and Yechieli Y. (2012): Dynamic dissolution of halite rock during flow of diluted saline solutions. *Geophysical Research Letters* 39, L09404. doi: 10.1029/2012GL051306.

Welder L., Ryberg D., Kotzur L., Grube T., Robinius M. and Stolten D. (2018): Spatio-temporal optimization of a future energy system for power-to-hydrogen applications in Germany. *Energy* 158, 1130–1149. doi: 10.1016/j.energy.2018.05.059.

Wittrup M. and Kyser T. (1990): The petrogenesis of brines in Devonian potash deposits of western Canada. *Chemical Geology* 82, 103–128. doi: 10.1016/0009-2541(90)90077-K.

Wolery T. and Jarek R. (2003): *Software user's manual EQ3/6, (Version 8.0)*. Tech. rep. Albuquerque, NM, USA: Sandia National Laboratories - U.S. Department of Energy, p. 48. url: https://wipp.energy.gov/library/CRA/CRA-2014/References/Others/Wolery_Jarek_2003_Software_Users_Manual_EQ36_Version_8_0.pdf (accessed on 03 September 2021)

Wooding R. A., Tyler S. W., White I. and Anderson P. A. (1997): Convection in groundwater below an evaporating Salt Lake: 2. Evolution of fingers or plumes. *Water Resources Research* 33 (6), 1219–1228. doi: 10.1029/96WR03534.

Xie M., Kolditz O. and Moog H. C. (2011): A geochemical transport model for thermo-hydro-chemical (THC) coupled processes with saline water. *Water Resources Research* 47 (2), 1–14. doi: 10.1029/2010WR009270.

Yang X. and Liu X. (2017): Numerical simulation of rock salt dissolution in dynamic water. *Environmental Earth Sciences* 76 (12), 427. doi: 10.1007/s12665-017-6768-5.

Yang X., Liu X., Zang W., Lin Z. and Wang Q. (2017): A Study of Analytical Solution for the Special Dissolution Rate Model of Rock Salt. *Advances in Materials Science and Engineering* 2017, 1–8. doi: 10.1155/2017/4967913.

Yuan-Hui L. and Gregory S. (1974): Diffusion of ions in sea water and in deep-sea sediments. *Geochimica et Cosmochimica Acta* 38 (5), 703–714. doi: 10.1016/0016-7037(74)90145-8.

Zarrouk S. J. and Sullivan M. O. (2001): The effect of chemical reactions on the transport properties of porous media. *23rd New Zealand Geothermal Workshop*, ed. by S. Simmons, M. Dunstall and O. Morgan. Auckland University, New Zealand, pp. 231–236.

Zhang G., Wang Z., Wang L., Chen Y., Wu Y., Ma D. and Zhang K. (2019): Mechanism of collapse sinkholes induced by solution mining of salt formations and measures for prediction and prevention. *Bulletin of Engineering Geology and the Environment* 78 (3), 1401–1415. doi: 10.1007/s10064-017-1173-6.

Zidane A., Zechner E., Huggenberger P. and Younes A. (2014): Simulation of rock salt dissolution and its impact on land subsidence. *Hydrology and Earth System Sciences* 18 (6), 2177–2189. doi: 10.5194/hess-18-2177-2014.

Ziegenbalg G. (2012): Grouting by Controlled Crystallization of Supersaturated Solutions: A New Technology to Seal Porous and Fractured Rock Formations and Stop Water Inflows into Mines. *Fourth International Conference on Grouting and Deep Mixing*, ed. by L. Lohnsen, D. Bruce and M. Byle. New Orleans, LA, USA: American Society of Civil Engineers (ASCE), pp. 1934–1947. doi: 10.1061/9780784412350.0168.

Publications of the Author

Steding, S., Kempka, T. and Kühn, M. (2021a): How insoluble inclusions and intersecting layers affect the leaching process within potash seams. *Applied Sciences*, 11, 9314. DOI: 10.3390/app11199314

Steding, S., Kempka, T., Zirkler, A. and Kühn, M. (2021b): Spatial and temporal evolution of leaching zones within potash seams reproduced by reactive transport simulations. *Water*, 13, 168. DOI: 10.3390/w13020168

Steding, S. and Schneider, W. (2021): Prognose des Schadstoffaustrags aus mehrphasigen DNAPL-Pools mittels semi-analytischem Berechnungsmodell. *Grundwasser*, 26, 241-253. DOI: 10.1007/s00767-021-00490-2

Steding, S., Zirkler, A. and Kühn, M. (2020): Geochemical reaction models quantify the composition of transition zones between brine occurrence and unaffected salt rock. *Chemical Geology*, 532, 119349. DOI: 10.1016/j.chemgeo.2019.119349

Strauch [Beeskow-Strauch], B., Arndt, J., Barth, J., Giese, R., Kühn, M., Myrttinen, A., Richter, H., **Steding, S.**, Zimmer, M. and Zirkler, A. (2019): Wo Salz, Wasser und Gas sich treffen - Kavernenrandbereiche unter Tage und unter der Lupe im Forschungsprojekt ProSalz. *System Erde*, 9, 20-25. DOI: 10.2312/GFZ.syserde.09.01.3

Steding, S., Bürkner, G., Törzs, T. and Grabe, J. (2018): Zum besonderen Quellverhalten von Tarrastonen. *geotechnik*, 41, 254-263. DOI: 10.1002/gete.201800003

Acknowledgements

The present thesis was partly carried out within the Geo:N project ProSalz (Grant 03A0014A). I would like to thank the German Federal Ministry for Education and Research (BMBF) for the received funding.

By the time I started my PhD, I only had a vague idea of what to expect. It became four intense years full of new experiences, impressions and challenges. Particularly the last 1.5 years, which were under the sign of Corona and characterized by numerous restrictions, turned out to be not easy. In the following, I would therefore like to thank a number of people for making this work possible.

My special thanks go to my first supervisor, Prof. Michael Kühn, who constantly supported and motivated me throughout my doctoral research. Even in times of Corona, he was always ready to listen to my questions, ideas and problems. His honest and trustful manner greatly contributed not only to my professional development, but also to my personal growth.

I would also like to thank my second supervisor, Dr. Thomas Kempka, for his extensive professional support. Without his profound expertise and advice, this work would not have been possible. In numerous meetings and discussions, also Axel Zirkler and Dr. Thomas Radtke, from the company K+S, shared their expertise with me and thus made an important contribution to the quality of this work.

Furthermore, I would like to thank Prof. Wilfried Schneider and Dr. Elke Bozau for their willingness to review this work. Many thanks also go to my working colleagues from the section Fluid Systems Modelling. The open, friendly atmosphere in our group has always given me inspiration and motivation. In addition, I would like to thank Theresa, Ina and Anja for proofreading parts of this work.

My deepest gratitude goes to my family, who always supported my decisions and picked me up in times of doubt. Especially the challenging situation during the last 9 months I would not have been able to manage without them.

Selbstständigkeitserklärung

Hiermit erkläre ich, Svenja Steding, dass ich als Autorin der vorliegenden Dissertation mit dem Titel: „*Geochemical and Hydraulic Modeling of Cavernous Structures in Potash Seams*“, die Arbeit selbstständig und ohne unerlaubte Hilfe angefertigt habe.

Ferner versichere ich, keine anderen als die angegebenen Quellen und Hilfsmittel benutzt zu haben. Alle Ausführungen, die anderen Schriften wörtlich oder inhaltlich entnommenen wurden, sind als solche kenntlich gemacht.

Die vorliegende Arbeit wurde in keinem anderen Promotionsverfahren angenommen oder abgelehnt.

_____

Datum, Ort

_____

Unterschrift